

Examining the Factors Controlling Transition Metal Surface Chemistry in terms of Local
Bonding Interactions and Metal Bond Conjugation

A Dissertation

Presented to
the faculty of the School of Engineering and Applied Science
University of Virginia

in partial fulfillment
of the requirements for the degree

Doctor of Philosophy

by

Craig Plaisance

August

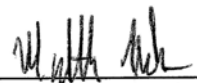
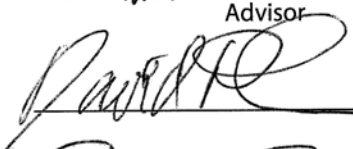
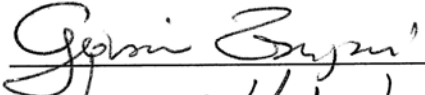
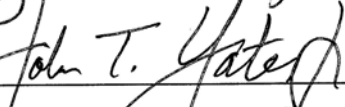

2012

APPROVAL SHEET

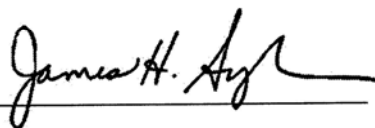
The dissertation
is submitted in partial fulfillment of the requirements
for the degree of
Doctor of Philosophy


AUTHOR

The dissertation has been read and approved by the examining committee:


Advisor





Accepted for the School of Engineering and Applied Science:



Dean, School of Engineering and Applied Science

August
2012

Abstract

Although a comprehension of adsorption to transition metal surfaces is crucial to understanding the principles that control catalytic chemistry on these surfaces, the nature of the metal-adsorbate bond is not understood to the same extent as bonding in organic molecules and organometallic complexes. This is due to the typical characterization of the metal-metal bonding within the transition metal surface as being delocalized over the entire crystal. In this work, a formalism is introduced that describes metal-metal bonding in terms of local fractional bonds that interact with each other through conjugation.

The resulting model is first used to describe the bonding in bulk $5d$ transition metals, using sd^n hybrid orbitals to form these bonds. It is found that conjugative interactions between vicinal metal-metal bonds account for a large portion of the cohesive energy, indicating that a strictly local representation of metal-metal bonding is insufficient. The trends in cohesive energy and surface energy of the (111) surface calculated from this model follow the same trend as the values calculated using density functional theory, indicating that the longer range delocalization excluded from this model is not required to describe the main features of the variation of bond strength among the different metals examined.

Application of this model to the chemisorption of atomic hydrogen also yields values of the adsorption energy that follow the same trend as the values calculated by density functional theory. The low adsorption energy on Au compared to the other $5d$ metals is found to be due to two effects. The first of these is due to the fact that the entire d shell is filled in the ground state of the Au atom so that the relevant d orbital cannot participate in forming a metal-hydrogen bond unless part of an electron is first promoted from this orbital into the higher energy s orbital. The second effect is due to the bond saturation of the Au atom by formation of a single bond to hydrogen so that it can no longer participate in conjugative interactions with neighboring metal atoms in the surface. These insights are applied qualitatively to a variety of other adsorbates, explaining a wide range of chemisorption behavior on these surfaces.

Acknowledgements

There are many people to whom my thanks are due for the vital roles they played in helping me to complete this dissertation. First, I would like to thank my advisor, Matthew Neurock for his guidance and instruction during my time working under him, and for helping me develop a such a solid understanding of catalysis. I would like to thank David Green, John Yates Jr., Robert Davis, and Giovanni Zangari for serving on my Ph.D. committee. Thanks to the Department of Energy and British Petroleum for funding during my study. Thanks to Vickie Faulconer for helping me get everything together to graduate. I would also like to thank my family for their support and encouragement over the past seven years. Last, but not least, I would like to thank my wonderful wife Tiana for her support, companionship, and patience while it took what must have seemed like an eternity for me to graduate.

Contents

Abstract	1
Acknowledgements	2
List of Figures	5
Preface	8
Chapter 1 – Development of a Local Bonding Description of Metallic Electronic Structure	12
1.1 Local bonding in molecular electronic structure	13
1.2 Local bonding in transition metal complexes	30
1.3 Application of local bonding formalism to metallic systems	40
1.3.1 Fractional bond orbitals	43
1.3.2 Conjugation in systems containing fractional orbitals	49
Chapter 2 – Local Bonding in the 5d Transition Metal fcc Crystals	62
2.1 Bonding in the Bulk	62
2.1.1 Zero order electronic structure	62
2.1.2 Conjugation	80
2.2 Bonding in Surfaces	92
2.2.1 Changes in zero order electronic structure due to surface cleavage	93

2.2.2	Surface Energy	95
Chapter 3 – Local Bonding Description of Chemisorption on 5d Transition Metal Surfaces...		101
3.1	Chemisorption of Atomic Hydrogen	102
3.1.1	Zero order bonding	103
3.1.2	Conjugation	127
3.2	Chemisorption Involving Multiple Interactions	138
Summary		146
Appendix A – Determination of Tight Binding Parameters		156
Appendix B – Method for DFT Calculations		157
Appendix C – Structures of Adsorbates on the (111) Surface		159
References		160

List of Figures

Figure 1.1 Occupied canonical molecular orbitals of ethane.....	15
Figure 1.2 Occupied localized molecular orbitals of ethane.....	16
Figure 1.3 Bonding (top) and antibonding (bottom) SLMOs in ethane	21
Figure 1.4 Construction of SLMOs for one of the C-H bonds in ethane.....	24
Figure 1.5 Hyperconjugative interaction in ethane.....	26
Figure 1.6 Decomposition of the resonance integral in ethane.....	29
Figure 1.7 Lewis dot structures for the normal valent 5d transition metal atoms	32
Figure 1.8 Zero order electronic structure of PtCl_4^{2-}	34
Figure 1.9 Zero order Electronic structure of PtCl_4^{2-} without use of hyperbonds.	36
Figure 1.10 Conjugative interactions in PtCl_4^{2-}	38
Figure 1.11 Decomposition of the resonance integral in PtCl_4^{2-}	39
Figure 1.12 Hybrid orbital of an Ir atom in the fcc lattice.....	42
Figure 1.13 Description of a hyperbond using fractional orbitals	45
Figure 2.1 An alternative representation of the fcc unit cell.....	64
Figure 2.2 Set fractional d orbitals for the fcc lattice.	65
Figure 2.3 Zero order bonding in fcc W	67

Figure 2.4 Distribution of lone pair charge density in the fcc lattice	68
Figure 2.5 Hybrid orbitals for fcc transition metals.....	70
Figure 2.6 Decomposition of the resonance integral for metal atoms in the fcc lattice	72
Figure 2.7 Decomposition of the zero order bond energy in fcc transition metal.	76
Figure 2.8 Set of atomic orbitals used to generate the conjugative interactions.....	80
Figure 2.9 Magnitudes of atomic orbitals used to generate conjugative interactions.....	82
Figure 2.10 Magnitudes of the conjugative interactions between metal atoms	84
Figure 2.11 Energy of conjugative interactions between metal atoms in the bulk	88
Figure 2.12 Cohesive energy of the fcc transition metal crystals	91
Figure 2.13 Effect of surface cleavage on zero order bonding	93
Figure 2.14 Process for cleavage of a two-layer slab from the bulk.....	96
Figure 2.15 Energies of conjugative interactions between surface and subsurface atoms	98
Figure 2.16 Loss of bond energy due to surface formation	99
Figure 3.1 DFT adsorption energies on the (111) surface of fcc transition metals	102
Figure 3.2 Two-layer infinite slab with a monolayer of hydrogen adsorbed on each side.....	104
Figure 3.3 Decomposition of chemisorption process	105
Figure 3.4 Hybridization in the metal-hydrogen bond.....	107

Figure 3.5 Formation of the metal-hydrogen bond	109
Figure 3.6 Atomic d orbitals used to construct hybrid orbitals in the adsorbate covered surface	112
Figure 3.7 Fractional d orbitals used to construct hybrids in the adsorbate covered surface	113
Figure 3.8 Distributions of lone pair charge density on the adsorbate covered surface	115
Figure 3.9 Decomposition of the zero order energy of surface bonds in the presence of an adsorbate layer of atomic hydrogen	119
Figure 3.10 Decomposition of the zero order energy of subsurface bonds in the presence of adsorbate layer of atomic hydrogen	121
Figure 3.11 Change in zero order metal-metal bond energy upon adsorption.....	124
Figure 3.12 Hydrogen adsorption energy on (111) fcc metal surfaces	126
Figure 3.13 Magnitudes of orbitals used to generate conjugative interactions.....	129
Figure 3.14 Magnitudes of conjugative interactions.....	131
Figure 3.15 Energies of conjugative interactions	136
Figure 3.16 Change in conjugation energy upon adsorption of hydrogen.....	137
Figure 3.17 Formation of three electron – two center bond	140
Figure 3.18 Bonding in the metal-adsorbate “molecule” formed between a single metal atom and each adsorbate	143

Preface

Due to the importance that metal surfaces play in heterogeneous catalytic reactions, a fundamental understanding of the chemical bonding on these surfaces is necessary to understand the chemistry and ultimately aid in the design of new materials. The most important factor controlling this reaction chemistry is the binding of chemical intermediates to the metal surface.¹ The structure and composition of the binding site and its local environment has a significant effect on how strong these intermediates bind to the surface. Thus a thorough understanding of the chemical effects by which these factors control binding of intermediates would lead to significant insight into the development of new catalysts.

Metal surfaces, however, present a unique challenge to our fundamental understanding of chemical bonding. While the bonding in organic molecules and transition metal complexes is well understood in terms of concepts such as hybridization, covalent bonding, and resonance,^{2,3} the chemistry of metal surfaces has so far eluded such a description. This is in a large part due to the complicated nature of the metallic bond which is commonly characterized as being delocalized over all the atoms in the system,⁴ making it difficult to utilize classic chemical bonding concepts. As a consequence of this, metals have not been studied extensively by the theoretical chemistry community in the same way that molecules and transition metal complexes have.

Most of our understanding of metals comes from the field of solid state physics where the electronic structure is described in terms of valence electrons occupying continuous bands of Bloch orbitals delocalized over all the atoms in the crystal.⁴ This description has been very successful at understanding nonlocal phenomena such as interactions with electromagnetic fields including electrical conductivity. Chemical bonding, however, is a local phenomenon occurring between neighboring atoms, making it cumbersome to describe in terms of delocalized orbitals. Nonetheless, a considerable amount of effort has gone into understanding metal surface chemistry in terms of this delocalized representation of the electronic structure, starting with the earliest model developed independently by Newns and Grimley^{5,6} to describe the chemisorption of atomic hydrogen on metal surfaces. A simplified version of this model was subsequently

developed by Hammer and Nørskov to correlate chemisorption strength of hydrogen and other atoms and molecular fragments with the average energy of the d-band relative to the Fermi level.⁷ This latter model, the d-band center model, has found widespread use for examining catalytic processes on transition metal surfaces.^{8–10}

While the Bloch orbital based models of chemisorption do explain some trends in chemisorption correctly, they do so in the language of solid state physics. Other approaches to understanding chemisorption, such as those by Hoffmann,¹¹ van Santen,¹² and Anderson,¹³ treat chemisorption in terms of charge transfer between molecular orbitals on the adsorbate and bands on the metal surface. This approach is analogous to Frontier Molecular Orbital Theory^{14,15} between molecular fragments, except that the electrons in the metal surface reside in a continuous band of delocalized orbitals instead of molecular orbitals with discrete energies. These interactions can be backed out from a band structure calculation using the crystal orbital overlap population analysis developed by Hoffman¹¹ or they can be estimated from perturbation theory. A drawback of this approach is that prior knowledge of the band structure of the surface is required. This is undesirable from a chemical perspective because delocalized bands are being used to describe a local chemical bond. Additionally, any predictive use of this approach is constrained to a perturbative treatment of the metal-adsorbate bond. This is only valid if the metal-adsorbate bond is much weaker than the metal-metal bonds. For adsorbates that are not stable species when not bound to the surface, including all atomic adsorbates, this assumption is not valid since the metal-adsorbate bond is significantly stronger than the metal-metal bonds.¹²

Another conceptual model of chemisorption¹² treats chemisorption in the surface-molecule limit in which the metal-adsorbate bond is much stronger than the metal-metal bonds. In this model, the overall process of adsorption is broken into three sub-processes. First, the metal atom in the adsorption site is removed from the surface to the vacuum, resulting in a loss of metal-metal bonding energy in the surface. Then, the metal atom and the adsorbate form a “surface molecule” in vacuum, leading to an increase in binding energy due to formation of the metal-adsorbate bond. Finally, the surface molecule is placed back into the surface and some of the original metal-metal bond energy lost is regained. In the limit of strong chemisorption in which the metal-adsorbate bond is much stronger than the metal-metal bonds, the chemisorption energy

can be approximated using a perturbative treatment. While in many cases this limit is somewhat valid, the metal-metal bonding is still often too strong to treat using perturbation theory and a more rigorous method is required. Also, even though this approach treats the metal-adsorbate bond in terms of valence bond concepts, it still does not treat the metal-metal bonding in such a manner.

All of the chemisorption models discussed so far treat bonding in the metal surface in terms of band theory. Since chemisorption is a local phenomenon,¹² it is somewhat unnatural to describe part of the system in terms of completely delocalized bands. It would be far better if a model of chemisorption could be developed using the traditional concepts of valence bond theory to treat all aspects of bonding in the system, including the metal-metal bond. This would help to unify our understanding of the interactions in these systems with our understanding of the interactions in more traditional chemical systems, especially in transition metal complexes. Until now, however, such a theoretical framework has not yet materialized. Is this because metallic systems are fundamentally different from other systems including those studied in organometallic chemistry? Or have the similarities simply been overlooked? We will shortly see that both of these are partially true and that by thinking about bonding in a slightly different way we can circumvent these differences to develop a framework that for the first time describes bonding in metals using the same concepts used for molecular systems.

To do so, we start out in Chapter 1 by reviewing some of the concepts of local bonding as applied to molecules and transition metal complexes. Much of this discussion is based on the Natural Bond Orbital Theory of Weinhold and Landis.³ We will see how, to a zero-order approximation, bonding in these species can be described in terms of two center bonding orbitals and one center lone pairs. In species that are well described by a single Lewis structure, this zero-order approximation is quite accurate in capturing the electronic structure. Other species, including most transition metal complexes, do not fall into this category and require the inclusion of conjugative interactions between filled and unfilled bond orbitals in the zero-order structure. Having introduced the concepts of local bonding, we then explore the issues involved in applying them to bonding in a metal crystal. We discover that it is necessary to use Lewis structures with fractional bonds to describe the zero-order bonding in metals. To describe these

fractional bonds, we introduce the concept of fractional bonding orbitals which are an adaptation of the conventional bonding orbitals associated with integer-order bonds in Lewis structures to fractional bonds. Finally, we extend the concepts of local bonding and conjugation discussed earlier to these fractional bonds.

In Chapter 2, this framework is applied to bonding in fcc transition metal crystals. We first determine a fractional hybridization scheme for the metal atoms that is consistent with the fcc symmetry of the unit cell and use these to form the fractional bonds in the zero-order structure. We then calculate the conjugative interactions between the fractional orbitals in the zero-order structure, which are found to contribute to the cohesive energy of the crystal to the same extent as the zero-order bonds. In the last section, we explore the changes in these interactions that occur upon cleavage of the a (111) surface from the bulk in preparation for the application of this model to chemisorption in the next chapter.

In the first part of Chapter 3, the semi-local model of bonding developed herein is used to examine chemisorption of atomic hydrogen on the atop site of the (111) surface of different transition metals. Several general features of metal-adsorbate bond are identified that are then used to rationalize the behavior of more complex adsorbates on the surfaces of different transition metals.

Chapter 1 – Development of a Local Bonding Description of Metallic Electronic Structure

In this chapter, we develop a model that describes the electronic structure of metallic systems in terms of local bonding. To begin, we review the concepts of local bonding first in molecules and then in transition metal complexes. To describe the electronic structure of these species in terms of local bonding, we use the ideas introduced by Weinhold and Landis in their Natural Bond Orbital Theory.³ In this theory, the zero order electronic structure of a species is described in terms of electron pairs occupying two center bonding orbitals and one center lone pairs. The zero order structure is improved by including conjugation involving electron transfer from filled bonding orbitals and lone pairs into empty antibonding orbitals. In the original form of this method, the bonding orbitals and lone pairs in the zero order structure are extracted from the output of a full electronic structure calculation. In this work, a modification is made allowing the zero order electronic structure to be determined directly from the one-electron Hamiltonian that describes the system, bypassing the need to perform a full electronic structure calculation.

After introducing the local model of electronic structure in molecules and transition metal complexes, we explore the application of this model to metallic systems. Due to the extreme hypervalency of metal atoms in the metallic state, we will see that it is necessary to describe the zero order structure of the metal in terms of fractional bonds and fractional lone pairs. With this modification, the zero order structure is constructed by placing fractional electron pairs into fractional bonding orbitals and fractional lone pair orbitals. We then develop a method of including conjugation between fractional bonds and lone pairs. It will be seen that treating conjugation between fractional orbitals is not as straightforward as treating conjugation between non-fractional orbitals due to the presence of interactions that do not conserve the total number of electrons in the system.

1.1 Local bonding in molecular electronic structure

In order to understand the bonding in metallic systems, we would first like to examine the less complicated bonding in molecular systems. To describe the electronic structure of molecules, as well as the other systems examined in this work, we will use the Kohn-Sham formulation of density functional theory¹⁶ which is used in the vast majority of electronic structure calculations carried out on metals.¹ In general, the electronic structure of a molecule in Kohn-Sham theory can be written in terms of a set of doubly occupied (for a species in a singlet state) mutually orthogonal molecular orbitals ψ_i that extend over all atoms of the molecule. The total electronic energy is then given by the sum of the doubly occupied orbital energies plus a term E_{dc} to cancel out the error due to double counting of electron-electron repulsion

$$E = 2 \sum_i \varepsilon_i + E_{dc} \quad (1.1)$$

The energy of each molecular orbital is equal to the expectation value of the Hamiltonian operator H for that orbital

$$\varepsilon_i = \varepsilon(\psi_i) = \langle \psi_i | H | \psi_i \rangle = \int d^3x \psi_i^*(x) H(x) \psi_i(x) \quad (1.2)$$

The above integral is carried out over all positions given by the vector coordinate x in three dimensional space. The Hamiltonian is given in atomic units by

$$H(x) = -\frac{1}{2} \nabla^2 + V(x) \quad (1.3)$$

In this expression for the Hamiltonian, $V(x)$ is an operator accounting for the combination of the local and nonlocal pseudopotentials, the Hartree potential, and the exchange correlation potential. These terms are described in further detail in the literature.¹⁷ To find the set of molecular orbitals representing the ground state of the molecule, the forms of these orbitals are

varied to minimize the total electronic energy of the system according to the variational principle.¹⁸

Calculations based on the Kohn-Sham introduced above are usually performed in such a way that the potential operator $V(x)$ in Equation (1.3) is consistent with the electron density $\rho(x)$ derived from the occupied molecular orbitals ψ_i , given by

$$\rho(x) = 2 \sum_i \psi_i^*(x) \psi_i(x) \quad (1.4)$$

where the sum is carried out over all doubly occupied molecular orbitals. This type of calculation is referred to as a self-consistent field (SCF) calculation. Through the potential operator $V(x)$, the Hamiltonian of such a calculation depends on the form of the occupied molecular orbitals, necessitating an iterative solution method. We can simplify the model considerably by ignoring the variation of the Hamiltonian with the form of the molecular orbitals. This is referred to as the tight binding model in solid state physics literature⁴ and the Extended Hückel model^{19,20} in theoretical chemistry literature. It is found that while these non-self-consistent calculations lead to energies that are quantitatively different from the self-consistent calculations, general qualitative features and trends are not affected.¹¹ Because of this and the much simpler model resulting from a tight binding or Extended Hückel calculation, we use this method in the remainder of this work.

While the calculations just described produce fairly accurate energies (when performed self-consistently) for a variety of systems,^{1,21} the extended nature of the molecular orbitals, as with the Bloch orbitals in metals, does not provide much insight into the bonding within the system. As an example, consider the seven occupied molecular orbitals shown in Figure 1.1 describing the ground state of ethane. These orbitals have amplitude on all atoms of the molecule and bear little resemblance to the diatomic bonding orbitals that underlie most of our chemical intuition.

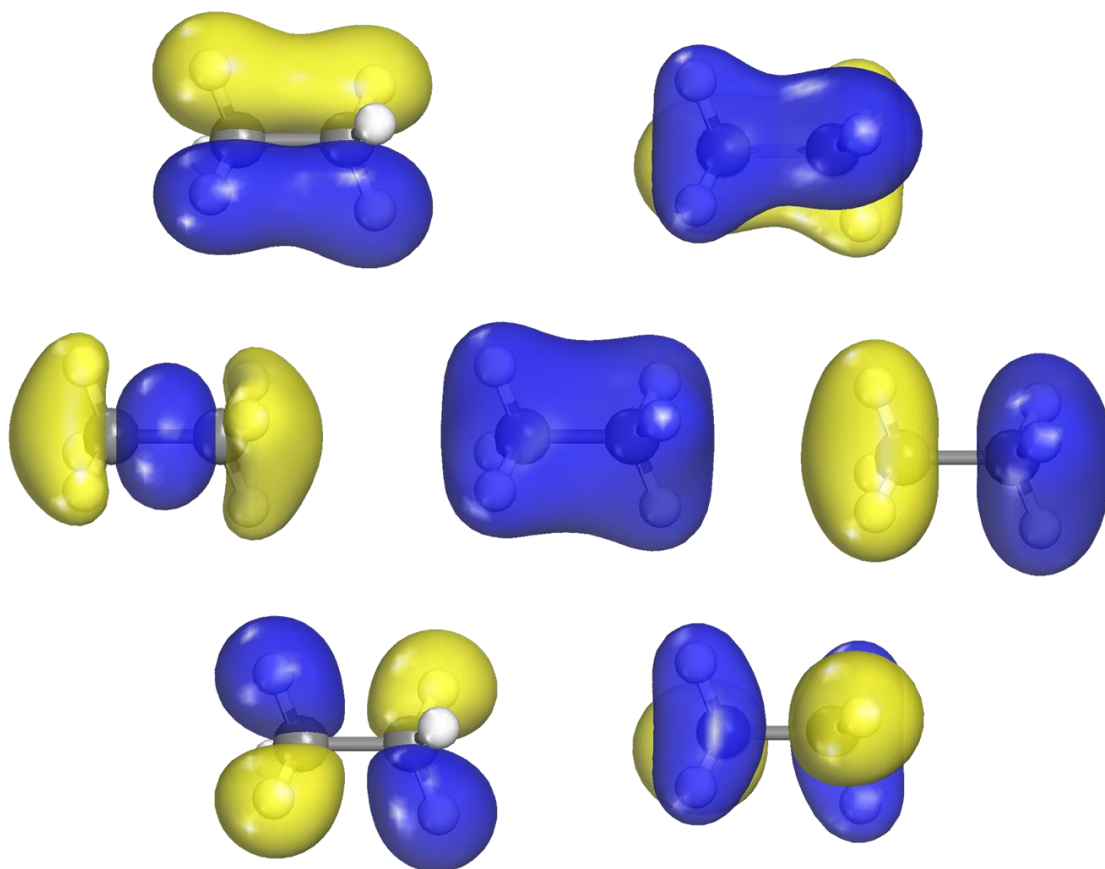


Figure 1.1 Occupied canonical molecular orbitals of ethane

In general, the set of molecular orbitals that determines the ground state electronic structure of a molecule are undetermined up to a unitary transformation that mixes the occupied orbitals with one another.²² The extended molecular orbitals shown in Figure 1.1 actually correspond to the orbitals that are eigenstates of the Hamiltonian. It is possible, using procedures in the literature,^{23,24} to obtain an equivalent set of molecular orbitals that very closely resemble the more familiar diatomic bonding orbitals. These localized molecular orbitals are shown for ethane in Figure 1.2. One can see that there are seven such orbitals in this set corresponding to the seven bonds in the molecule. Unlike the canonical molecular orbitals, these localized orbitals are concentrated on the two atoms forming the corresponding bond, although they do have small nonzero amplitude on the neighboring atoms that are not visible in the figure, often called delocalization tails,²⁵ that leads to some chemically significant effects as we will see later.

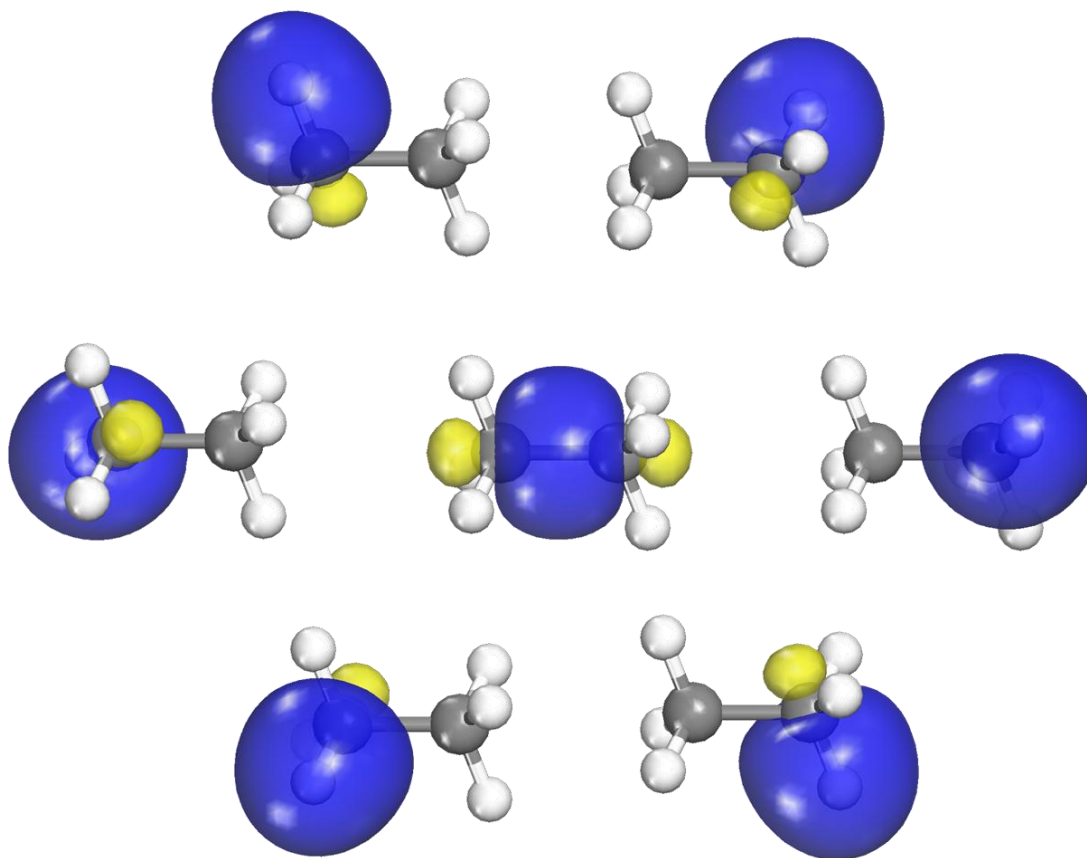


Figure 1.2 Occupied localized molecular orbitals of ethane

Another way to describe the electronic structure of a molecule in a localized form is with the use of strictly localized molecular orbitals (SLMOs) such as the natural bond orbitals that Weinhold and Landis use in their Natural Bond Orbital Theory.³ SLMOs are molecular orbitals constructed from atomic orbitals located on at most two different atoms. Every bond in a Lewis structure is associated with bonding (and antibonding) SLMO that is constructed from atomic orbitals on the two bound atoms. Each lone pair in the Lewis structure is associated with a nonbonding SLMO constructed from atomic orbitals located on the atom containing the lone pair. The natural bond orbitals (NBOs) of Weinhold and Landis^{3,26,27} are SLMOs constructed from the one electron density matrix of a full electronic structure calculation. The optimal set of natural bond orbitals is the one that most closely reproduces this density matrix. In their monograph,³ they use this method to rationalize a wide range of chemical behavior for both organic molecules and transition metal complexes in terms of localized bonding concepts.

Similar methods have been introduced by other authors,^{28–30} though the work herein is inspired mainly by the work of Weinhold and Landis.

Like the localized molecular orbitals, there is one NBO corresponding to each bond or lone pair in the molecule. The bonding NBOs (called bonding orbitals from here on) are formed from a linear combination of atomic orbitals on two bonded atoms, and unlike the localized molecular orbitals, have no amplitude on other atoms. Such an orbital corresponding to a bond between atoms A and B can be written in terms of hybrid orbitals h_A and h_B on each of the two atoms

$$\sigma_{AB} = c_A h_A + c_B h_B \quad (1.5)$$

where each hybrid is a linear combination of the atomic orbitals ϕ on the corresponding atom (A in the upper limit of the sum denotes that the sum is carried out over all atomic orbitals on atom A).

$$h_A = \sum_{\mu}^A a_{\mu} \phi_{\mu} \quad (1.6)$$

The polarization coefficients c_A and c_B determine the amplitude of the bonding orbital on each of the two hybrids and the sum of their squares must equal one so that the orbital is normalized. The squares of the polarization coefficients determine the fraction of the electron pair in the bonding orbital that resides on each of the corresponding atoms. We can get the partial charges on atoms A and B (q_{AB} and q_{BA}) induced by this bond according to

$$q_{AB} = 1 - 2 c_A^2 \quad (1.7a)$$

$$q_{BA} = 1 - 2 c_B^2 \quad (1.7b)$$

so that the total partial charge on an atom A is given by the sum of the charge given by this expression over all bonds with neighboring atoms B

$$q_A = \sum_B q_{AB} \quad (1.8)$$

The energy of the bonding orbital given by Equation (1.5) is determined by Equation (1.2) to be

$$\varepsilon_{AB} = c_A^2 \varepsilon(h_A) + c_B^2 \varepsilon(h_B) + 2 c_A c_B V_{AB} \quad (1.9)$$

where V_{AB} is the resonance integral between the two hybrids forming the bond (H is the Hamiltonian given by Equation (1.3))

$$V_{AB} = \langle h_A | H | h_B \rangle = \int d^3x h_A^*(x) H(x) h_B(x) \quad (1.10)$$

and $\varepsilon(h_A)$ and $\varepsilon(h_B)$ are the energies of the two hybrids given by Equation (1.2). If the reference state is taken to be the two separated hybrids, each containing one unpaired electron, the bond energy (positive for a stabilizing bond) associated with the doubly occupied bonding orbital is

$$\Delta\varepsilon_{AB} = - \underbrace{\overbrace{(c_A^2 - c_B^2)}^{\text{ionicity}} [\varepsilon(h_A) - \varepsilon(h_B)]}_{\text{ionic}} - \underbrace{\overbrace{2 c_A c_B}_{\text{covalency}} 2 V_{AB}}_{\text{covalent}} \quad (1.11)$$

It can be seen that the bond energy is composed of separate ionic and covalent contributions. The ionic bond energy is the difference in energy between the two hybrids weighted by the ionicity of the bond. The magnitude of the ionicity is zero for a purely covalent bond and one for a purely ionic bond, having a positive (negative) value for a bond polarized towards A (B). The covalent bond energy is equal to twice the resonance integral weighted by the covalency of the bond, which is unity for a purely covalent bond and zero for a purely ionic bond. The covalency and ionicity are related by the expression

$$\text{covalency}^2 + \text{ionicity}^2 = 1 \quad (1.12)$$

showing that as one value increases, the other decreases.

In addition to the bonding NBOs, there are also nonbonding NBOs (called nonbonding orbitals or lone pair orbitals from here on) that contain lone pairs. These orbitals are formed from a linear combination of atomic orbitals ϕ on the atom on which the lone pair resides. Such an orbital on atom A, n_A , takes the form

$$n_A = \sum_{\mu}^A a_{\mu} \phi_{\mu} \quad (1.13)$$

For an atom with an sp^3 valence shell, the number of lone pairs will be equal to $n = 4 - v$ where v is the valence of the atom.

The bond energy given in Equation (1.11) above was defined with respect to atoms containing one unpaired electron in each bonding hybrid and a pair of electrons in each nonbonding orbital. The energy of this reference state depends on the hybridization of the atoms so must be defined with respect to a reference configuration for each atom. This leads to a total binding energy for the system that is composed of one sum of bond energies for all pairs of bound atoms A and B and another sum of hybridization energies over all atoms A

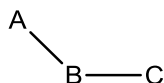
$$\Delta E = \sum_{AB} \Delta \varepsilon_{AB} + \sum_A \Delta \varepsilon_A \quad (1.14)$$

where the hybridization energy of atom A is given by a sum over the energies of all singly occupied bonding hybrids and a sum over the energies of the doubly occupied lone pairs with respect to the reference energy of the atom ε_A^0 .

$$\Delta \varepsilon_A = \varepsilon_A^0 - \sum_i \varepsilon(h_A^i) - 2 \sum_j \varepsilon(n_A^j) \quad (1.15)$$

In the method of Weinhold and Landis, the ground state electronic structure is determined by finding the set of polarization coefficients in Equation (1.5) and the hybridization coefficients in Equations (1.6) and (1.13) that lead to a one electron density matrix closest to that of the full electronic structure calculation. The NBOs determined in this way, however, are limited in their usefulness because they are generated from a full electronic structure calculation rather than determined *a priori*. This makes it difficult to determine how their forms are directly related to the structure of the molecule via the Hamiltonian. Because of this, we choose in this work to instead determine the NBOs by finding the set that minimizes the total energy in Equation (1.15) subject to the constraint that the SLMOs are mutually orthogonal so that the overall wavefunction obeys the Pauli Exclusion Principle. This method has similarities to the method Coulson and Goodwin.³¹

The condition that the set of SLMOs must be mutually orthogonal is automatically met for any two SLMOs that have no atoms in common as long as an orthogonal set of atomic orbitals is used such as the natural atomic orbitals,³² also developed by Weinhold. For two SLMOs that do have an atom in common such as σ_{AB} and σ_{BC} in the structure shown here



the orthogonality condition is met if the two hybrids on atom B are orthogonal. As a result, we can replace the orthogonality requirement for the SLMOs with a simpler requirement that the set of all bonding and nonbonding hybrids h_A and n_A on each atom A must be mutually orthogonal. As a consequence of this condition, a sum rule can be written for each atomic orbital of the form³

$$\sum_i^A (a_\mu^i)^2 = 1 \quad (1.16)$$

When applied to an atom with an sp^3 valence shell, this rule implies that the total amount of s character among all the hybrids is conserved according to

$$\sum_i^A (a_s^i)^2 = 1 \quad (1.17)$$

so that if one hybrid increases in s character, the other hybrids must decrease in s character.

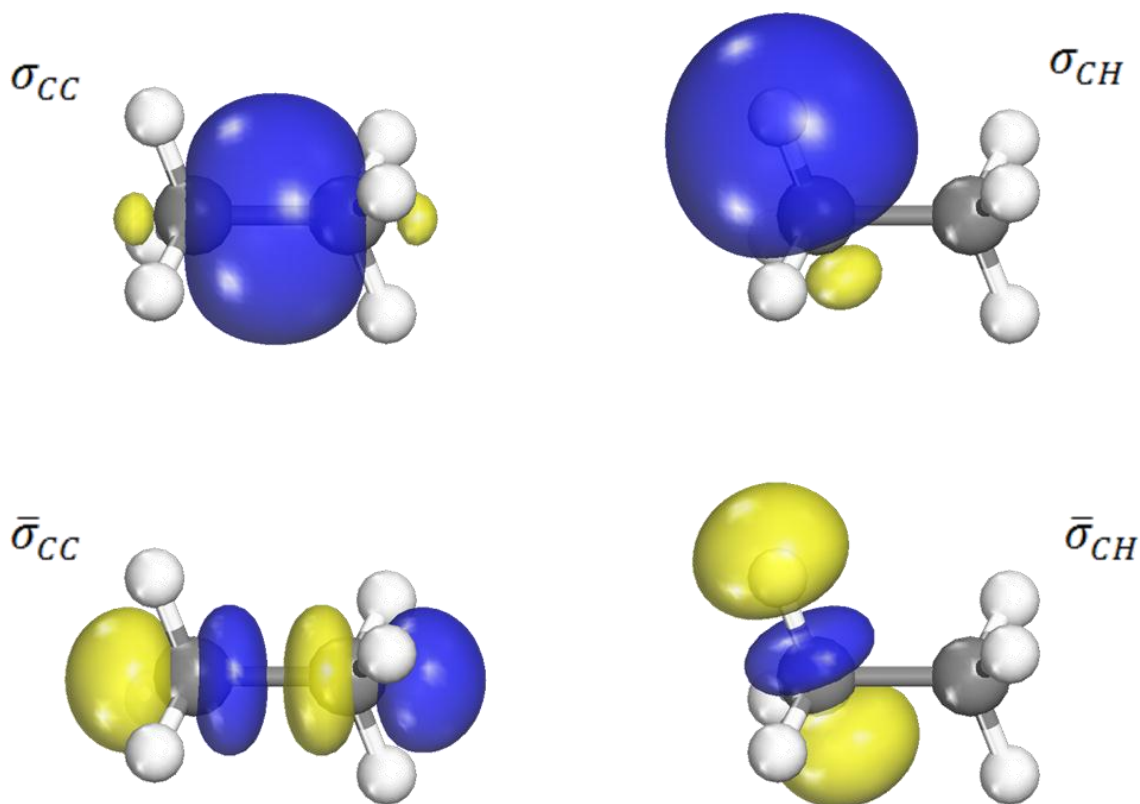


Figure 1.3 Bonding (top) and antibonding (bottom) SLMOs associated with the C-C bond and with one of the six C-H bonds in ethane

Two of the seven bonding SLMOs of ethane, the C-C bonding orbital and one of the C-H bonding orbitals, are shown in Figure 1.3, where it can be seen that they are almost identical in shape to the corresponding localized molecular orbitals from Figure 1.2. These SLMOs are built up from the atomic orbitals on carbon and hydrogen, as shown in Figure 1.4 for one of the C-H bonds. First, a hybrid h_C is constructed on the carbon atom from the carbon s orbital and a p orbital oriented towards the hydrogen atom.

$$h_C = a_s s_C + a_p p_C \quad (1.18)$$

This hybrid then combines with the hydrogen s orbital to form a bonding orbital given by

$$\sigma_{CH} = c_C h_C + c_H s_H \quad (1.19)$$

Since the C-H bond is polarized towards the more electronegative carbon atom, the magnitude of the bond on the carbon atom given by c_C^2 is equal to 0.59 and the corresponding magnitude on the hydrogen atom is 0.41, leading to a positive charge of 0.18 e⁻ on each hydrogen atom and a negative charge of 0.54 e⁻ on the carbon atoms as determined by Equation (1.8). The amount of s character in the carbon hybrid is given by a_s^2 and is equal to 0.24, very close to the value of 0.25 corresponding to an ideal sp^3 hybrid.

Likewise, the bonding orbital corresponding to the C-C bond can be written as a linear combination of hybrids h_{C1} and h_{C2} on the two carbon atoms

$$\sigma_{CC} = \frac{1}{\sqrt{2}}(h_{C1} + h_{C2}) \quad (1.20)$$

Each hybrid is a linear combination of the s orbital on the corresponding carbon atom and a p orbital oriented in the direction of the C-C bond

$$h_{C1} = a_s s_1 + a_p p_1 \quad (1.21a)$$

$$h_{C2} = a_s s_2 + a_p p_2 \quad (1.21b)$$

Since this bond is nonpolar, the magnitude of the bonding orbital on each of the two carbon atoms is equal to 0.5 (leading to the factor of $1/\sqrt{2}$ in Equation (1.20)). The amount of s character in the carbon hybrid is equal to 0.28, again very close to an ideal sp^3 composition. Note that the s compositions of the C-C hybrid and the three C-H hybrids obey the sum rule in Equation (1.16).

In addition to these bonding orbitals discussed so far, there is a corresponding set of unoccupied antibonding orbitals $\bar{\sigma}_i$ that take the form

$$\bar{\sigma}_{AB} = c_B h_A - c_A h_B \quad (1.22)$$

and are orthogonal to the bonding orbitals. There are seven of these antibonding orbitals in ethane, one corresponding to each of the bonds in the molecule. The process of building up the antibonding orbitals is shown in Figure 1.4 for one of the C-H bonds. Two of these orbitals are shown in Figure 1.3 – for the C-C bond and for one of the C-H bonds. The energy of this antibonding orbital is equal to

$$\bar{\epsilon}_{AB} = c_B^2 \epsilon(h_A) + c_A^2 \epsilon(h_B) - 2 c_A c_B V_{AB} \quad (1.23)$$

where V_{AB} is the resonance integral between the two hybrids given by Equation (1.10).

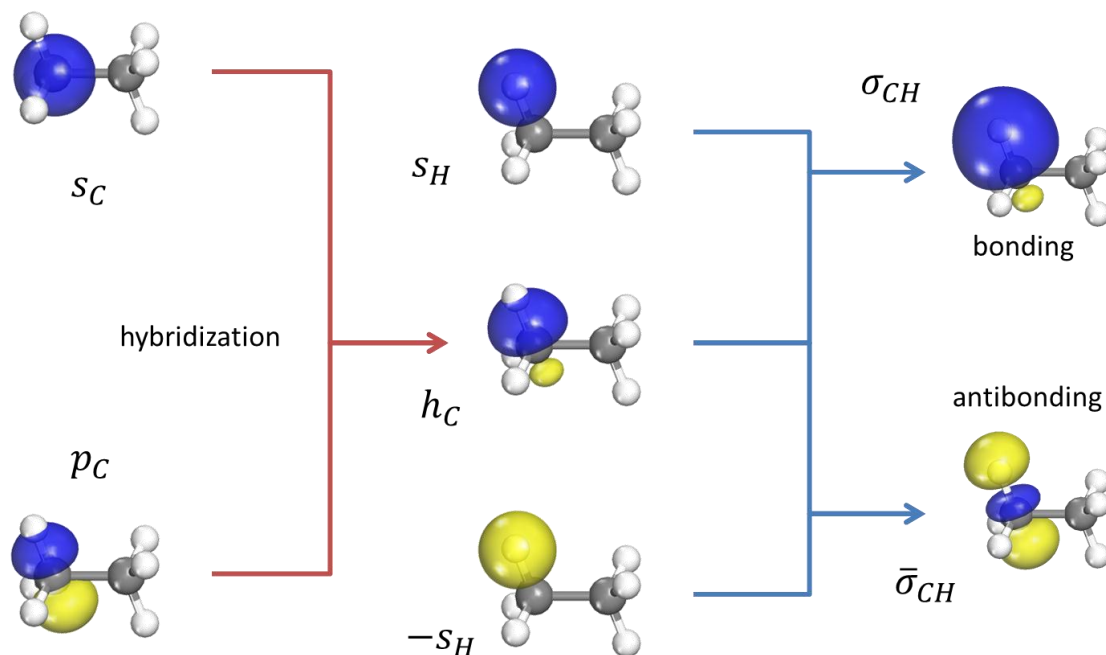


Figure 1.4 The construction of SLMOs for one of the C-H bonds in ethane begins by first forming an sp^n hybrid h_C on the carbon atom according to Equation (2.6). This hybrid then combines with the hydrogen s orbital to form bonding (σ_{CH}) and antibonding ($\bar{\sigma}_{CH}$) orbitals according to Equation (1.60).

Because the bonding orbitals were artificially constrained to have amplitude on only two atoms, the electronic structure derived from them is not the true ground state of the system. The energy of the molecule can be further reduced by allowing the bonding orbitals to partially mix with the antibonding orbitals,³ as shown in Figure 1.5 for two such C-H orbitals on ethane, labeled σ_1 and $\bar{\sigma}_2$.

$$\sigma_1 = c_C h_{C1} + c_H s_{H1} \quad (1.24a)$$

$$\bar{\sigma}_2 = c_H h_{C2} - c_C s_{H2} \quad (1.24b)$$

This interaction results in a modified bonding orbital given by

$$\sigma_1 \rightarrow \sigma_1 + \alpha \bar{\sigma}_2 \quad (1.25)$$

which has a lower energy than the zero order bonding orbital. Although the antibonding orbital is higher in energy than the bonding orbital, the decrease in kinetic energy of the electron pair gained by delocalizing into the antibonding orbital more than compensates for this. The amount of admixture represented by α can be obtained from perturbation theory according to

$$\alpha = -\frac{\langle \bar{\sigma}_2 | H | \sigma_1 \rangle}{\varepsilon(\bar{\sigma}_2) - \varepsilon(\sigma_1)} \quad (1.26)$$

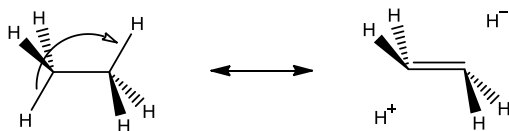
where the numerator contains the resonance integral between the two orbitals

$$\langle \bar{\sigma}_2 | H | \sigma_1 \rangle = \int d^3x \bar{\sigma}_2(x) H(x) \sigma_1(x) \quad (1.27)$$

where H is the Hamiltonian operator given by Equation (1.3), and the denominator contains the difference in energies of the two orbitals given by Equation (1.2). The resonance integral Since the resonance integral is only appreciable if two atoms of the bonding and antibonding orbitals are close, these interactions are restricted to orbitals on bonds that have a vicinal relationship. To second order in the resonance integral, the decrease in energy of the σ_{CH} orbital is equal to

$$\Delta\varepsilon(\sigma_1) = -\frac{|\langle \bar{\sigma}_2 | H | \sigma_1 \rangle|^2}{\varepsilon(\bar{\sigma}_2) - \varepsilon(\sigma_1)} \quad (1.28)$$

This decrease in energy comes from the delocalization of the electrons in the bonding orbital into the antibonding orbital, resulting in a modified bonding orbital that has amplitude on more than two atoms as shown in Figure 1.5 and is the origin of the delocalization tails in the localized molecular orbitals discussed earlier. This delocalization energy offsets the energy required to promote an electron pair from the bonding orbital to the higher energy antibonding orbital. Weinhold and Landis refer to this mechanism as a donor-acceptor conjugative interaction in which an electron pair is donated from the occupied bonding orbital into the unoccupied antibonding orbital.³ This has the effect of weakening the two original bonds and strengthening the bond between the two vicinal atoms, described by the admixture of the following resonance structure



in which the two C-H bonds are heterolytically broken forming a C-C double bond.

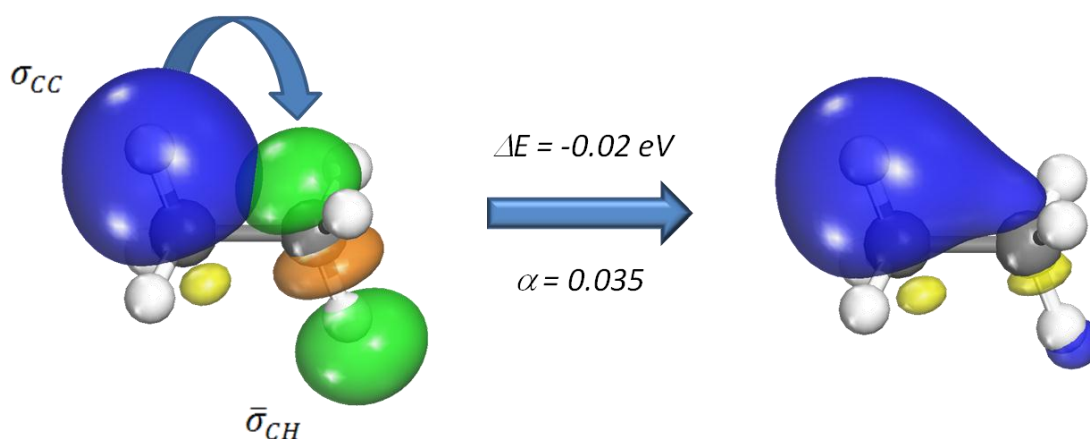


Figure 1.5 A C-H bonding orbital (blue/yellow) of ethane can mix with a C-H antibonding orbital (green/orange) forming a perturbed bonding orbital with lower energy than the original (degree of mixing is exaggerated so it is visible in the orbital isosurface). This hyperconjugative interaction can be described as donation of an electron pair from the bonding orbital into the antibonding orbital.

If we ignore any resonance integrals between atomic orbitals on non-bonded atoms, the integral in Equation (1.27) between the bonding and antibonding orbitals is proportional to the integral between the two hybrids on the carbon atoms

$$\langle \bar{\sigma}_2 | H | \sigma_1 \rangle = c_C^1 c_H^2 \langle h_C^2 | H | h_C^1 \rangle \quad (1.29)$$

If we write each of the hybrids in terms of the constituent atomic orbitals as in Equation (1.10), then the remaining resonance integral can be written as a sum of Slater-Koster integrals between the atomic orbitals, shown graphically in Figure 1.6

$$\langle h_C^2 | H | h_C^1 \rangle = \left[\underbrace{a_s^1 a_s^2 V_{ss\sigma} + a_s^1 a_{p_z}^2 V_{sp\sigma} + a_{p_z}^1 a_s^2 V_{ps\sigma} + a_{p_z}^1 a_{p_z}^2 V_{pp\sigma}}_{\sigma \text{ interactions}} + \underbrace{a_{p_x}^1 a_{p_x}^2 V_{pp\pi} + a_{p_y}^1 a_{p_y}^2 V_{pp\pi}}_{\pi \text{ interactions}} \right] \quad (1.30)$$

The first four terms involve σ interactions between the s orbitals and the p orbitals oriented along the bond axis (along the z axis), while the last two terms involve π interactions between the p orbitals perpendicular to the bond axis. The first four terms can actually be reduced to two terms by taking appropriate combinations of the s and p_z orbitals to form the hybrids h_{σ_+} and h_{σ_-} shown in Figure 1.6. The two σ_+ hybrids point inwards along the bond axis while the σ_- hybrids point outwards along the bond axis. The σ_+ hybrid on one atom only has a nonzero resonance integral V_{σ_+} with the σ_+ hybrid on the other atom, while the same is true for the σ_- hybrids with a resonance integral V_{σ_-} - thus the σ_+ hybrid on one atom does not interact with the σ_- hybrid on the other atom. These two sets of hybrids, along with the two remaining sets of p orbitals, constitute a set of characteristic interactions between the two carbon atoms. The resonance integral between the two hybrids in Equation (1.30) can be written in terms of the three associated characteristic integrals.

$$\langle h_C^2 | H | h_C^1 \rangle = \left[\begin{aligned} &\langle h_C^2 | h_{\sigma_+}^2 \rangle \langle h_{\sigma_+}^1 | h_C^1 \rangle V_{\sigma_+} + \langle h_C^2 | h_{\sigma_-}^2 \rangle \langle h_{\sigma_-}^1 | h_C^1 \rangle V_{\sigma_-} \\ &+ [\langle h_C^2 | p_x^2 \rangle \langle p_x^1 | h_C^1 \rangle + \langle h_C^2 | p_y^2 \rangle \langle p_y^1 | h_C^1 \rangle] V_{\pi} \end{aligned} \right] \quad (1.31)$$

Since the σ_+ hybrids point inward along the bond axis, the associated resonance integral will be much larger than the resonance integral for the σ_- hybrids, since they point outwards along the bond axis. This can be seen in the values for the C-C bond in ethane where $V_{\sigma_+} = -9.97 \text{ eV}$ and $V_{\sigma_-} = -0.30 \text{ eV}$. The value of the resonance integral for the π interactions typically lies between these two - in ethane $V_{\pi} = -2.65 \text{ eV}$. In addition to the values of the characteristic integrals, it is also important to consider overlap integrals between the hybrids participating in the conjugative interaction (h_C^2, h_C^1) and the hybrids associated with the characteristic interactions ($h_{\sigma_+}, h_{\sigma_-}, p_x, p_y$), which we will refer to as the overlap of the hybrid with the characteristic interaction. For ethane, the hybrids h_C^1 and h_C^2 have very little overlap with the σ_+ interaction

$(\langle h_C^2 | h_{\sigma_+}^2 \rangle = \langle h_{\sigma_+}^1 | h_C^1 \rangle = 0.05)$ so that this interaction is only present at 0.3% of its full value and only contributes -0.03 eV to the resonance integral in Equation (1.31). This makes sense because the σ_+ hybrid is very close in composition to the hybrids forming the C-C bond, which themselves are orthogonal to the hybrids forming the C-H bonds. One can say that the σ_+ interaction is already saturated by the C-C bond in the zero order electronic structure so it is not available to participate in conjugative interactions. In contrast, the σ_- interaction is present at 33% of its full strength, but only contributes -0.10 eV to the resonance integral since V_{σ_-} is so small. The two π interactions account for almost all of the resonance integral, being present at 67% of their full value and contributing -1.76 eV to the total value of the resonance integral of -1.92 eV. This means that the conjugative interaction between the two C-H bonds is almost entirely due to π interactions between the two carbon atoms and the σ interactions can be ignored to a good approximation. The sum of all eighteen conjugative interactions involving charge transfer across the C-C bond leads to an additional stabilization of the molecule by 0.60 eV.

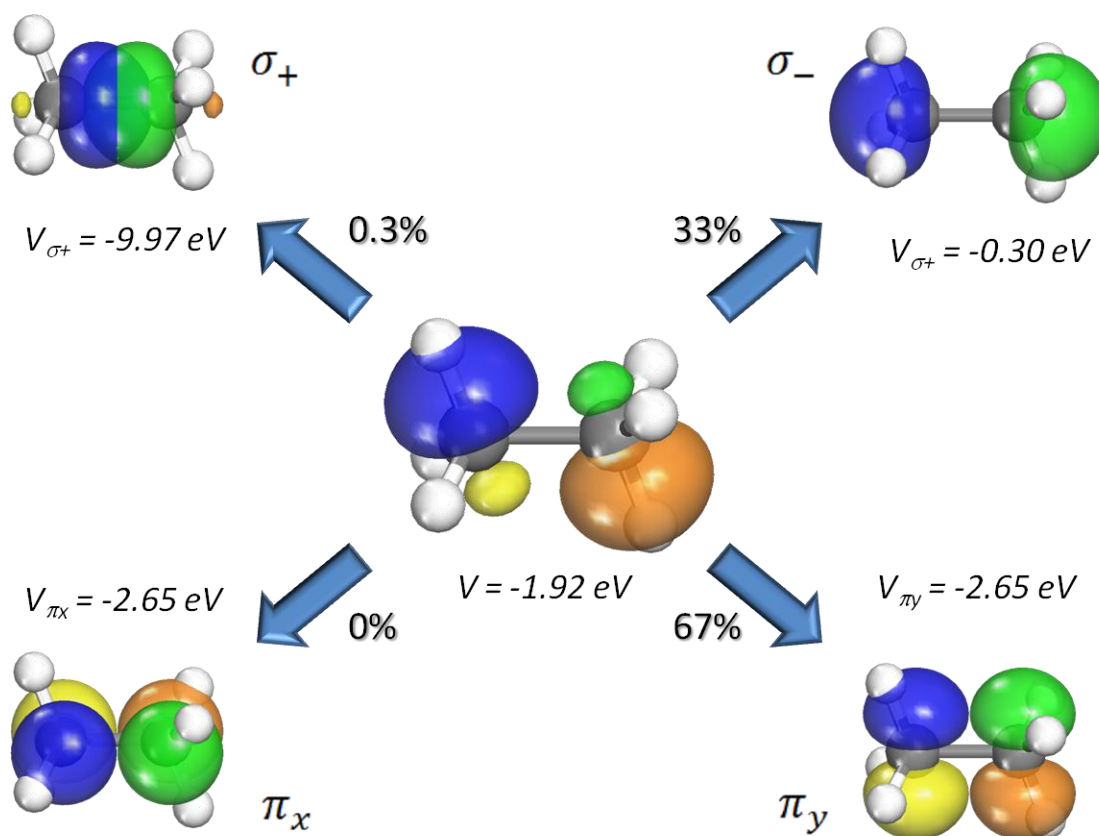


Figure 1.6 The resonance integral between the bonding and antibonding orbitals in Figure 1.5 is approximated by the integral between the two corresponding carbon hybrids. The resonance integral between these two hybrids can be decomposed into four characteristic interactions – two with σ symmetry (top) and two with π symmetry (bottom).

Looking back at Equation (1.26) that determines the degree of mixing between the bonding and antibonding orbitals participating in a conjugative interaction, one can see that this value is the ratio of the resonance integral to the difference in energy between the two orbitals. Taking the energies of the bonding and antibonding orbitals from Equations (1.9) and (1.23) for two identical nonpolar bonds, this energy difference is equal to twice the value of the resonance integral between the two hybrids forming the bond given in Equation (1.10), so for the interaction in ethane, it is approximately equal to

$$\varepsilon(\bar{\sigma}_2) - \varepsilon(\sigma_1) \cong 2 \langle h_c | H | s_H \rangle \quad (1.32)$$

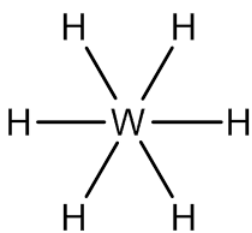
The resonance integral in this equation is equal to -8.89 eV, significantly greater than the resonance integral in the numerator of Equation (1.26) (-0.94 eV) that was mainly due to the π interaction between the two carbon atoms. This leads to a very small amount of the antibonding orbital being mixed with the bonding orbital with $\alpha = 0.053$ and the stabilization energy from Equation (1.28) is only 0.05 eV. This is due to the fact that the σ_+ interaction between the two carbon atoms is nearly saturated in the zero order electronic structure due to the C-C bond. The remaining π interactions that are available are much weaker than the strong σ interaction in the C-H bonds. Therefore, it is very unfavorable to weaken the strong C-H bonds to form a relatively weak π bond between the two carbon atoms, leading to only weak conjugative interactions.

1.2 Local bonding in transition metal complexes

Transition metal complexes form a natural bridge between molecules and metal crystals. For this reason, we would first like to look at the SLMO description of transition metal complexes before applying it to metallic systems. We will see that the SLMOs of these species have many similarities to the SLMOs of molecular species, with two main differences. First, the valence shell of a transition metal atoms consists of one s orbital and five d orbitals while the valence shell of the $2p$ atoms, which are the primary constituents of molecular species, consists of one s orbital and three p orbitals. This leads to several important differences in hybridization and geometric structure.^{3,33,34} The other difference is that, while conjugation involving σ bonds (hyperconjugation) gave only a small correction to the zero order structure of molecular species, it leads to a much greater contribution in most common transition metal complexes due to hypervalency of the metal atom. Both of these characteristics are present in metallic systems, so it is instructive to first examine them in the simpler transition metal complexes.

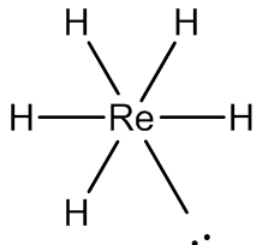
As already mentioned, the transition metal atoms forms bonds using a valence s orbital and five valence d orbitals. While historically, the p orbitals have been included in the valence space of

transition metal atoms, more recent computational studies show that they are too high in energy to participate in bonding and remain mostly unoccupied.³⁵ Utilizing the set of one *s* orbital and five *d* orbitals for each transition metal atom, it can be predicted that these elements should follow a twelve-electron rule just as the main group elements follow an eight electron rule.^{3,33,34} Figure 1.7 shows Lewis diagrams for the normal-valent (those that can satisfy the twelve-electron rule by covalent bonding) 5*d* transition metals W to Au. It is seen that W has six unpaired electrons and can thus form six covalent bonds, giving it a valence of six. The additional electrons added from Re to Au go into lone pairs with entirely *d* character so that the valence decreases from six for W to one for Au. At the same time, the ideal composition of the hybrids changes from sd^5 for W to sd^0 for Au as *d* orbitals are taken away to house the increasing number of lone pairs.



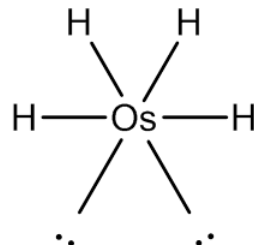
$$v = 6$$

$$n = 0$$



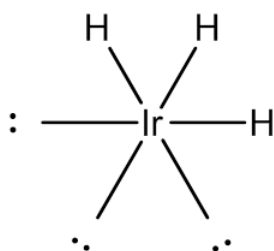
$$v = 5$$

$$n = 1$$



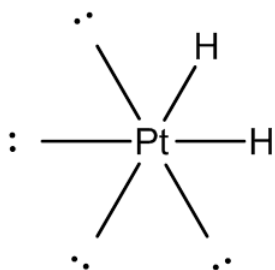
$$v = 4$$

$$n = 2$$



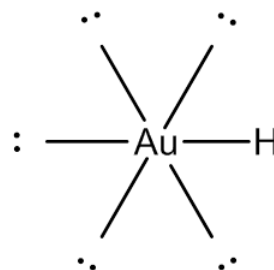
$$v = 3$$

$$n = 3$$



$$v = 2$$

$$n = 4$$



$$v = 1$$

$$n = 5$$

Figure 1.7 Lewis dot structures for the normal valent 5d transition metal atoms based on the 12 electron rule. Hydrogen is used to represent any monovalent ligand. Valence (v) decreases from six to one moving right from W to Au while number of lone pairs (n) increases from zero to five. Adapted from Weinhold and Landis³

The valences for the transition metal atoms shown in Figure 1.7 seem to be at odds with the structures that are actually found in nature. For example, Pt would be predicted to form PtCl_2 molecules, since it is divalent, while it is known that this compound dissolves in aqueous solution as the square planar PtCl_4^{2-} by combining with two Cl^- ions. Traditionally, it was assumed that the Pt atom achieves this configuration by forming four equivalent sdp^2 hybrids.³⁶ Weinhold and Landis show that this can alternately be achieved without including the metal p orbitals by using three-center/four-electron hyperbonds.³ For PtCl_4^{2-} , there are two such hyperbonds connecting opposing pairs of Cl ligands as shown in Figure 1.8. The two hyperbonds ω_x and ω_y are formed from sd^n hybrids h_{Pt}^x and h_{Pt}^y on the Pt atom and sp^n hybrids

h_{Cl}^x and h_{Cl}^y orbitals on the Cl ligands as shown in the figure. The two Pt hybrids have sd^1 composition, with the d component derived from the $d_{x^2-y^2}$ orbital, which lies in the molecular plane. As required for all the molecular orbitals to be mutually orthogonal, the two Pt hybrids h_{Pt}^x and h_{Pt}^y are orthogonal to each other. Each set of three orbitals combines to form a filled bonding orbital, a filled nonbonding orbital, and an empty antibonding orbital, also shown in the figure. Thus the approximate electronic structure of this complex can be described as two pairs of electrons occupying each of the two hyperbonds composed of Pt sd^1 hybrids with the other four lone pairs on Pt occupying nonbonding d orbitals.

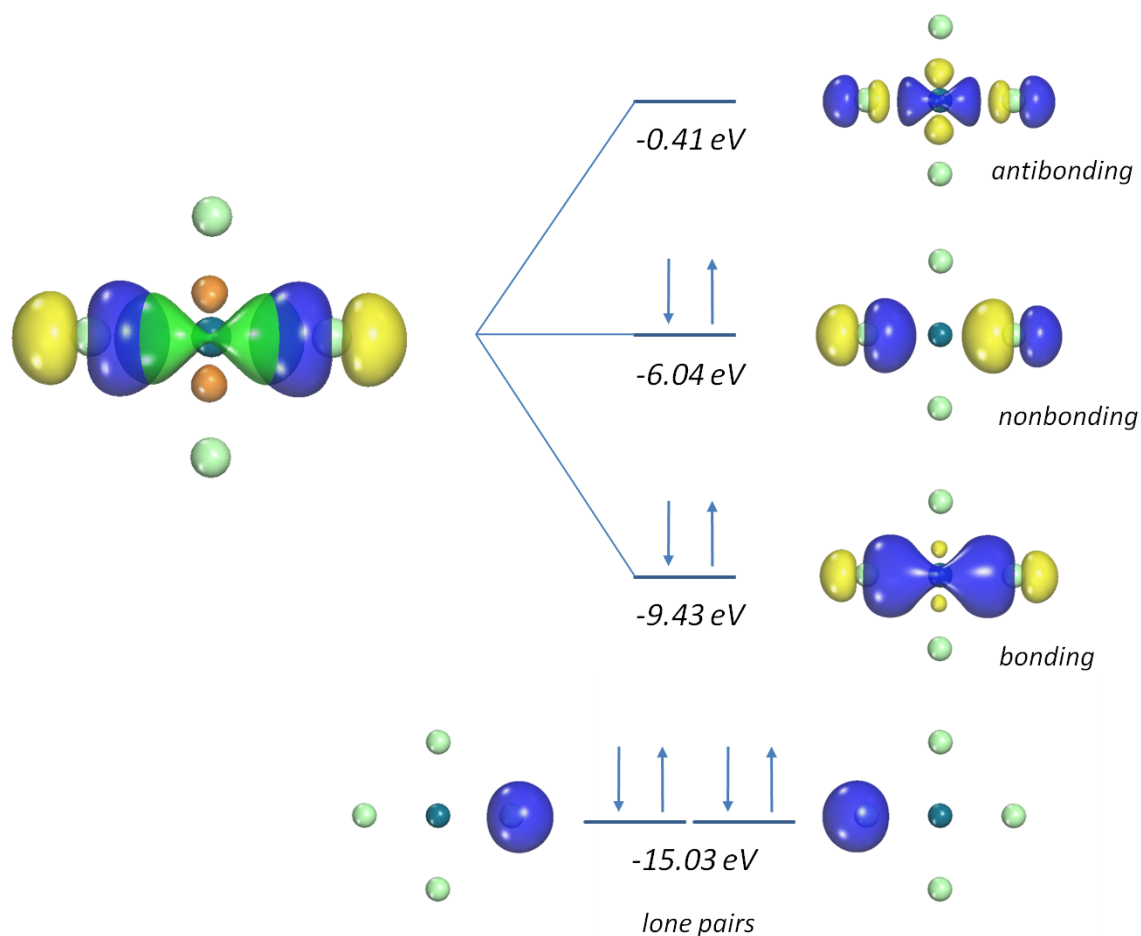
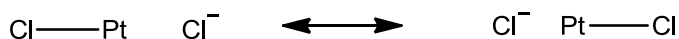
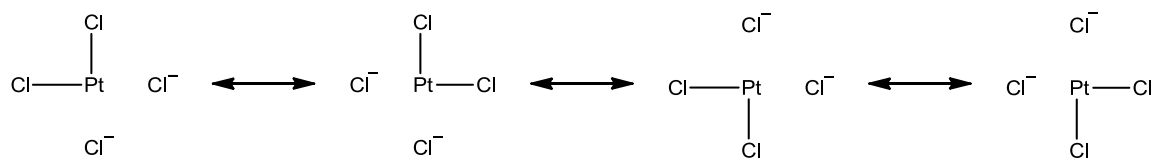


Figure 1.8 An sd hybrid on the Pt atom (green/orange) in PtCl_4^{2-} mixes with the two sp^n hybrids (blue/yellow) on the Cl atoms to form three orbitals that make up a four electron / three center hyperbond. The bonding and nonbonding orbitals are doubly occupied while the antibonding orbital is unoccupied. Also shown is an additional set of sp^n orbitals on the Cl atoms that contain lone pairs but do not participate in the hyperbond.

Although the hyperbonds allow us to describe the electronic structure in transition metal complexes, they do so at the price of including three center bonds in addition to the more familiar two center bonds. Actually, each hyperbond can be described as a resonance between two structures³



Each of these structures consists of a two-center bond between the Pt atom and the Cl ligand with the other Cl ligand along the bond axis existing as an unbound anion. For PtCl_4^{2-} , then, there are in total four resonance structures



In each of these structures, the Pt atom forms bonds with two adjacent Cl atoms while the other two Cl atoms are present as Cl^- anions. Since these four resonance structures are equivalent, we can take any one of them to form a zero order model of the electronic structure built from only two-center bonding orbitals and one-center lone pairs. One of these structures, shown in Figure 1.9, has four of the eight electrons from the two hyperbonds in two bonding orbitals σ_x and σ_y , which have the compositions

$$\sigma_x = c_{Pt}h_{Pt}^x + c_{Cl}h_{Cl}^x \quad (1.33a)$$

$$\sigma_y = c_{Pt}h_{Pt}^y + c_{Cl}h_{Cl}^y \quad (1.33b)$$

The other four electrons from the hyperbonds go into nonbonding orbitals on the Cl^- anions on the x and y axes, respectively.

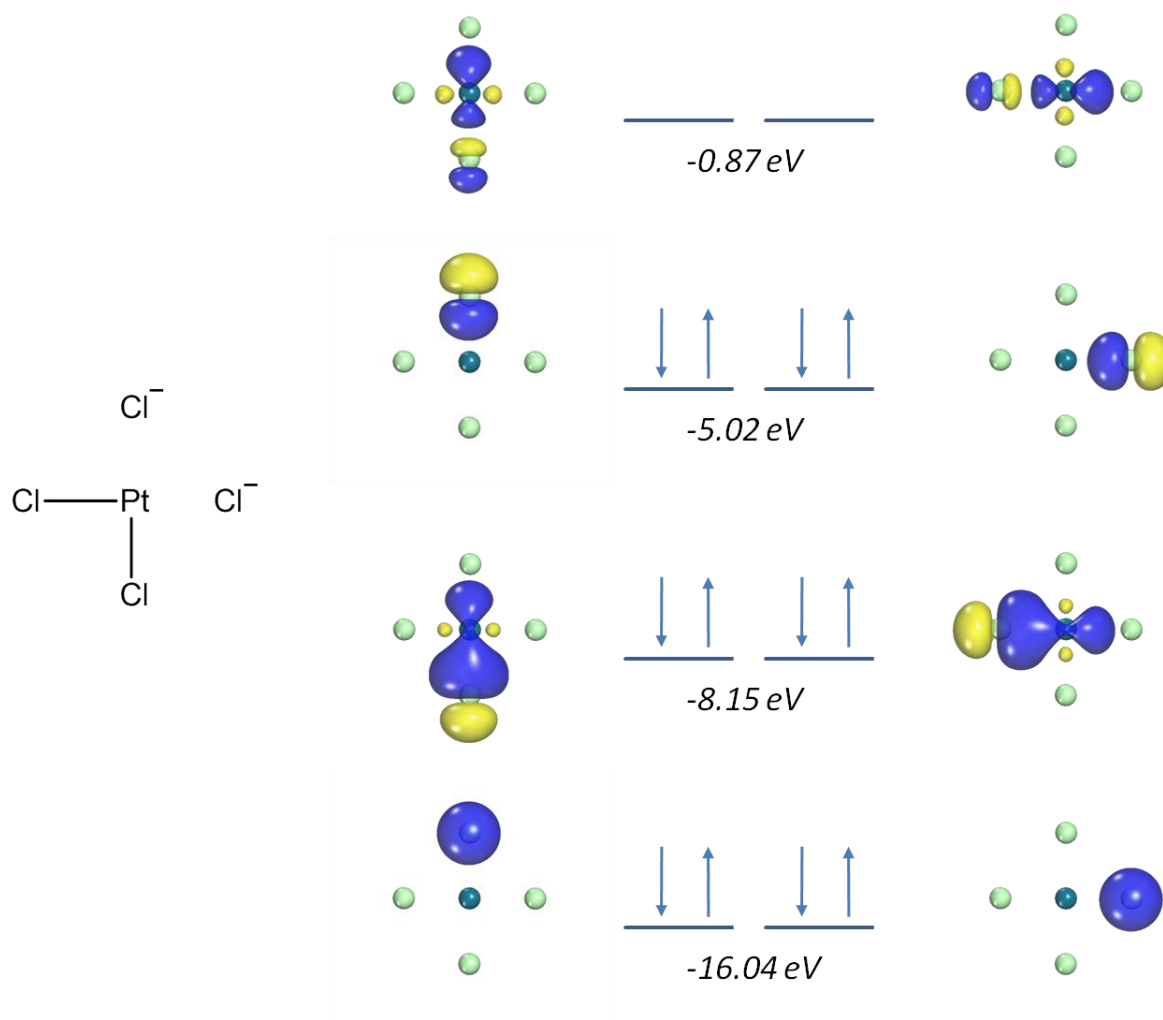


Figure 1.9 Zero order Electronic structure of PtCl_4^{2-} associated with one of the four resonance structures without use of hyperbonds. Two electron pairs go into each set of Pt-Cl bonding orbitals, Cl^- s orbitals, and Cl^- p orbitals. There are also two unoccupied Pt-Cl antibonding orbitals.

The zero-order binding energy from Equation (1.14) of this structure (8.47 eV) is significantly weaker than the zero-order binding energy of the structure composed of hyperbonds (13.67 eV). As it turns out, the higher energy of this structure is offset by stronger stabilization due to conjugation, since in the end, the exact ground state energies for these two representations must be the same. The energy of the zero-order electronic structure can be reduced by considering donation of electrons from filled Cl^- lone pairs into empty Pt-Cl antibonding orbitals. The electrons in the s or p orbital on one of the Cl^- can donate into either of the two Pt-Cl

antibonding orbitals leading to four unique conjugative interactions shown in Figure 1.10. The first two interactions (a_s and a_p) involve donation into a Pt-Cl antibonding orbital in a trans orientation to the Cl^- while the other two interactions (b_s and b_p) involve donation into an antibonding orbital in a cis orientation to the Cl^- . These antibonding orbitals have the form

$$\bar{\sigma}_x = c_{\text{Cl}} h_{\text{Pt}}^x - c_{\text{Pt}} h_{\text{Cl}}^x \quad (1.34a)$$

$$\bar{\sigma}_y = c_{\text{Cl}} h_{\text{Pt}}^y - c_{\text{Pt}} h_{\text{Cl}}^y \quad (1.34b)$$

and were shown in Figure 1.9. The two trans interactions a_s and a_p are particularly strong, each stabilizing the molecule by 0.81 eV and 2.19 eV, respectively, much stronger than the interactions present in ethane, as well as the cis interactions b_s and b_p which stabilize the molecule by less than 0.02 eV each. The interactions involving donation from the Cl^- p orbitals are significantly stronger than those involving the s orbitals because the s orbital is much lower in energy and is thus a weaker donor, as can be seen in Figure 1.9. One set of the strong interactions (a_s and a_p) is associated with each of the two formal hyperbonds, accounting for the large difference in zero order binding energy between the structure composed of hyperbonds and the structure that is not. The stabilization calculated using perturbation theory is 6.01 eV, somewhat larger than the actual difference in zero order binding energies of 5.18 eV. This is expected since second order perturbation theory tends to overestimate the stabilization energy when the interactions are particularly strong. If one were to go to higher orders in perturbation theory, this error should eventually vanish.

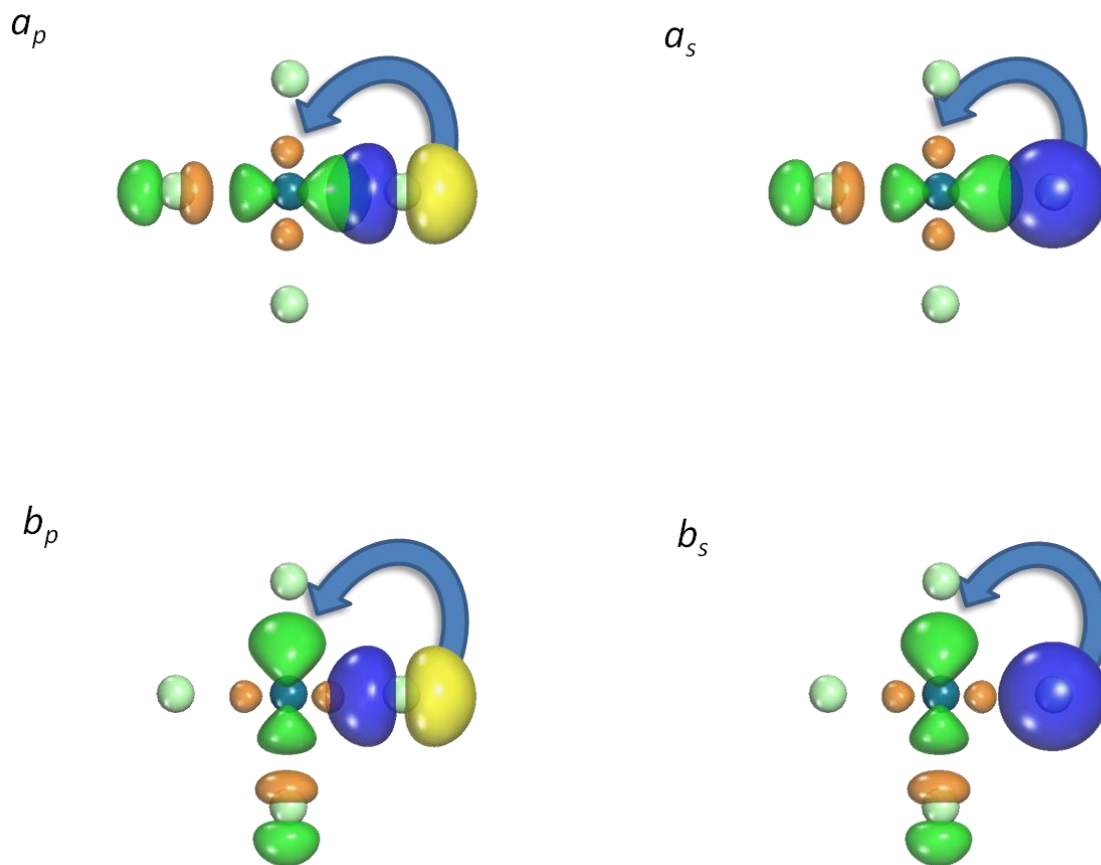


Figure 1.10 Four of the eight conjugative interactions associated with the zero order electronic structure in Figure 1.9. Two involve donation from a Cl^- p orbital into a Pt-Cl antibonding orbital oriented either trans (a_p) or cis (b_p), while the other two involve donation from a Cl^- s orbital (a_s and b_s). The two trans interactions are very strong and contribute significantly to the stability of the molecule.

To understand why these two trans interactions are so strong, we separate the interaction between the Pt and Cl^- into a set of characteristic interactions as we did for the C-C interaction in ethane in the previous section. Because the Pt atom contains an sd^5 valence shell, these interactions will be different from those between the two sp^3 carbon atoms in ethane. As with ethane, there are four such interactions as shown in Figure 1.11, two having σ symmetry and two having π symmetry. The two π interactions are between the d_{xz} and d_{yz} orbitals on Pt (with the bond oriented along the z axis) and the p_x and p_y orbitals on Cl^- , respectively, and have resonance integrals of -0.90 eV and -0.84 eV. The two σ interactions are between two sd^n

hybrids on Pt, $h_{\sigma+}^{Pt}$ and $h_{\sigma-}^{Pt}$, and two sp^n hybrids on Cl^- , $h_{\sigma+}^{Cl}$ and $h_{\sigma-}^{Cl}$. The two σ hybrids on Cl^- are similar to those on the carbons atoms of ethane, however, the hybrids on Pt have quite different shapes as shown in Figure 1.11. The σ_+ hybrid is concentrated along the axis between the Pt and Cl^- while the σ_- hybrid is concentrated in a ring around the Pt atom in the xy plane. As with ethane, the σ_+ interaction is stronger than both the π interactions and the σ_- interaction, having a resonance integral of -4.20 eV, while the σ_- interaction is weaker than all the other interactions, having a resonance integral of -0.25 eV.

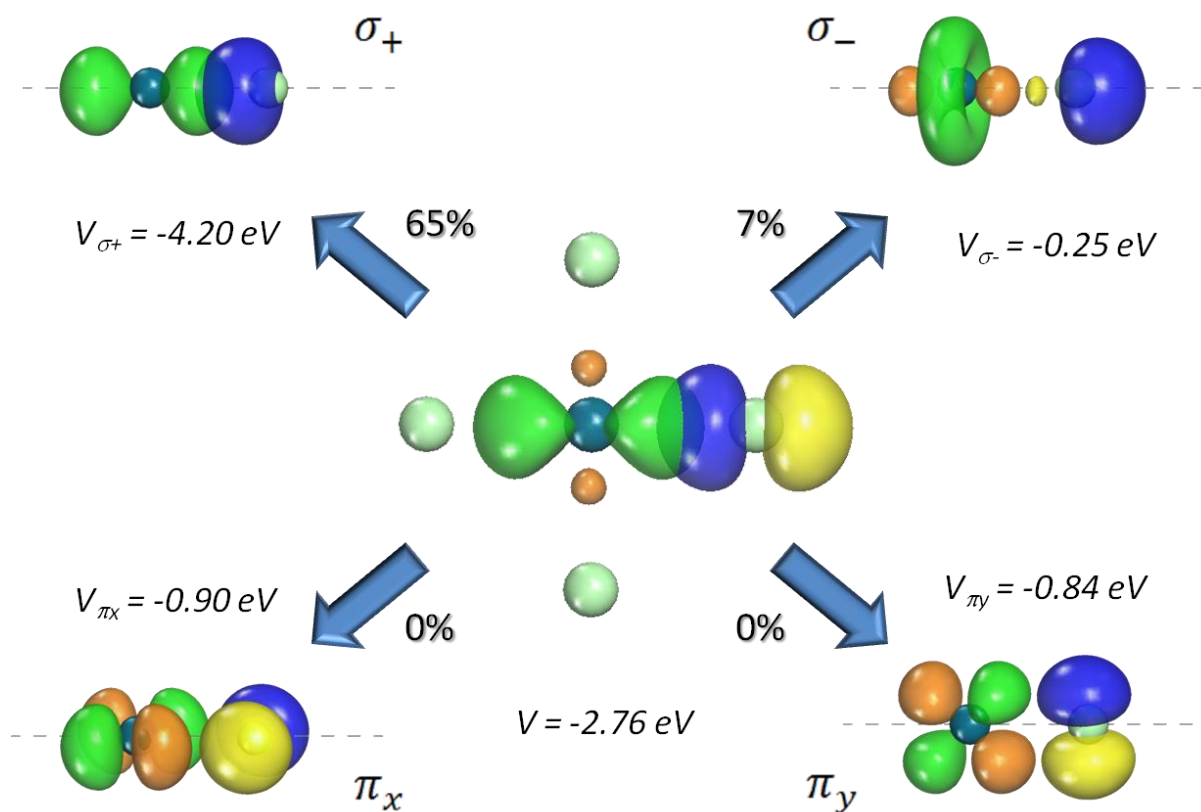


Figure 1.11 As with ethane in Figure 1.6, the resonance integral between the lone pair and antibonding orbital of interaction a_p in Figure 1.10 is approximated by the integral between the Pt sd hybrid and the Cl^- p orbital. The resonance integral between these two hybrids can be decomposed into two characteristic interactions with σ symmetry (top). For a generalized interaction between an sd^n hybrid and an sp^n hybrid, there also exist two characteristic interactions with π symmetry (bottom). A similar decomposition applies to the interaction in a_s .

The strong trans conjugative interaction between the Pt and Cl^- atoms (consider the pair along the x axis) is due to donation from the p_x orbital on Cl^- into the Pt-Cl antibonding orbital $\bar{\sigma}_x$. The overlap of the Pt hybrid h_{Pt}^x forming the antibonding orbital with the σ_+ interaction is 0.995, a very high value compared to the almost negligible value for ethane. The overlap of the Cl^- p_x orbital with the σ_+ interactions is also high, having a value of 0.66, so altogether the σ_+ interaction is present at 65% of its maximum strength so that the associated resonance integral between the Cl^- p_x orbital and the Pt h_{Pt}^x orbital is -2.73 eV. Why is this interaction so strong while the same interaction was negligible for ethane? The difference is that in ethane, the σ_+ interaction was already saturated by the C-C bond present in the zero order structure, while in PtCl_4^{2-} , there is no bond at all between the Pt and Cl^- to limit the strength of the conjugative interactions. This suggests a concept that will be useful later on when we discuss transition metal crystals – *the stronger the zero-order bond is between two atoms, the less potential there is for conjugative interactions between these two atoms.*

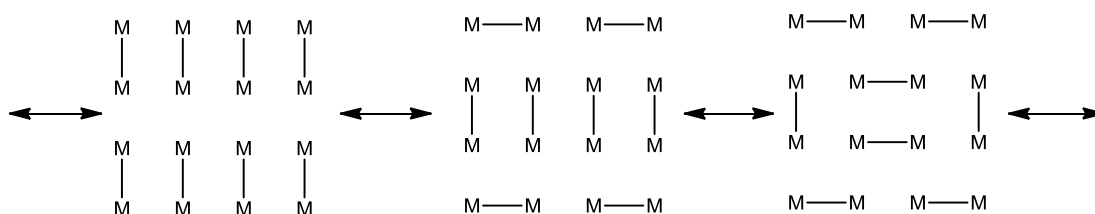
Unlike the trans conjugative interaction, the cis interactions b_x and b_y in Figure 1.10 are much weaker. Considering the interaction between the Pt and Cl^- that lies along the x axis, it involves donation from the Cl^- p_x orbital (or s orbital) into the $\bar{\sigma}_y$ Pt-Cl antibonding orbital. The projection of the h_{Pt}^y hybrid forming the $\bar{\sigma}_y$ orbital on the σ_+ interaction is only 0.10, much lower than the projection of these orbitals in a trans orientation. This is not surprising since the $h_{\sigma_+}^{Pt}$ hybrid is similar in shape to the h_{Pt}^x hybrid in the other Pt-Cl bond. Since the h_{Pt}^x hybrid is orthogonal to the h_{Pt}^y orbital in the σ_y acceptor orbital it is expected that the h_{Pt}^y would have very little overlap with the $h_{\sigma_+}^{Pt}$ orbital.

1.3 Application of local bonding formalism to metallic systems

Unlike transition metal complexes, in which the ligands are free to adopt a coordination structure consistent with the hybridization of the metal atom, the ligands of a metal atom in a transition metal crystal are constrained by the symmetry of the crystal lattice. As will be seen shortly, this leads to significant complications when attempting to describe the zero order electronic structure

of these systems in terms of SLMOs, which we overcome by the introduction of fractional bonds and fractional orbitals.

Most of the catalytically active late transition metals (groups VII – XI) adopt an fcc or hcp close packed structure in which each metal atom in the bulk is coordinated by twelve other metal atoms. Since the valences of these elements according to the twelve electron rule range from one to five, none of these elements can accommodate twelve ligands using classical bonding concepts, even when using hyperbonds. One way to overcome this would be to describe the bonding using multiple resonance structures such as



In a large crystal, however, this requires an intractable number of resonance structures in order to describe the extensive hypervalency that is present. For example, the coinage metal atoms have only one unpaired *s* electron that can be used to form covalent bonds, but each atom has a coordination of twelve in the fcc crystal structure – this would require on the order of 12^N resonance structures (where *N* is the number of atoms in the lattice). Furthermore, these resonance structures are interconnected and thus cannot be separated into smaller subsystems. An attempt by Pauling to apply the valence bond model to metallic systems never achieved widespread use due to these complications.³⁷

An alternative to considering all possible resonance structures in a transition metal crystal is to choose only one of them to form a zero order electronic structure, much as we did when choosing one of the two resonance structures to describe a hyperbond in transition metal complexes. This approach has problems of its own, however, even if one is not bothered by the fact that this electronic structure does not conform to the symmetry of the crystal lattice. The problem with this approach is that the spatial arrangement of the ligands around a transition metal atom in the crystal is not consistent with its hybridization in many cases. To illustrate this,

consider the fcc crystal of Ir in which each Ir atom has three d orbitals occupied with lone pairs and three sd^2 hybrid orbitals that can participate in bonding. As shown in Figure 1.12, the sd^2 orbitals are oriented along three perpendicular axes, having octahedral symmetry. A transition metal complex in which the metal atom has the same hybridization would have ligands that occupy the vertices of an octahedron. However, the coordination shell around an Ir atom in this crystal does not conform to an octahedron – it is not possible to pick out three (or six with hyperbonding) ligands that would overlap perfectly with these sd^2 hybrids. Therefore, any zero order electronic structure constructed from these hybrids would have to have bent bonds and is unlikely to describe the true electronic structure well. This was not a problem for transition metal complexes because the ligands are, in most cases, free to align with the hybrids; however, this rearrangement cannot occur in a crystal lattice for obvious reasons.

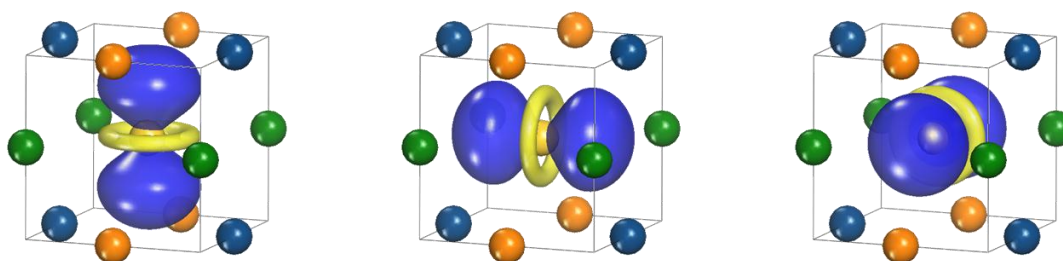


Figure 1.12 The three sd^2 hybrids that are available for covalent bonding in an Ir atom cannot be oriented towards three pairs of collinear ligands in the fcc crystal lattice.

Thus, we seem to be at an impasse in attempting to describe the bonding in a transition metal crystal in terms of valence bond concepts. Before giving up this approach completely and resigning to be content with the cumbersome description of bonding using band theory, perhaps it is worth considering whether a modification of valence bond theory will make it more conformable to these systems. As we have observed, the difficulty lies in the fact that it is not possible to construct a good Lewis structure, or even a good set of resonance structures, for a transition metal crystal so that the bonds in a given Lewis structure correspond to a set of mutually orthogonal diatomic bonding orbitals, each occupied by a pair of electrons. As discussed already, this stems from the extreme hypervalency of transition metal atoms in a crystal caused by the fact that each metal atom has far more atoms in its coordination shell than it

has unpaired electrons with which it can form covalent bonds. However, what if we could draw Lewis structures with fractional order bonds instead of only integer order bonds? That would allow us to distribute the available unpaired electrons equally among all of the bonds to atoms in the first coordination shell. If a metal atom has v unpaired electrons and N atoms in the coordination shell, then we could form a bond of order v/N with each neighboring atom using v/N of an electron pair. In that case, it would be trivial to draw a single Lewis structure for a metal crystal regardless of the number of unpaired electrons on each metal atom. This is similar in spirit to the depiction of benzene as consisting of six σ carbon-carbon bonds and six half π bonds.

The difficulty introduced by including fractional bonds in the Lewis structure is that, in classical valence bond theory, each bond in a Lewis structure corresponds to a diatomic bonding molecular orbital that is orthogonal to the orbitals corresponding to the other bonds in the structure. How does one, then, construct such an orbital for a fractional bond? It turns out that there is a simple way to allow for this, which we discuss in the next section.

1.3.1 Fractional bond orbitals

A simple way to construct a diatomic bonding molecular orbital corresponding to a fractional bond in a Lewis structure is to do away with the usual constraint that the magnitude of such an orbital ψ , given by

$$\langle\psi|\psi\rangle = \int d^3x \psi_i^*(x)\psi_i(x) \quad (1.35)$$

be normalized to unity. Instead, we set the magnitude equal to the magnitude of the fractional bond, which we denote $\eta(\psi)$. Each fractional orbital ψ corresponds to a non-fractional properly normalized orbital ψ^R having the same shape, but a magnitude of unity

$$\psi = \sqrt{\eta} \psi^R \quad (1.36)$$

The energy of the fractional orbital is obtained by scaling the energy of the corresponding non-fractional orbital by the magnitude η

$$\varepsilon(\psi) = \eta \varepsilon(\psi^R) \quad (1.37)$$

so that the bond energy of a fractional bond given by Equation (1.11) is directly proportional to the bond magnitude.

As an illustration, we will represent the hyperbonds previously discussed for transition metal complexes in terms of fractional orbitals. We can describe a hyperbond as consisting of two bonds, each of magnitude one half, between the hybrid on the metal atom and the two ligands as shown in Figure 1.13. To describe the electronic structure, we can create two bonding orbitals of magnitude one half – one between the metal hybrid and an orbital on ligand X and the other between the metal hybrid and an orbital on ligand Y. Additionally, there is a nonbonding orbital of magnitude one half on each of the two ligands. One half of an electron pair is placed into each of these four orbitals for a total of four electrons.

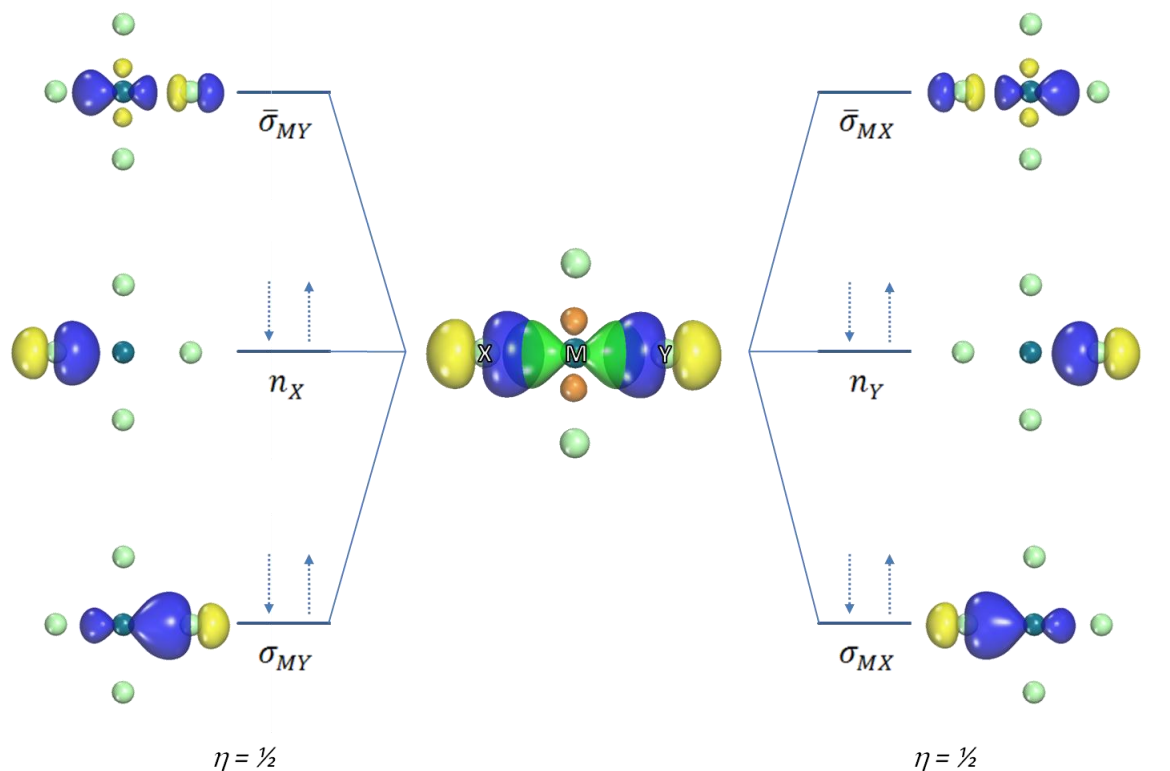


Figure 1.13 A hyperbond between metal atom M and collinear ligands X and Y can be represented in terms of four fractional orbitals of magnitude $1/2$ (two bonding σ_{MX}/σ_{MY} and two nonbonding n_X/n_Y), each occupied by one half of an electron pair. Additionally, there are two unoccupied fractional antibonding orbitals $\bar{\sigma}_{MX}$ and $\bar{\sigma}_{MY}$, each of magnitude $1/2$.

Recall that when introducing SLMOs we stated that each hybrid on an atom must be orthogonal to the other hybrids on that atom in order to preserve the Pauli Exclusion Principle. Obviously, this constraint can no longer be met in this case since there are more bonds than there are atomic orbitals on a given atom. One way around this is to introduce a virtual atomic orbital space in addition to the space associated with the normal atomic orbitals (which are referred to as the real atomic orbitals). We specify that these virtual orbitals do not interact with each other or with the real atomic orbitals and have no physical meaning – they are simply a convenient mathematical tool for treating fractional orbitals in the same way as normal bond orbitals. As an example, the hyperbond just discussed in Figure 1.8 can be described by introducing one extra virtual atomic orbital on each of the three atoms forming the bond. We can then form two orthogonal fractional hybrid orbitals on each of the atoms by mixing the real atomic orbital with the virtual orbital.

The three hybrid orbitals forming the hyperbond (h_M , h_X , and h_Y) are mixed with the corresponding virtual orbitals (χ_M , χ_X , and χ_Y) to create six mutually orthogonal fractional hybrids

(1.38)

$$\begin{aligned}\tilde{h}_{M1} &= \frac{1}{\sqrt{2}}(h_M + \chi_M) & \tilde{h}_{M2} &= \frac{1}{\sqrt{2}}(h_M - \chi_M) \\ \tilde{h}_X &= \frac{1}{\sqrt{2}}(h_X + \chi_X) & \tilde{n}_X &= \frac{1}{\sqrt{2}}(h_X - \chi_X) \\ \tilde{h}_Y &= \frac{1}{\sqrt{2}}(h_Y + \chi_Y) & \tilde{n}_Y &= \frac{1}{\sqrt{2}}(h_Y - \chi_Y)\end{aligned}$$

that can be used to form the two fractional bonding orbitals σ_{MX} and σ_{MY} and the two fractional lone pairs n_X and n_Y

(1.39)

$$\begin{aligned}\bar{\sigma}_{MX} &= c_M \tilde{h}_{M1} + c_X \tilde{h}_X & \sigma_{MY} &= c_M \tilde{h}_{M2} + c_Y \tilde{h}_Y \\ n_X &= \tilde{n}_X & n_Y &= \tilde{n}_Y\end{aligned}$$

Each fractional bonding orbital and lone pair is filled with one half of a real electron pair and one half of a virtual electron pair, since the magnitude of each fractional orbital is one half. Like the virtual atomic orbitals, the virtual electrons have no real physical meaning and are introduced simply for convenience. If the Hamiltonian describing the system does not contain any interactions between the real and virtual atomic orbitals, then the virtual orbitals will have no influence on the behavior of the real part of the system and can be completely ignored except for the fact that they make the fractional bond orbitals orthogonal to one another. However, if one insists in assigning physical significance to the virtual orbitals, they can be thought of as forming

a Hilbert space that is entangled with the real Hilbert space in order to form a pure quantum state. Without them, the fractional orbitals would describe a mixed quantum state in the real orbital space. Since many of the tools in quantum chemistry only apply to pure quantum states, it is much easier to work with the entangled system.

As a consequence of the orthogonality of the fractional orbitals, a set of sum rules can be written concerning the orbital content of the hybrids analogous to Equation (1.16) for non-fractional orbitals. To illustrate this, consider a generalized set of hybrid orbitals on a transition metal atom written as a linear combination of the s orbital, the five d orbitals d_μ , and a virtual orbital χ_M

$$h_i = a_s^i s + \sum_{\mu} a_{d_\mu}^i d_\mu + a_\chi^i \chi_i \quad (1.40)$$

This hybrid has a real magnitude given by

$$\eta(h_i) = (a_s^i)^2 + \sum_{\mu} (a_{d_\mu}^i)^2 \quad (1.41)$$

For each of the six atomic orbitals, there is a sum rule of the following form:

$$\sum_i (a_s^i)^2 = 1 \quad (1.42)$$

Thus there are six such sum rules for the six valence atomic orbitals indicating that the distribution of each atomic orbital across all of the hybrids on that atom is conserved. These are exactly the same as the sum rules developed earlier for non-fractional orbitals in molecular systems. Combining these sum rules with the expression for the magnitudes of the hybrids in Equation (1.41) leads to an additional sum rule

$$\sum_i^{\text{bonding}} \eta(h_i) + \sum_j^{\text{non-bonding}} \eta(n_j) = 6 \quad (1.43)$$

which states that the sum of the magnitudes of all hybrids on an atom must be equal to the number of atomic orbitals in the valence shell of that atom. If we then consider a transition metal atom that has a valence of v and $n = 6 - v$ lone pairs, two more sum rules can also be written

$$\sum_i^{\text{bonding}} \eta(h_i) = v \quad (1.44)$$

$$\sum_i^{\text{non-bonding}} \eta(n_i) = n \quad (1.45)$$

These state that the sum of the magnitudes of the bonding hybrids must equal the valence and the sum of the magnitudes of the nonbonding hybrids must be equal to the number of formal lone pairs. It should be noted that these last two sum rules are just generalizations of the traditional concepts of valency to work with fractional orbitals.

Before continuing, it is useful to introduce two functions to work with the real and virtual components of fractional orbitals. The function R returns the normalized real component (denoted as ψ^R in Equation (1.36)) of a fractional orbital ψ while the function V returns the normalized virtual component. Using these functions, a fractional orbital ψ with magnitude η can be written as

$$\psi = \sqrt{\eta} R(\psi) + \sqrt{(1 - \eta)} V(\psi) \quad (1.46)$$

The energy ε of ψ can then be written as

$$\varepsilon = \langle \psi | H | \psi \rangle = \eta \varepsilon^R = \eta \langle R(\psi) | H | R(\psi) \rangle = \eta \langle \psi | H | \psi \rangle^R \quad (1.47)$$

since any Hamiltonian matrix elements involving the virtual space are zero. We will use ε^R as shorthand for the energy of the normalized real component of a fractional orbital. Likewise, $\langle \psi_1 | H | \psi_2 \rangle^R$ is shorthand for the resonance integral between the normalized real components of two fractional orbitals and $\langle \psi_1 | \psi_2 \rangle^R$ is shorthand for the overlap integral between the normalized real components. Using this notation, a resonance integral between two fractional orbitals ψ_1 and ψ_2 with magnitudes η_1 and η_2 can be written as

$$\langle \psi_1 | H | \psi_2 \rangle = \sqrt{\eta_1 \eta_2} \langle R(\psi_1) | H | R(\psi_2) \rangle = \sqrt{\eta_1 \eta_2} \langle \psi_1 | H | \psi_2 \rangle^R \quad (1.48)$$

This notation will be used in the next section when we discuss conjugation between fractional orbitals.

1.3.2 Conjugation in systems containing fractional orbitals

As with systems containing only integer order bonds, metal crystals employing fractional order bonds to describe the zero order electronic structure have a set of fractional antibonding orbitals that can interact with the filled bonding orbitals leading to conjugation and reduction in energy. The conjugative interactions in transition metal crystals are expected to be far more extensive than those in organic molecules and transition metal complexes due to the delocalized nature of metallic electrons. Therefore, these interactions are expected to make a large contribution to the total binding energy of the metal crystal, as was the case with hyperbonds in the transition metal complexes, and ultimately should have a large effect on chemisorption energies.

The fractional bond orbitals that we use to describe the zero order electronic structure of metals lead to a significant complication if we attempt to treat the conjugative interactions in metals in the same way we did for organic molecules and transition metal complexes by applying Equation (1.28). The problem occurs because donating electrons from one fractional orbital to another leads to a change in the total number of electrons in the system if the two orbitals have different magnitudes, and the energy denominator of Equation (1.28) loses any physical meaning. Thus

the individual donor-acceptor interactions between pairs of fractional orbitals are not independent since any changes in the total number of electrons must cancel out in the end.

In order to avoid this problem, we need to approach the conjugative interactions in a different way. Specifically, we must devise a set of donor-acceptor interactions that individually conserve the number of electrons in the system. This can be done as follows. Suppose there is an occupied fractional orbital a of magnitude η_a and an unfilled fractional orbital r of magnitude η_r . If $\eta_a > \eta_r$, we can come up with an electron number conserving interaction by splitting a into two additional fractional orbitals a_1 and a_2 . The first orbital a_1 has the same magnitude as r while a_2 contains the remainder of a , having a magnitude $\eta_{a_2} = \eta_a - \eta_r$. We can then achieve an electron number conserving interaction involving donation from a_1 into r . The remaining orbital, a_2 , does not participate in any interaction with r . Using Equation (1.28), this leads to a second order interaction energy of

$$\Delta E_{a_1 \rightarrow r} = - \frac{|\langle a_1 | H | r \rangle|^2}{\varepsilon_r - \varepsilon_{a_1}} \quad (1.49)$$

where the resonance integral in the numerator is equal to

$$\langle a_1 | H | r \rangle = \left(\frac{\eta_r}{\eta_a} \right)^{\frac{1}{2}} \langle a | H | r \rangle = \eta_r \langle a | H | r \rangle^R \quad (1.50)$$

and the energy difference in the denominator is equal to

$$\varepsilon_r - \varepsilon_{a_1} = \varepsilon_r - \frac{\eta_r}{\eta_a} \varepsilon_a = \eta_r [\varepsilon_r^R - \varepsilon_a^R] \quad (1.51)$$

where ε_r^R and ε_a^R are the energies of the normalized orbitals constructed from the real components of a and r

$$\varepsilon_a^R = \langle a | H | a \rangle^R \quad (1.52)$$

$$\varepsilon_r^R = \langle r|H|r \rangle^R \quad (1.53)$$

The second order conjugation energy can now be written in terms of the normalized real components as

$$\Delta E_{a_1 \rightarrow r} = \eta_r \Delta E_{a \rightarrow r}^R = -\eta_r \frac{|\langle a|H|r \rangle^R|^2}{\varepsilon_r^R - \varepsilon_a^R} \quad (1.54)$$

In the case that $\eta_a < \eta_r$, the solution is similar, except r is split into two orbitals r_1 and r_2 with magnitudes $\eta_{r_1} = \eta_a$ and $\eta_{r_2} = \eta_r - \eta_a$, with r_1 interacting with a , giving a second order conjugation energy equal to

$$\Delta E_{a \rightarrow r_1} = \eta_a \Delta E_{a \rightarrow r}^R = -\eta_a \frac{|\langle a|H|r \rangle^R|^2}{\varepsilon_r^R - \varepsilon_a^R} \quad (1.55)$$

Thus, the second order conjugation energy between two fractional orbitals is equal to the conjugation energy between the two orbitals formed from the normalized real components, scaled by the lowest magnitude of the two fractional orbitals. We can write this generically as

$$\Delta E_{a \rightarrow r} = F_{a \rightarrow r} \Delta E_{a \rightarrow r}^R = -F_{a \rightarrow r} \frac{|\langle a|H|r \rangle^R|^2}{\varepsilon_r^R - \varepsilon_a^R} \quad (1.56)$$

where $F_{a \rightarrow r}$ is the magnitude of the interaction given by

$$F_{a \rightarrow r} = \begin{cases} \eta_a & \text{if } \eta_a < \eta_r \\ \eta_r & \text{if } \eta_a > \eta_r \end{cases} \quad (1.57)$$

and $\Delta E_{a \rightarrow r}^R$ is the energy of the interaction between the normalized real components of the two orbitals.

Even these individually electron number conserving interactions just described can still lead to a change in the total number of electrons if a single fractional orbital participates in separate interactions with two fractional orbitals in which the real components are not orthogonal. To illustrate this, we introduce the electron number operator N which has matrix elements between two fractional orbitals i and j defined by

$$N_{ij} = \langle i|N|j \rangle = (\eta_i \eta_j)^{\frac{1}{2}} \langle i|j \rangle^R \quad (1.58)$$

Thus, the electron number operator is just equal to the overlap of the unnormalized real components of the two fractional orbitals, with the diagonal elements N_{ii} equal to the magnitudes η_i . The total number of electrons in a system can then be determined by the expectation value of this operator on the system's wavefunction $\langle N \rangle$.

The electron number operator can be used to specify the change in the number of electrons associated with a set of conjugative interactions from occupied orbitals denoted by the indices a and b into unoccupied orbitals denoted by the indices r and s , with the result accurate to second order in the conjugative interaction being equal to

$$\Delta \langle N \rangle = \sum_{ar} c_a^r N_{ar} + \sum_{ar} (c_a^r)^2 (\eta_r - \eta_a) + \sum_{ars} c_a^r c_a^s N_{rs} - \sum_{abr} c_a^r c_b^r N_{ab} \quad (1.59)$$

In order for a set of interactions to conserve the total number of electrons in the system, the change in the expectation value of the electron number operator $\Delta \langle N \rangle$ must be zero regardless of the values of the amplitudes of the individual interactions c_a^r . This can only occur if the factors which multiply these amplitudes are all zero. The factors in the first sum (N_{ar}) are zero as long as the orbitals donor and acceptor orbitals do not both have nonzero amplitude on any given atom. The factors in the second sum ($\eta_r - \eta_a$) are already zero for interactions of the type described earlier in which the donor and acceptor orbitals a and r have the same magnitudes.

The factors in the third sum of Equation (1.59), N_{rs} , arises from the coupling of two interactions $a \rightarrow r$ and $a \rightarrow s$ involving donation from the same orbital a to two different orbitals r and s .

This situation arises when r and s are two antibonding orbitals with amplitude on atom B that are interacting with either a lone pair or bonding orbital a having amplitude on neighboring atom A. If the real components of the two acceptor orbitals are orthogonal, then $N_{rs} = 0$ and the two interactions independently conserve the number of electrons. If r and s do not have amplitude on a shared atom N_{rs} is automatically zero since the real components of the fractional hybrid orbitals making up the antibonding orbitals r and s are automatically orthogonal if the two hybrid orbitals are on different atoms.

Similarly, the factors in the fourth sum of Equation (1.59), N_{ab} , arises from the coupling of two interactions $a \rightarrow r$ and $b \rightarrow r$ from two different donor orbitals a and b into the same acceptor orbital r . This situation occurs when a and b are bonding orbitals or lone pairs both having amplitude on a common atom A that are interacting with an antibonding orbital with amplitude on neighboring atom B. If the real components of the two donor orbitals are orthogonal, then $N_{ab} = 0$ and the interactions independently conserve the number of electrons. Again, if a and b do not have amplitude on a common atom, then N_{ab} is automatically zero.

We can now state three requirements for composing a set of conjugative interactions between fractional orbitals that independently conserve the number of electrons in the system.

1. For an interaction $a \rightarrow r$, the donor and acceptor orbitals must have equal magnitudes so that $\eta_a = \eta_r$.
2. For two interactions $a \rightarrow r$ and $a \rightarrow s$ involving donation from the same donor orbital into two different acceptor orbitals, the real components of the two acceptor orbitals r and s must be orthogonal.
3. For two interactions $a \rightarrow r$ and $b \rightarrow r$ involving donation from two different donor orbitals into the same acceptor orbital, the real components of the two donor orbitals a and b must be orthogonal.

The first criterion is fulfilled using the procedure described earlier of using only a fraction of the orbital with the higher magnitude. The easiest way to fulfill the other two criteria is if we construct a set of occupied orbitals a, b, \dots on atom A whose real components are mutually

orthogonal and a set of unoccupied orbitals r, s, \dots on atom B whose real components are also mutually orthogonal

$$N_{ab} = \langle R(a) | R(b) \rangle = \eta_a \delta_{ab} \quad (1.60a)$$

$$N_{rs} = \langle R(r) | R(s) \rangle = \eta_r \delta_{rs} \quad (1.60b)$$

There will be six such orbitals on each transition metal atom corresponding to the six atomic orbitals in the sd^5 valence space. The set of bonding orbitals, antibonding orbitals, and lone pairs corresponding to the SMLO representation of the zero order ground state in general does not fulfill the orthogonality relations in Equation (1.60). Furthermore, it is cumbersome to construct a set of orbitals that fulfill these relations from the SMLOs since they have amplitude on more than a single atom (except for the lone pairs). To get around these problems, we instead use the set of atomic orbitals on atoms A and B as the basis for constructing the conjugative interactions and use a procedure described later to account for bonding in the zero order structure.

In order to use the atomic orbitals to define the conjugative interactions, it is first necessary to divide them into occupied and unoccupied sets of fractional orbitals. To do this, we first split the bonding hybrids on atom A into occupied \underline{h}_{AC} and unoccupied \bar{h}_{AC} parts defined by

$$\underline{h}_{AC} = \frac{1}{\sqrt{2}} [h_{AC} + \chi_{AC}] \quad (1.61a)$$

$$\bar{h}_{AC} = \frac{1}{\sqrt{2}} [h_{AC} - \chi_{AC}] \quad (1.61b)$$

where χ_{AC} is a virtual orbital, so that each bond in the zero order electronic structure can be described as a combination of the two interactions $\underline{h}_{AB} \rightarrow \bar{h}_{BA}$ and $\underline{h}_{BA} \rightarrow \bar{h}_{AB}$. Thus, a covalent bond between atoms A and B can be thought of occurring in the following way. Initially, each hybrid contains half an electron of each spin in the occupied fractional hybrids \underline{h}_{AB} and \underline{h}_{BA} .

The covalent bond is formed by the transfer of the half electron on atom A in \underline{h}_{AB} into \bar{h}_{BA} on atom B and the simultaneously occurring transfer of the half electron on atom B in \underline{h}_{BA} into \bar{h}_{AB} on atom A. In this way, we can think of covalent bond formation in the same way we think of conjugation – in molecular orbital theory and band theory, there is no distinction between the two phenomena anyway.

We now use the occupied and unoccupied hybrids on atom A to split the atomic orbitals into occupied bonding $\{\underline{\phi}_\mu\}$, unoccupied bonding $\{\bar{\phi}_\mu\}$, and occupied nonbonding (lone pair) $\{\ddot{\phi}_\mu\}$ sets. This is done by projecting the atomic orbital onto the sets of occupied bonding hybrids $\{\underline{h}_{AC}\}$, unoccupied bonding hybrids $\{\bar{h}_{AC}\}$, and lone pairs $\{n_i^A\}$ on atom A and normalizing the resulting orbitals by adding a virtual component $\underline{\chi}_\mu$, $\bar{\chi}_\mu$, or $\ddot{\chi}_\mu$

$$\underline{\phi}_\mu = \sum_C \langle \underline{h}_{AC} | \phi_\mu \rangle \underline{h}_{AC} + (1 - \underline{\eta}_\mu)^{\frac{1}{2}} \underline{\chi}_\mu \quad (1.62a)$$

$$\bar{\phi}_\mu = \sum_C \langle \bar{h}_{AC} | \phi_\mu \rangle \bar{h}_{AC} + (1 - \bar{\eta}_\mu)^{\frac{1}{2}} \bar{\chi}_\mu \quad (1.62b)$$

$$\ddot{\phi}_\mu = \sum_i \langle n_i^A | \phi_\mu \rangle n_i^A + (1 - \ddot{\eta}_\mu)^{\frac{1}{2}} \ddot{\chi}_\mu \quad (1.62c)$$

$$\underline{\eta}_\mu = \sum_C |\langle \underline{h}_{AC} | \phi_\mu \rangle|^2 \quad (1.63a)$$

$$\bar{\eta}_\mu = \sum_C |\langle \bar{h}_{AC} | \phi_\mu \rangle|^2 \quad (1.63b)$$

$$\ddot{\eta}_\mu = \sum_i |\langle n_i^A | \phi_\mu \rangle|^2 \quad (1.63c)$$

$$\underline{\eta}_\mu + \bar{\eta}_\mu + \ddot{\eta}_\mu = 1 \quad (1.63d)$$

where $\underline{\eta}_\mu$, $\bar{\eta}_\mu$, and $\ddot{\eta}_\mu$ are the magnitudes of the corresponding fractional orbitals. The possible conjugative interactions then involve donation from an occupied orbital $\underline{\phi}_\mu$ or $\ddot{\phi}_\mu$ on atom A into an unoccupied orbital $\bar{\phi}_\mu$ on atom B.

If the bonding environment around the atom has certain symmetry, as occurs for an atom in an fcc crystal, each of the three sets $\{\underline{\phi}_\mu\}$, $\{\ddot{\phi}_\mu\}$, and $\{\bar{\phi}_\mu\}$ obeys the number operator relations in Equation (1.60)

$$\langle \underline{\phi}_\mu | N | \underline{\phi}_\nu \rangle = \delta_{\mu\nu} \underline{\eta}_\mu \quad (1.64a)$$

$$\langle \bar{\phi}_\mu | N | \bar{\phi}_\nu \rangle = \delta_{\mu\nu} \bar{\eta}_\mu \quad (1.64b)$$

$$\langle \ddot{\phi}_\mu | N | \ddot{\phi}_\nu \rangle = \delta_{\mu\nu} \ddot{\eta}_\mu \quad (1.64c)$$

and thus forms a suitable basis for constructing electron number conserving conjugative interactions. All of the systems studied in the present work have such a symmetry, thus we will only mention briefly that if the appropriate symmetry is not present, a suitable basis for constructing conjugative interactions can still be constructed using the eigenvectors of the electron number operator in the vector space spanned by each of the three sets of orbitals.

Once the appropriate sets of atomic orbitals are constructed, the energy of each conjugative interaction between an occupied orbital a and an unoccupied orbital r is equal to

$$\Delta E_{a \rightarrow r} = \frac{1}{2} F_{a \rightarrow r} \Delta E_{a \rightarrow r}^R = \frac{1}{2} F_{a \rightarrow r} \frac{|\langle a | H | r \rangle^R|^2}{\varepsilon_r^R + e_r^R - \varepsilon_a^R - e_a^R} \quad (1.65)$$

This energy is equal to the magnitude of the interaction $F_{a \rightarrow r}$ multiplied by the interaction energy between the normalized real components of the two orbitals, or intrinsic interaction energy $\Delta E_{a \rightarrow r}^R$. The numerator of the real interaction energy is the square of the resonance integral between the normalized real components of the two orbitals defined by Equation (1.48). The denominator consists of the difference in the energies of the normalized real components of the two orbitals (given by Equation (1.47)) in addition to two terms e_a^R and e_r^R that account for bonding interactions in which the donor and acceptor orbitals a and r participate in the zero order structure. The term e_a^R is negative and lowers the effective energy of the donor orbital, increasing the magnitude of the denominator and weakening any interactions in which this orbital participates. The terms e_r^R is positive and raises the effective energy of the acceptor orbital, also weakening any interactions in which it participates. The expressions for these correction terms are equal to

$$e_a^R = \frac{1}{\eta_a} \sum_c \langle a | \underline{h}_{AC} \rangle \langle \bar{h}_{CA} | H | a \rangle \quad (1.66a)$$

$$e_r^R = -\frac{1}{\eta_r} \sum_c \langle r | \bar{h}_{AC} \rangle \langle \underline{h}_{CA} | H | r \rangle \quad (1.66b)$$

for occupied and unoccupied bonding orbitals a and r with magnitudes η_a and η_r , with the sum carried out over all bonds that atom A forms in the zero order structure. Thus, we can see that every bond in which a donor orbital participates in the zero order structure lowers its effective energy and weakens conjugative interactions in which it participates. Likewise, every bond in which an acceptor orbital participates in the zero order structure raises its effective energy, also weakening the conjugative interaction in which it participates. For a nonbonding donor orbital, this energy correction is zero since lone pairs do not form bonds in the zero order structure.

The magnitude of the conjugative interaction in Equation (1.65), $F_{a \rightarrow r}$, is given by the expression in Equation (1.57) with one modification. This modification is due to the fact that even if the matrix elements of the electron number operator are zero between orbitals in any one of the three sets in Equation (1.62), they are still nonzero between orbitals in different sets, of particular importance for orbitals in the occupied bonding $\{\underline{\phi}_\mu\}$ and occupied nonbonding $\{\ddot{\phi}_\mu\}$ sets

$$\langle \underline{\phi}_\mu | N | \ddot{\phi}_\nu \rangle = \delta_{\mu\nu} (\eta_\mu \ddot{\eta}_\mu)^{\frac{1}{2}} \quad (1.67)$$

This is important when considering an acceptor orbital $\bar{\phi}_\nu$ interacting with both $\underline{\phi}_\mu$ and $\ddot{\phi}_\mu$ on atom A. The coupling between these two interactions violates the requirements in Equation (1.60) and thus the two interactions do not independently conserve the number of electrons in the system. In order for the acceptor $\bar{\phi}_\nu$ to interact with both of these donor orbitals, it must be split into two smaller orbitals $\bar{\phi}_\nu^1$ and $\bar{\phi}_\nu^2$ where the first of these interacts with $\underline{\phi}_\mu$ and the second interacts with $\ddot{\phi}_\mu$ in the following two interactions

$$\underline{\phi}_\mu \rightarrow \bar{\phi}_\nu^1 \quad (1.68a)$$

$$\ddot{\phi}_\mu \rightarrow \bar{\phi}_\nu^2 \quad (1.68b)$$

The sum of the magnitudes of the two new acceptor orbitals $\bar{\eta}_\nu^1$ and $\bar{\eta}_\nu^2$ must be less than magnitude of the original acceptor orbital $\bar{\eta}_\nu$.

$$\bar{\eta}_\nu^1 + \bar{\eta}_\nu^2 \leq \bar{\eta}_\nu \quad (1.69)$$

Thus, the sum of the magnitudes of these two interactions must be less than or equal to the magnitude of the acceptor orbital $\bar{\phi}_\nu$ and is given by combining Equation (1.69) with Equation (1.57)

$$F_{\underline{\phi}_\mu \rightarrow \bar{\phi}_\nu} + F_{\ddot{\phi}_\mu \rightarrow \bar{\phi}_\nu} = \begin{cases} \underline{\eta}_\mu + \dot{\eta}_\mu & \text{if } \underline{\eta}_\mu + \dot{\eta}_\mu < \bar{\eta}_\nu \\ \bar{\eta}_\nu & \text{if } \bar{\eta}_\nu < \underline{\eta}_\mu + \dot{\eta}_\mu \end{cases} \quad (1.70)$$

In the case that $\underline{\eta}_\mu + \dot{\eta}_\mu < \bar{\eta}_\nu$, the magnitudes of these two interactions are simply equal to the magnitudes of the corresponding orbitals. If $\bar{\eta}_\nu < \underline{\eta}_\mu + \dot{\eta}_\mu$, then there is some degree of freedom as to how to split the total magnitude of the acceptor orbital between the two donor orbitals. In this case, we chose to maximize the interaction involving donation from the lone pair orbital $\ddot{\phi}_\mu$ since its effective energy in the denominator of Equation (1.65), ε_μ , is higher than the effective energy $\varepsilon_\mu + e_\mu$ of the bonding orbital $\underline{\phi}_\mu$, and thus results in a stronger interaction. This results in the following expressions for the magnitudes of the two interactions

$$F_{\ddot{\phi}_\mu \rightarrow \bar{\phi}_\nu} = \begin{cases} \dot{\eta}_\mu & \text{if } \dot{\eta}_\mu < \bar{\eta}_\nu \\ \bar{\eta}_\nu & \text{if } \dot{\eta}_\mu > \bar{\eta}_\nu \end{cases} \quad (1.71a)$$

$$F_{\underline{\phi}_\mu \rightarrow \bar{\phi}_\nu} = \begin{cases} \underline{\eta}_\mu & \text{if } \underline{\eta}_\mu < \bar{\eta}_\nu - F_{\ddot{\phi}_\mu \rightarrow \bar{\phi}_\nu} \\ \bar{\eta}_\nu - F_{\ddot{\phi}_\mu \rightarrow \bar{\phi}_\nu} & \text{if } \underline{\eta}_\mu > \bar{\eta}_\nu - F_{\ddot{\phi}_\mu \rightarrow \bar{\phi}_\nu} \end{cases} \quad (1.71b)$$

This means that the $\underline{\phi}_\mu \rightarrow \bar{\phi}_\nu$ interaction will only occur if the $\ddot{\phi}_\mu \rightarrow \bar{\phi}_\nu$ interaction does not saturate the acceptor orbital $\bar{\phi}_\nu$.

Finally, there is one modification that must be made to Equation (1.71) to take into account the bond that already exists between atoms A and B in the zero order structure. Using the atomic orbital basis to generate the conjugative interactions leads to a double counting of the A-B bond energy – once from the zero order energy and again from the conjugation energy. To correct for this, we subtract the energy of the A-B bond calculated from second order perturbation theory in Equation (1.28). This corresponds to the energy of the original A-B bond calculated in the same way that the conjugation energy is calculated. This energy is given by

$$\Delta E_{\underline{h}_{AB} \rightarrow \bar{h}_{BA}} = \eta_{AB} \Delta E_{\underline{h}_{AB} \rightarrow \bar{h}_{BA}}^R = -\eta_{AB} \frac{|\langle \underline{h}_{AB} | H | \bar{h}_{BA} \rangle^R|^2}{\varepsilon_{\bar{h}_{BA}}^R + e_{\bar{h}_{BA}}^R - \varepsilon_{\underline{h}_{AB}}^R - e_{\underline{h}_{AB}}^R} \quad (1.72)$$

where \underline{h}_{AB} and \bar{h}_{BA} are the occupied and unoccupied hybrids on atoms A and B given by Equation (1.61) that form the zero order A-B bond. We can further show that this energy is equal to a quarter of the zero order bond energy calculated exactly using Equation (1.11), which in the case of a nonpolar bond, is equal to

$$\Delta E_{\underline{h}_{AB} \rightarrow \bar{h}_{BA}} = \frac{1}{4} \Delta \varepsilon_{AB} = \frac{1}{2} \langle h_{AB} | H | h_{BA} \rangle \quad (1.73)$$

There are two reasons for the factor of 1/4. The first is simply that we are only considering electron transfer in one direction, from A to B. This corresponds to only half of a bond, leading to a factor of 1/2. The other factor of 1/2 comes from the approximations used to calculate the conjugation energy. This method double counts the effect of the zero order A-B bond on the effective energies of \underline{h}_{AB} and \bar{h}_{BA} given by Equation (1.66), leading to an under prediction of the energy of this bond by 1/2.

Applying the correction in Equation (1.73) also necessitates a modification of the expressions for $F_{\underline{\phi}_\mu \rightarrow \bar{\phi}_\nu}$ and $F_{\ddot{\phi}_\mu \rightarrow \bar{\phi}_\nu}$ in Equations (1.71) for the magnitudes of interactions involving donation from the bonding and nonbonding occupied orbitals $\underline{\phi}_\mu$ and $\ddot{\phi}_\mu$ on atom A into unoccupied orbital $\bar{\phi}_\nu$ on atom B. That is because the hybrids forming the A-B bond are generated from the $\underline{\phi}_\mu$ bonding orbital and not the $\ddot{\phi}_\mu$ nonbonding orbital. To account for this, the zero-order bonding interaction $\underline{h}_{AB} \rightarrow \bar{h}_{BA}$ is decomposed into separate interactions involving the occupied bonding orbitals on atom A and the unoccupied bonding orbitals on atom B

$$\underline{h}_{AB} \rightarrow \bar{h}_{BA} = \eta_{AB} \sum_{\mu\nu} |\langle \phi_\mu | h_{AB} \rangle^R|^2 |\langle \phi_\nu | h_{BA} \rangle^R|^2 \{ \underline{\phi}_\mu \rightarrow \bar{\phi}_\nu \} \quad (1.74)$$

where μ runs over all atomic orbitals on atom A and ν runs over all atomic orbitals on atom B. We then define the interaction magnitudes $F_{\underline{\phi}_\mu \rightarrow \bar{\phi}_\nu}^0$ that correspond to these interactions according to

$$F_{\underline{\phi}_\mu \rightarrow \bar{\phi}_\nu}^0 = \eta_{AB} \sum_{\mu\nu} |\langle \phi_\mu | h_{AB} \rangle^R|^2 |\langle \phi_\nu | h_{BA} \rangle^R|^2 \quad (1.75)$$

Finally, the expression for $F_{\ddot{\phi}_\mu \rightarrow \bar{\phi}_\nu}$ is modified to account for this interaction, and along with the expression for $F_{\underline{\phi}_\mu \rightarrow \bar{\phi}_\nu}$ stated previously in Equation (1.71b), make up the final set of expressions for determining the interaction magnitudes

$$F_{\ddot{\phi}_\mu \rightarrow \bar{\phi}_\nu} = \begin{cases} \ddot{\eta}_\mu & \text{if } \ddot{\eta}_\mu < \bar{\eta}_\nu - F_{\underline{\phi}_\mu \rightarrow \bar{\phi}_\nu}^0 \\ \bar{\eta}_\nu - F_{\underline{\phi}_\mu \rightarrow \bar{\phi}_\nu}^0 & \text{if } \ddot{\eta}_\mu > \bar{\eta}_\nu - F_{\underline{\phi}_\mu \rightarrow \bar{\phi}_\nu}^0 \end{cases} \quad (1.76a)$$

$$F_{\underline{\phi}_\mu \rightarrow \bar{\phi}_\nu} = \begin{cases} \underline{\eta}_\mu & \text{if } \underline{\eta}_\mu < \bar{\eta}_\nu - F_{\ddot{\phi}_\mu \rightarrow \bar{\phi}_\nu} \\ \bar{\eta}_\nu - F_{\ddot{\phi}_\mu \rightarrow \bar{\phi}_\nu} & \text{if } \underline{\eta}_\mu > \bar{\eta}_\nu - F_{\ddot{\phi}_\mu \rightarrow \bar{\phi}_\nu} \end{cases} \quad (1.76b)$$

These expressions mean that a given acceptor orbital $\bar{\phi}_\nu$ on atom B first interacts with the occupied bonding orbital $\underline{\phi}_\mu$ on atom A with an interaction magnitude of $F_{\underline{\phi}_\mu \rightarrow \bar{\phi}_\nu}^0$, corresponding to the A-B bond in the zero order structure. If $\bar{\phi}_\nu$ is not saturated by this first interaction, a second interaction involving donation from $\ddot{\phi}_\mu$ into $\bar{\phi}_\nu$ will occur until either orbital is saturated. Then, if $\bar{\phi}_\nu$ is still not saturated, it interacts further with $\underline{\phi}_\mu$ until one of these two orbitals is saturated.

Chapter 2 – Local Bonding in the 5d Transition Metal fcc Crystals

We finally have the tools necessary to describe bonding in a transition metal crystals to zero order in terms of two center bonding orbitals and one center nonbonding lone pairs. As a first application, we examine the hybridization and bonding in the bulk fcc crystals of the late 5d transition metals W to Au using fractional orbitals. After introducing the zero order structure, we will examine the contribution of conjugation to the bonding in metallic systems. It will be seen that conjugation contributes about as much to the cohesive energy of the crystal as the bonding in the zero order structure, similar to the hyperbonds in transition metal complexes. At the end of the chapter, we examine the effects of surface cleavage on the bonding between metal atoms in preparation for the discussion of chemisorption in Chapter 3.

2.1 Bonding in the Bulk

Since we are interested ultimately in describing chemisorption on transition metal surfaces, we need to understand the local bonding in the surface layer. However, the creation of a surface breaks the fcc symmetry of the system that is present in the bulk, making the bonding at the surface more complicated than the bonding in the bulk. We will therefore take the approach of first understanding in detail the electronic structure in the bulk and then make a few modifications to apply these results to surfaces.

2.1.1 Zero order electronic structure

Metal atom hybridization

Based on the sum rules in Equation (1.44), a metal atom of valence v in an fcc crystal lattice will form fractional bonds with its twelve neighbors, each having a magnitude of $v/12$. Similar to the transition metal complexes, each metal atom will have $n = 6 - v$ lone pairs that are contained in nonbonding fractional hybrids of d character so that the bonding hybrids will be sd^{v-1} . So even though we are describing hypervalent atoms with fractional bonds, the hybrids

will still have the same composition as they would in the transition metal complexes, although their arrangement and orientation will be different.

We would now like to take a closer look at the arrangement and orientation of the bonding and nonbonding hybrids to see how they differ from the hybrids in a corresponding transition metal complex. Figure 2.1 shows an alternative representation of an fcc unit cell in which one atom lies in the center of the cell and is surrounded by twelve ligands placed on the edges of the cube. The ligands can be arranged into three equivalent groups, each lying in one plane passing through the center of the cubic cell. In order to obtain a set of hybrid orbitals on the central atom to form bonds with the ligands, it is easiest if the canonical set of five orthogonal d orbitals is transformed into the set of nine fractional d orbitals that is shown in Figure 2.2. From the figure, one can see that all nine of the fractional d orbitals have the same shape as the canonical d_{z^2} orbital but are oriented in different directions. Six of these orbitals (d_{xy+} , d_{xy-} , d_{xz+} , d_{xz-} , d_{yz+} , d_{yz-}) have magnitudes of $2/3$ and are oriented along the axes connecting the six pairs of collinear ligands while the other three (d_{z^2} , d_{y^2} , d_{x^2}) have magnitudes of $1/3$ and are oriented towards the faces of the cubic unit cell. The first set is defined by the vertices of a cuboctahedron so it will be labeled d_{co} while the second set is defined by the vertices of an octahedron so it will be labeled d_o . The d_{co} set has a dimension of four while the d_o set has a dimension of one so that this is the $sd_{co}^4 d_o^1$ representation of the sd^5 valence space. This means that the d_{co} set effectively contains four of the five d orbitals while the d_o set effectively contains the remaining d orbital – but this should not be taken too literally due to the fractional nature of the representation.

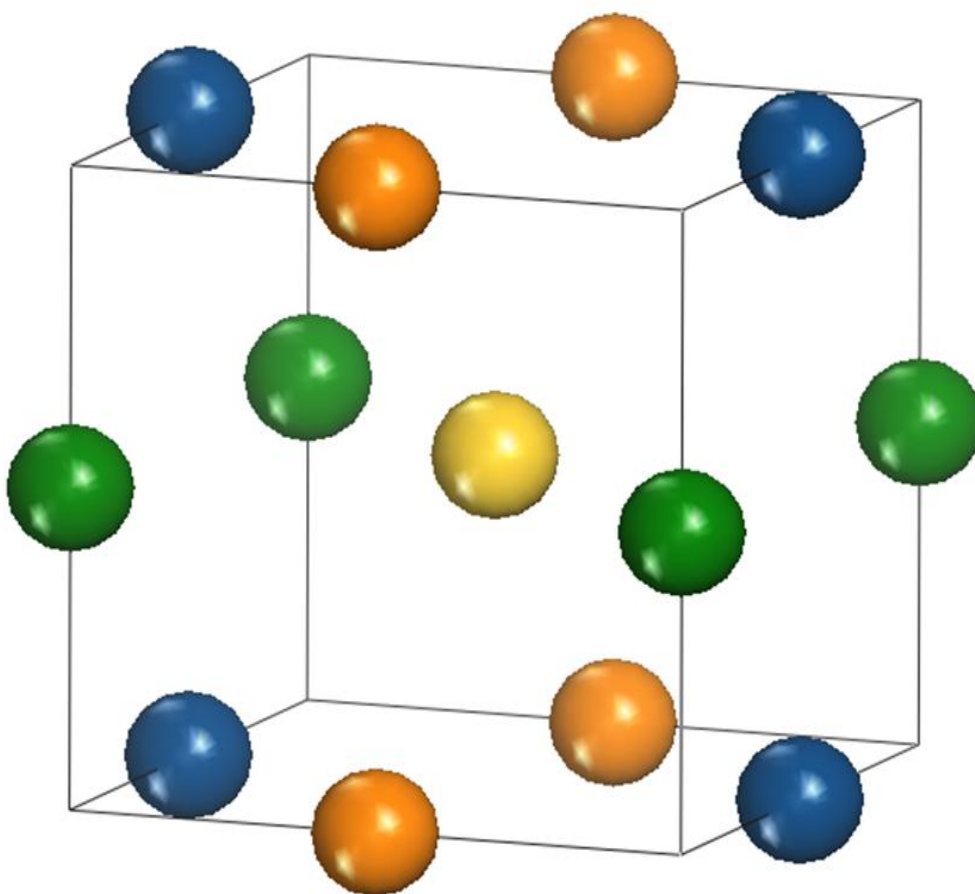


Figure 2.1 An alternative representation of the fcc unit cell in which one atom is at the center surrounded by its twelve neighbors lying on the edges of the cell. The ligands can be arranged into three groups of four, each group lying in a plane containing the central atom.

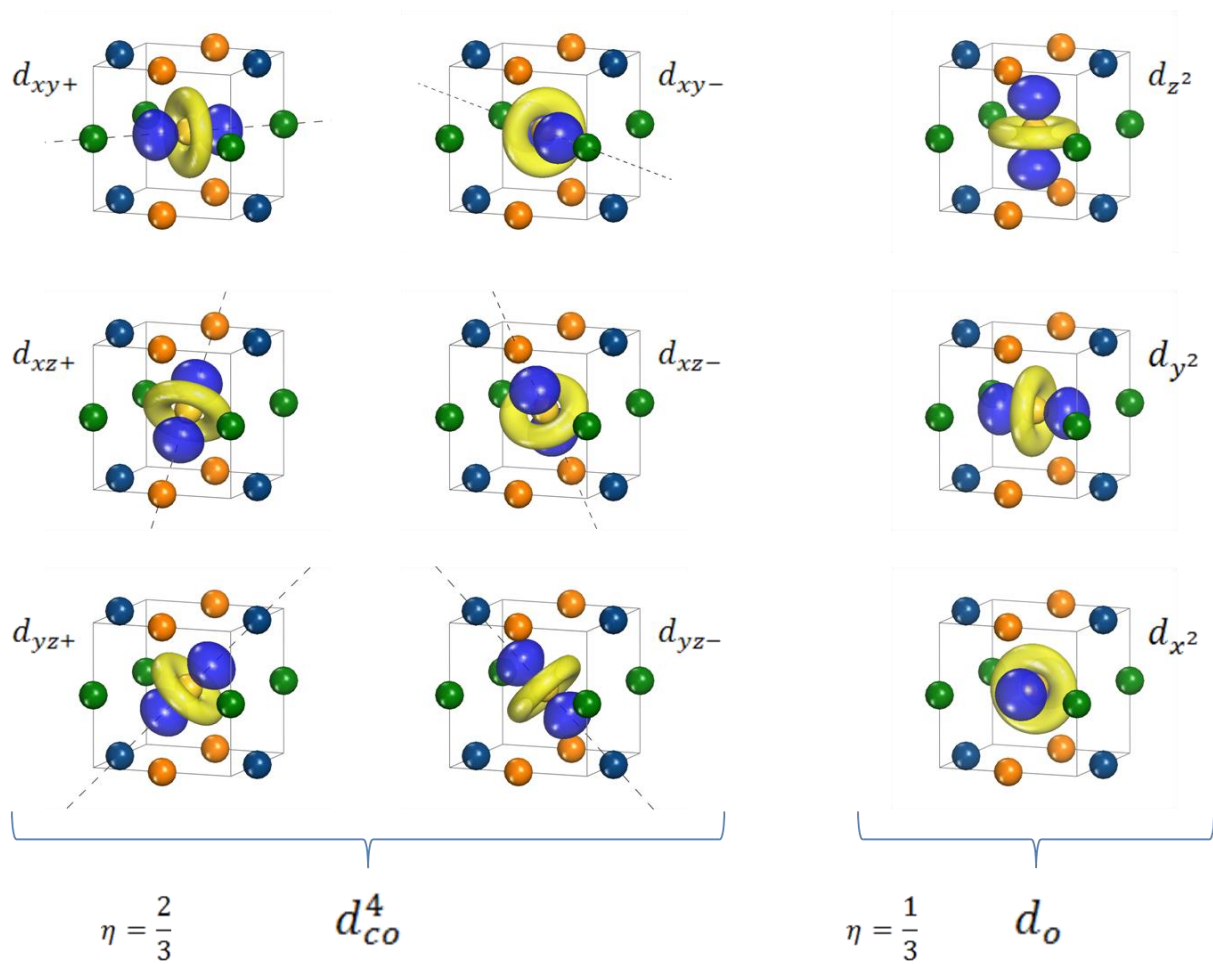


Figure 2.2 The set of nine fractional d orbitals that conform to the symmetry to the fcc lattice and have the shape of the canonical d_{z^2} orbital. The six d_{co} orbitals shown on the left are oriented towards the six pairs of collinear ligands on the edges of the unit cell. The three d_o orbitals on the right are oriented towards the faces of the unit cell. The d_{co} orbitals have magnitude $2/3$ and span a fractional Hilbert space of dimension four while the d_o orbitals have magnitude $1/3$ and span a space of dimension one.

Bonding in fcc W

Other than Au, which forms bonds using a single s orbital, fcc W displays the next simplest hybrid configuration of the late $5d$ transition metals. Since W has a valence of six, it will form a bond of magnitude $1/2$ with each of its twelve ligands according to Equation (1.44). As there are no lone pairs, all six atomic orbitals participate in bonding so the hybrids should have sd^5 composition or $sd_{co}^4 d_o^1$ in our alternative representation of the d orbital space. This leads to six

mutually orthogonal hybrids of magnitude one, each directed towards one of the six pairs of collinear ligands. Since one hybrid is shared by two ligands, it forms a bonding orbital of magnitude $1/2$ with each of these as shown in Figure 2.3, bearing similarities to the hyperbonds in transition metal complexes. Such a hybrid h_{AB} on atom A forming a bond with atom B takes the form

$$h_{AB} = \frac{1}{\sqrt{12}} [s + \sqrt{4}d_{AB} - (\sqrt{2} - 1)d_o] \quad (2.1)$$

where d_{AB} is a d_{co} orbital oriented along the A-B bond and the d_o orbital is oriented perpendicular to this bond. The d component of this hybrid deviates somewhat from the ideal d_{co} form due to the mixture of d_o character – this leads to a form that is not symmetric about the bond axis as can be seen in Figure 2.3. It has two large lobes directed along the A-B bond axis and circular lobe around the axis that is elongated in the direction of a pair of ligands perpendicular to this axis.

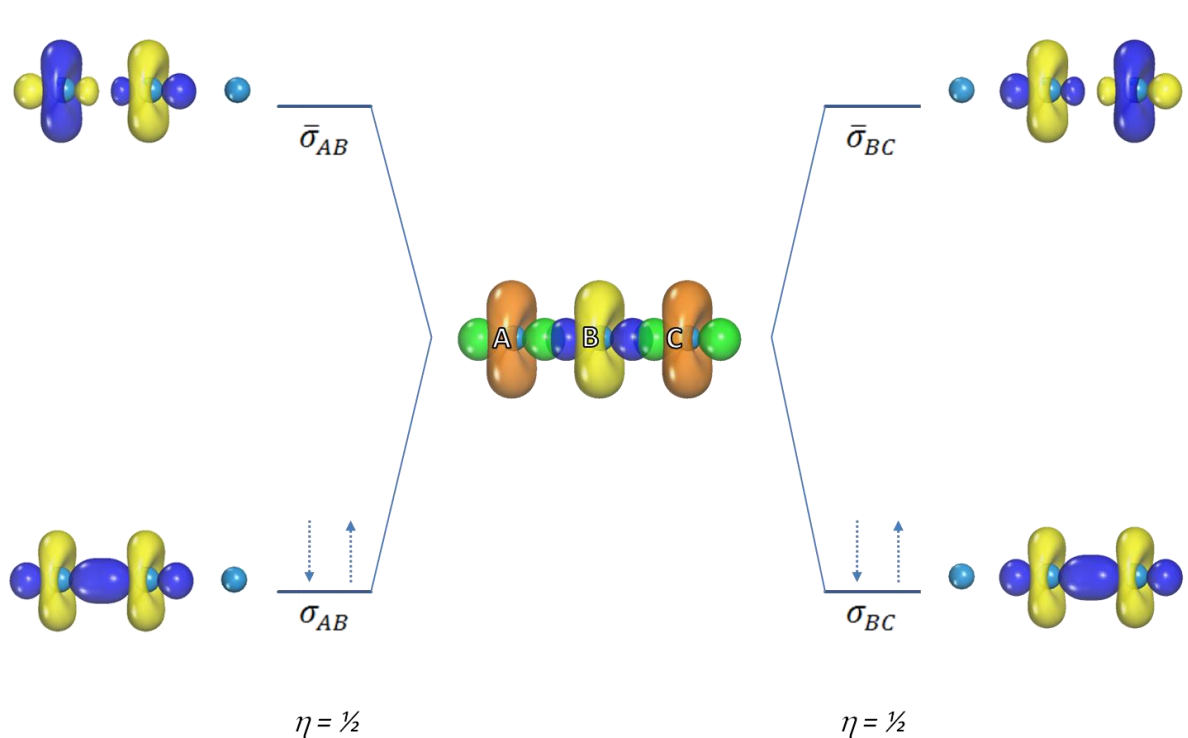


Figure 2.3 In an fcc W crystal, each atom B has six $sd^4co d_o$ hybrids containing unpaired electrons, each oriented along an axis connecting to collinear ligands A and C. Each of these hybrids can form two fractional bonds of magnitude $1/2$ with the corresponding pair of collinear ligands, leading to two bonding orbitals σ_{AB} and σ_{BC} , each occupied by half an electron pair, and two empty antibonding orbitals $\bar{\sigma}_{AB}$ and $\bar{\sigma}_{BC}$.

Bonding in fcc Re to Au

The sd^5 hybridization scheme presented so far should accurately represent the bonding of a group VI transition metal (W, Mo, Cr) in an fcc lattice since they have six unpaired electrons. The $3d$ and $4d$ metals will have the exact same hybridization as the $5d$ metal in the same group since the electron configuration is identical. Elements in groups VII-XI, as shown in the Lewis structures in Figure 1.7, have nonbonding electrons that also must be included. As already discussed, this leads to the inclusion of lone pairs in nonbonding d orbitals and a resulting reduction in the magnitude of the bonding hybrids according to Equation (1.44). Although the bonding hybrids in Au are simple to describe since they have entirely s character, the bonding hybrids in the elements Re to Pt are more difficult due to the inclusion of d character in them. Unlike the lone pairs in transition metal complexes that each occupy a single nonbonding d

orbital, doing so in the present case would break the symmetry of the fcc lattice. Therefore, the lone pair must fractionally occupy several d orbitals in order to preserve this symmetry. As an illustration, consider an fcc crystal of Re which has one lone pair per metal atom. There are two different ways to place this lone pair into d orbitals that do not violate the lattice symmetry. The first is to place $1/6$ of the lone pair into each of the six d orbitals of the d_{co} set while the other is to place $1/3$ of the lone pair into each of the three d orbitals of the d_o set. These configurations lead to a charge distribution shown in Figure 2.4 having the symmetry of the fcc lattice. One can see that the d_o configuration places lone pair density directed at the six faces of the cubic unit cell while the d_{co} configuration places it directed at the eight corners of the cell. Of course, any linear combination of these two configurations also has the correct symmetry. These two independent lone pair configurations apply to the other transition metal atoms having lone pairs as well.

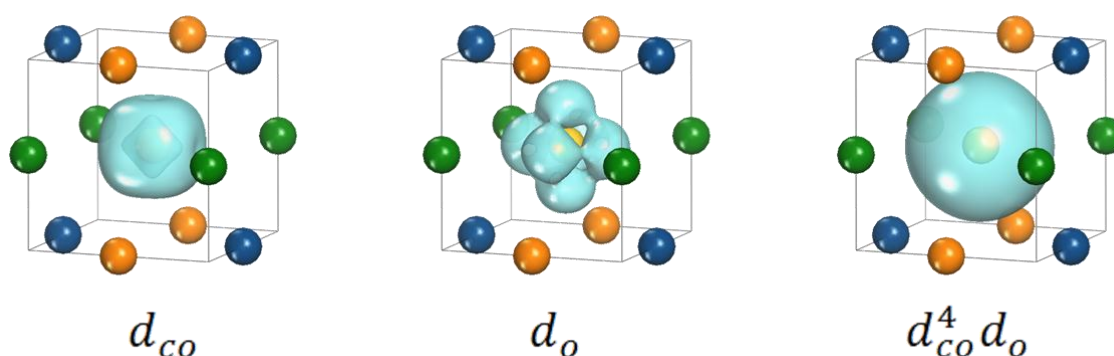


Figure 2.4 Lone pairs can occupy the d orbitals from the fractional representation shown in Figure 2.2 in two different configurations that have the same symmetry as the fcc lattice. In the first configuration, shown on the left, $1/6$ of the lone pair occupies each of the six d_{co} orbitals leading to a charge distribution concentrated towards the corners of the unit cell. In the second configuration, shown in the center, $1/3$ of the lone pair occupies each of the three d_o orbitals leading to a charge distribution concentrated towards the faces of the unit cell. In the coinage metals, both sets of d orbitals are completely filled so that the charge distribution is spherical as shown on the right.

When a portion of the d orbital space has been set aside as fractional nonbonding orbitals that contain lone pairs, these orbitals are no longer available to form bonding hybrids. Consequently, the valence of the atom decreases by one for each lone pair present. This manifests as a reduction in magnitude of the bonding hybrids that were found to have magnitudes of $1/2$ in fcc W. The resulting magnitude of these hybrids is then

$$\eta(h_i) = \frac{v}{12} = \frac{6 - n}{12} \quad (2.2)$$

This is a direct result of the Pauli Exclusion Principle and is obtained from the sum rules in Equation (1.44).

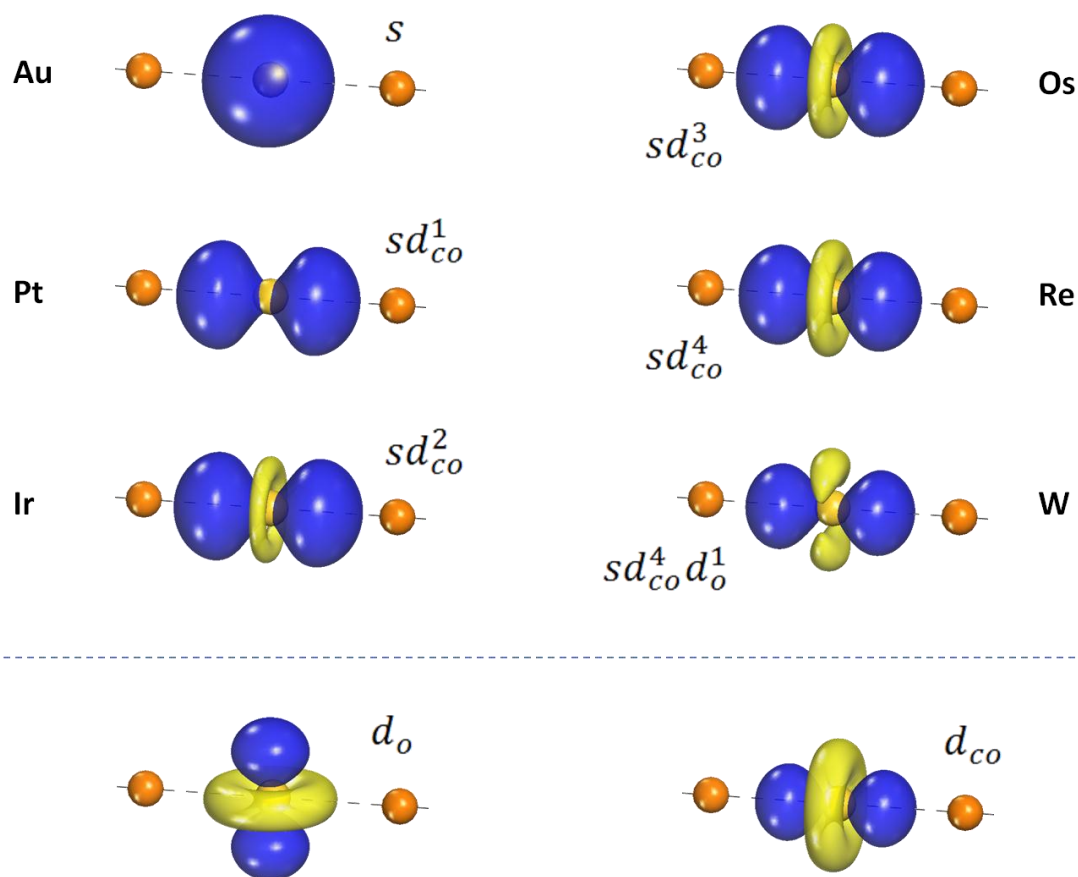


Figure 2.5 The sd^{v-1} hybrids participating in metal-metal bonding for the later 5d transition metals. The hybrid is purely s character on Au since the d orbitals are completely occupied with lone pairs. On Pt to Re, the d component of the hybrid is rotationally symmetric about the bond axis since it is made up of only d_{co} orbitals. On W, the d_o orbitals participate in hybridization as well, breaking this symmetry.

The exact form of the hybrids will depend on the distribution of the lone pairs between the d_{co} and the d_o orbitals. In fcc Re, it is most energetically favorable to place the single lone pair into the d_o orbitals since they have weaker overlap with the ligand orbitals than the d_{co} set. Since this set of orbitals has dimension one, it is completely filled with the lone pair and can no longer participate in bonding, leading to twelve hybrids of magnitude 5/12 with sd_{co}^4 character. The subsequent lone pairs for Os to Au go into d_{co} orbitals, so that the bonding hybrids have sd_{co}^{v-1} character and magnitudes given by Equation (2.2). The form of a hybrid h_{AB} on an atom A forming a bond with atom B is then given by

$$h_{AB} = \frac{1}{\sqrt{12}}(s + \sqrt{v-1} d_{AB}) \quad (2.3)$$

where the d component, d_{AB} , has the shape of a d_{co} orbital directed along the A-B bond axis. These hybrids are illustrated in Figure 2.5 where it can be seen that they become progressively more concentrated along the bond axis as the d_{co} component increases.

Zero-order bond energies

The bond energy of each metal-metal bond between a hybrid h_{AB} on atom A and a hybrid h_{BA} on atom B is shown by Equation (1.11) in Chapter 1 for a purely covalent bond to be twice the resonance integral between the two hybrids.

$$\Delta\varepsilon_{AB} = 2 V_{AB} = 2 \langle h_{AB} | H | h_{BA} \rangle \quad (2.4)$$

When calculating this bond energy, it is useful to decompose the resonance integral into characteristic interactions as we did for molecular species in the previous chapter. For two adjacent metal atoms in a crystal, there will be six such characteristic interactions shown in Figure 2.6 – two σ interactions involving sd^n hybrids, and two sets of π and δ interactions involving d orbitals. The two σ interactions, σ_+ and σ_- , occur between two sets of hybrids composed of the s orbital and a d orbital that is oriented along the bond axis. The hybrids in the σ_+ set are formed by a constructive (in the region of the bond) superposition of the s and d orbitals and are concentrated along the bond axis in both directions, having a strong resonance integral (-1.58 eV in Au). The hybrids in the σ_- set are formed by a destructive (in the region of the bond) superposition of the s and d orbitals and is concentrated in a ring around the bond axis, having much weaker resonance integral (-0.17 eV in Au). The π and δ interactions (-0.39 eV and -0.07 eV in Au) are also weaker than the σ_+ interactions.

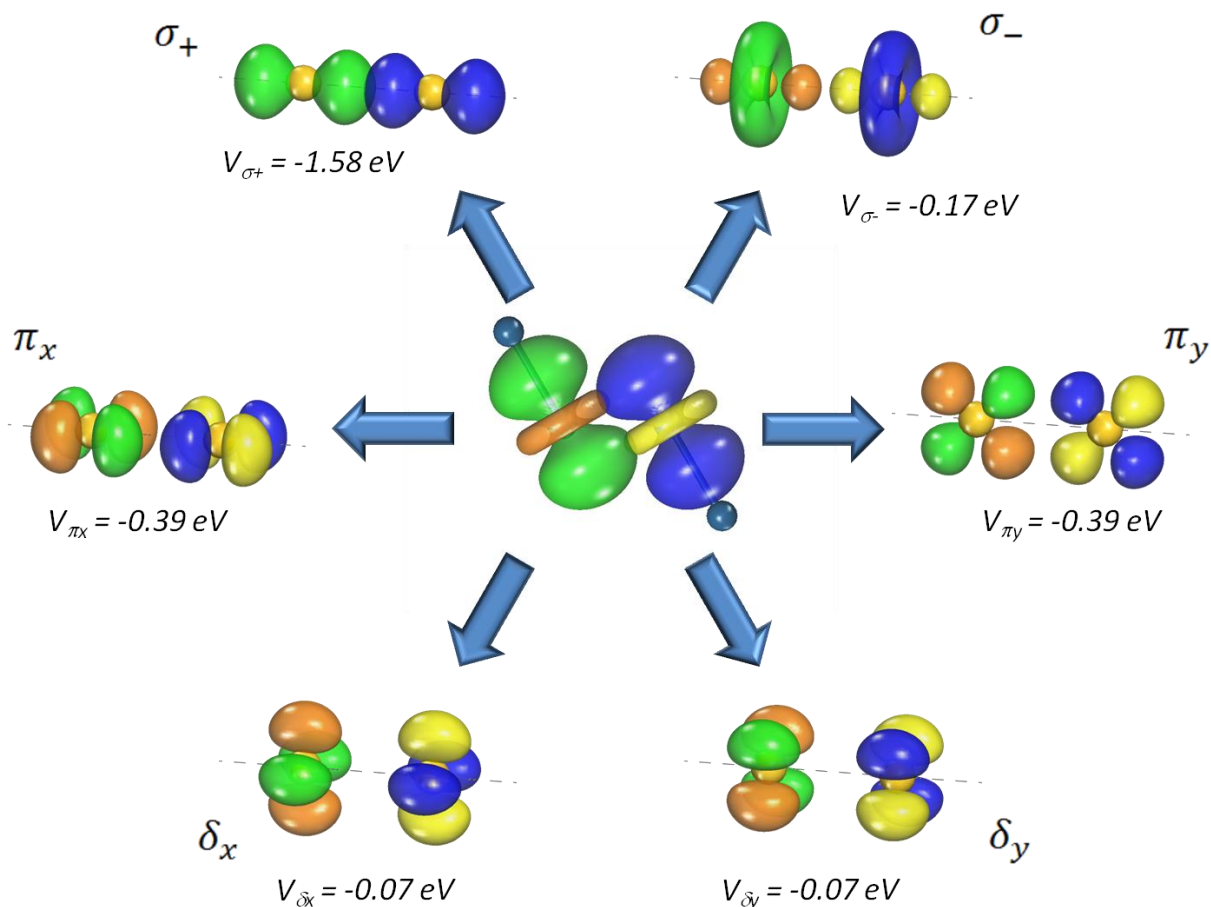


Figure 2.6 As with ethane in Figure 1.6 and PtCl_4^{2-} in Figure 1.11, the resonance integral between two hybrids on neighboring atoms can be decomposed into two characteristic interactions with σ symmetry (top), two with π symmetry (middle), and two with δ symmetry (bottom). Of these, the σ_+ interaction makes the largest contribution.

As we did in Equation (1.31) of Chapter 1, the resonance integral in the above equation for the bond energy can be written as a sum of the six characteristic interactions

$$\langle h_{AB} | H | h_{BA} \rangle = \left[\begin{aligned} & \langle h_{AB} | h_{\sigma_+}^A \rangle \langle h_{\sigma_+}^B | h_{BA} \rangle V_{\sigma_+} + \langle h_{AB} | h_{\sigma_-}^A \rangle \langle h_{\sigma_-}^B | h_{BA} \rangle V_{\sigma_-} \\ & + \left[\langle h_{AB} | h_{\pi_x}^A \rangle \langle h_{\pi_x}^B | h_{BA} \rangle + \langle h_{AB} | h_{\pi_y}^A \rangle \langle h_{\pi_y}^B | h_{BA} \rangle \right] V_{\pi} \\ & + \left[\langle h_{AB} | h_{\delta_x}^A \rangle \langle h_{\delta_x}^B | h_{BA} \rangle + \langle h_{AB} | h_{\delta_y}^A \rangle \langle h_{\delta_y}^B | h_{BA} \rangle \right] V_{\delta} \end{aligned} \right] \quad (2.5)$$

Calculation of the bond energy is greatly simplified if only the σ_+ interaction is considered to contribute. This is not a bad approximation since the resonance integral of this interaction is at least four times larger than those for the other interactions. In this case, the bond energy can be approximately written as

$$\Delta\varepsilon_{AB} = 2 \langle h_{AB} | h_{\sigma_+}^A \rangle \langle h_{\sigma_+}^B | h_{BA} \rangle V_{\sigma_+} \quad (2.6)$$

The hybrids associated with the σ_+ interaction have the form

$$h_{\sigma_+}^A = b_s s + b_d d_{AB} \quad (2.7)$$

where d_{AB} is oriented along the bond axis as in the definition of the bonding hybrid h_{AB} in Equation (2.3). The bond energy in Equation (2.6) consists of the product of three integrals – two of these integrals, $\langle h_{AB} | h_{\sigma_+}^A \rangle$ and $\langle h_{\sigma_+}^B | h_{BA} \rangle$, measure the overlap of the two hybrids with the σ_+ interaction, while the third integral, V_{σ_+} , is a resonance integral that measures the intrinsic strength of the σ_+ interaction.

Table 2.1 Tight binding parameters used in the model. From first to last row – resonance integral of the σ_+ interaction between two metal atoms; resonance integral of the σ interaction between two metal s orbitals; resonance integral of the σ interaction between two metal d orbitals; energy difference between the metal d and s orbitals; resonance integral between the metal hybrid h_a and the hydrogen s orbital; energy difference between the hydrogen s orbital and the metal hybrid h_a . The parameters for Ir in bold are used for all metals in the simplest form of the model. These parameters were calculated using the procedure in Appendix A.

	W	Re	Os	Ir	Pt	Au
V_{σ_+}	2.23	2.16	2.17	1.98	1.81	1.42
$b_s^2 V_{\sigma_+}$	1.10	1.00	1.11	1.09	1.12	0.93
$b_d^2 V_{\sigma_+}$	1.13	1.16	1.05	0.89	0.69	0.49
$\epsilon_d - \epsilon_s$	-1.27	-1.24	-1.93	-2.04	-2.31	-2.09
V_{MH}	3.79	3.77	3.66	3.57	3.45	2.89
$\epsilon_H - \epsilon_M$	-0.56	0.22	1.14	1.73	1.71	0.96

In addition to depending on the metal atom valence, the bond energy in Equation (2.6) also depends on the values of the atomic parameters V_{σ_+} and b_d (b_s is related to b_d through $b_s^2 + b_d^2 = 1$). Two quantities derived from these parameters, $b_s^2 V_{\sigma_+}$ and $b_d^2 V_{\sigma_+}$, are listed for the late 5d transition metals in Table 2.1, extracted from DFT calculations on the bulk metal using the procedure in Appendix A. The first quantity measures the strength of the σ interaction between the s orbitals while the second measures the strength of the σ interaction between two d orbitals. It is seen that $b_d^2 V_{\sigma_+}$ increases in magnitude moving from Au to Re while $b_s^2 V_{\sigma_+}$ is relatively constant. The increase in the strength of the σ interaction between d orbitals is due to an increase in the radial extent of the d orbitals, whereas the extent of the s orbitals does not change significantly. While the variation of these atomic parameters surely has an effect on the energies calculated by the present model, we will ignore these variations for now and focus only on the effect of metal atom valence, using the parameters for Pt for all of the metals. At the end of this section, we will come back and examine the effect of these variations.

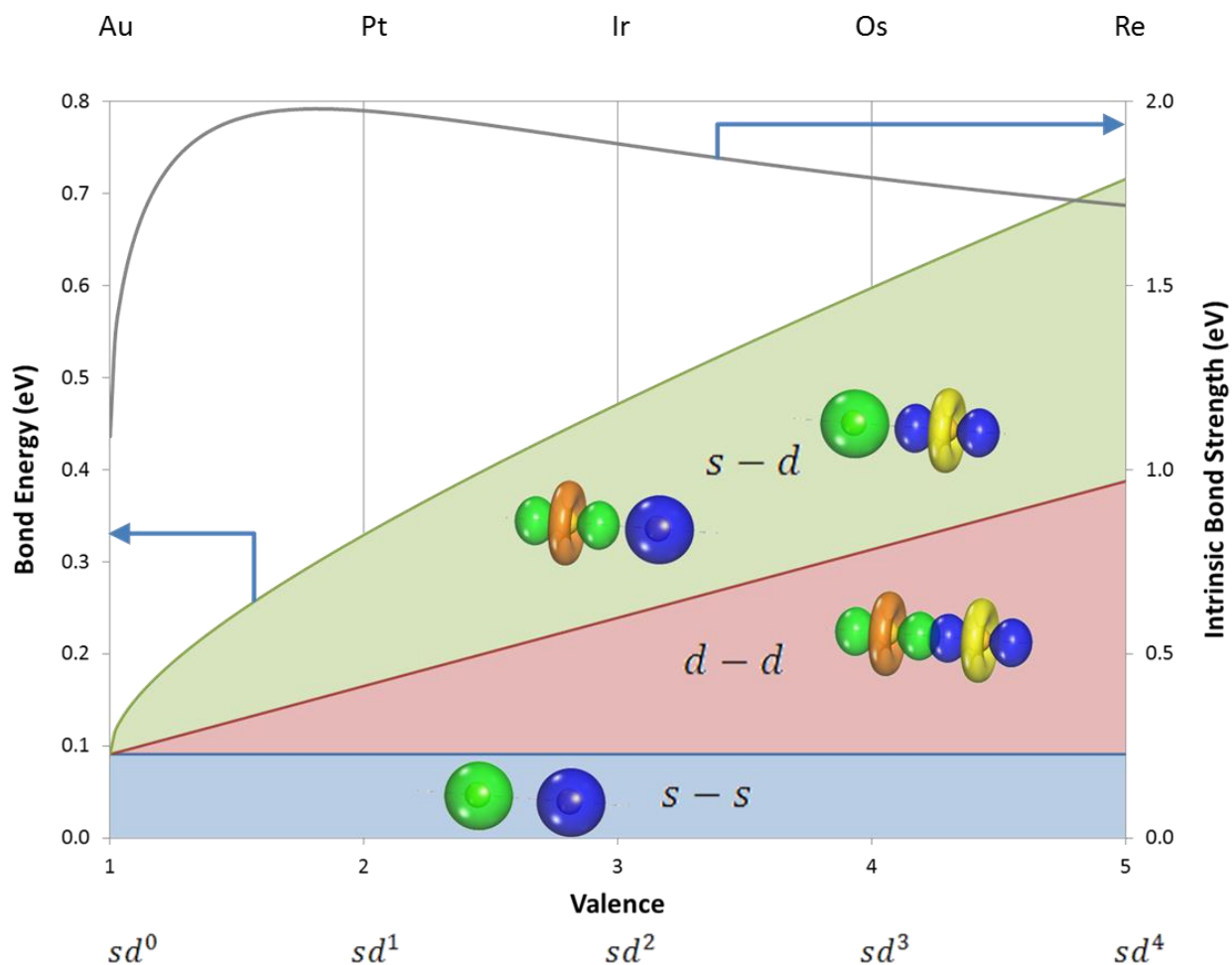


Figure 2.7 The total zero-order metal-metal bond energy for fcc Au to Re can be split into three parts due to interactions between the individual s and d components of the two hybrids forming the bond, as shown in Equation (2.10). Also shown is the intrinsic bond strength defined as the bond energy normalized to the bond magnitude.

The bond energy given by Equation (2.6) is plotted for metal atoms of differing valence in Figure 2.7. It can be seen that the bond energy increases from Au to Re as the d components of the hybrids h_{AB} and h_{BA} increase in magnitude. As the magnitude of the d component becomes higher, though, its effect on the bond energy diminishes so that the increase in bond energy between Au and Pt is significantly higher than the increases between other elements. The intrinsic strength of the metal-metal bond is given by normalizing the bond energy to the bond magnitude in Equation (2.2). This value is shown to be highest for Pt, which has hybrids closest in composition to the optimal composition of 45% d character. This intrinsic strength decreases

moving towards Re as the bonding hybrids become more concentrated in d character and towards Au as they become depleted of d character. However, the composition and shape of the hybrid orbitals has only a secondary impact on the binding energy compared to the effect due to an increase in bond magnitudes as the valence increases. In contrast, we will see in the next section that the shape of the hybrids has a much stronger impact on the conjugation within the crystal.

Decomposition of the bond energy

Since the bonding hybrids are composed of s and d_{co} orbitals, the overlap integrals in Equation (2.6) can be written in terms of these individual components

$$\langle h_{AB} | h_{\sigma_+}^A \rangle = \langle h_{AB} | s \rangle \langle s | h_{\sigma_+}^A \rangle + \langle h_{AB} | d_{AB} \rangle \langle d_{AB} | h_{\sigma_+}^A \rangle \quad (2.8a)$$

$$\langle h_{\sigma_+}^B | h_{BA} \rangle = \langle h_{\sigma_+}^B | s \rangle \langle s | h_{BA} \rangle + \langle h_{\sigma_+}^B | d_{BA} \rangle \langle d_{BA} | h_{BA} \rangle \quad (2.8b)$$

This means that the overlap of h_{AB} with the σ_+ interaction is equal to the sum of the individual overlaps of its s and d_{AB} components with the σ_+ interaction. Using the form of the hybrids defining the σ_+ interaction in Equation (2.7), these equations can be written as

$$\langle h_{AB} | h_{\sigma_+}^A \rangle = b_s \langle h_{AB} | s \rangle + b_d \langle h_{AB} | d_{AB} \rangle \quad (2.9a)$$

$$\langle h_{\sigma_+}^B | h_{BA} \rangle = b_s \langle s | h_{BA} \rangle + b_d \langle d_{BA} | h_{BA} \rangle \quad (2.9b)$$

The ratio of b_s to b_d determines the relative weightings of the s and d_{AB} components in the σ_+ interaction. If $b_s > b_d$, then increasing the magnitude of the s component of the bonding hybrid h_{AB} will cause a greater increase in the σ_+ interaction than increasing the magnitude of the d_{AB} component. This is the case in practice since the s orbital has a greater radial extent than the d orbitals.

Using the overlap integrals in Equation (2.9), the bond energy can be written in terms of interactions between the individual components of the two hybrids

$$\Delta\varepsilon_{AB} = 2 \left[\underbrace{b_s^2 \langle h_{AB}|s\rangle \langle s|h_{BA}\rangle}_{s-s} + \underbrace{b_d^2 \langle h_{AB}|d_{AB}\rangle \langle d_{BA}|h_{BA}\rangle}_{d-d} \right. \\ \left. + \underbrace{b_s b_d \langle h_{AB}|s\rangle \langle d_{BA}|h_{BA}\rangle}_{s-d} + \underbrace{b_s b_d \langle h_{AB}|d_{AB}\rangle \langle s|h_{BA}\rangle}_{d-s} \right] V_{\sigma_+} \quad (2.10)$$

We can see from this expression that there are four interactions that make up the total bond energy – one between the s components of the two hybrids, one between the d components of the two hybrids, and two between the s component on one hybrid and the d component on the other. Each term in this expression is equal to the product of the intrinsic strength of the interaction and the amplitude of the interaction. To illustrate this, consider the term accounting for the s - s interaction. The intrinsic strength of this interaction is equal to $b_s^2 V_{\sigma_+}$ and is defined solely by the hybrids that define the σ_+ interaction. The amplitude of the interaction is equal to the product of the two integrals $\langle h_{AB}|s\rangle$ and $\langle s|h_{BA}\rangle$ that measure the amplitudes of the s components of the two hybrids.

Using the forms of the hybrids given in Equation (2.3), the values of the integrals in Equation (2.10) for the bond energy are equal to

$$\langle h_{AB}|s\rangle = \langle s|h_{BA}\rangle = \frac{1}{\sqrt{12}} \quad (2.11a)$$

$$\langle h_{AB}|d_{AB}\rangle = \langle d_{BA}|h_{BA}\rangle = \frac{1}{\sqrt{12}} \sqrt{v-1} \quad (2.11b)$$

so that the bond energy is

$$\Delta\varepsilon_{AB} = \frac{1}{6} \left[\underbrace{b_s^2}_{s-s} + \underbrace{b_d^2 (v-1)}_{d-d} + 2 \underbrace{b_s b_d \sqrt{v-1}}_{s-d} \right] V_{\sigma_+} \quad (2.12)$$

From this expression, we can see that the amplitudes of the four different interactions depend differently on the valence of the metal atoms. Since the amplitudes of the s components of the hybrids are the same for all metals, the s - s interaction has no dependence on the valence and contributes a constant amount to the bond energy of all the $5d$ metals as shown in Figure 2.7. The amplitude of the d - d interaction is proportional to the square of the amplitude of the d component on the hybrids, which itself is proportional to the number of d orbitals included in the hybridization ($v - 1$). It therefore contributes an equal amount to the bond energy for each addition d orbital added, leading to a linear increase in the strength of this interaction with valence. The amplitudes of the s - d interactions are proportional to the amplitude of the d component of each hybrid, which is itself proportional to the square root of the number of d orbitals included in hybridization. As a result, the addition of the first d orbital on Pt leads to a large increase in bond energy relative to Au. Each subsequent addition of a d orbital to the hybridization leads to an increasingly diminishing increase in bond energy. Thus it is the s - d interactions that lead to the large increase in total bond energy between Au and Pt as was seen in Figure 2.7.

For all $5d$ elements except Au, the s - d interactions contribute more than half of the total bond energy. This is in contrast to the popular qualitative model of transition metal electronic structure that separates the bands into independent s states and d states.³⁸ From the present model, it appears that the s and d orbitals are hybridized to the same extent that the s and p orbitals are hybridized in the $2p$ elements.

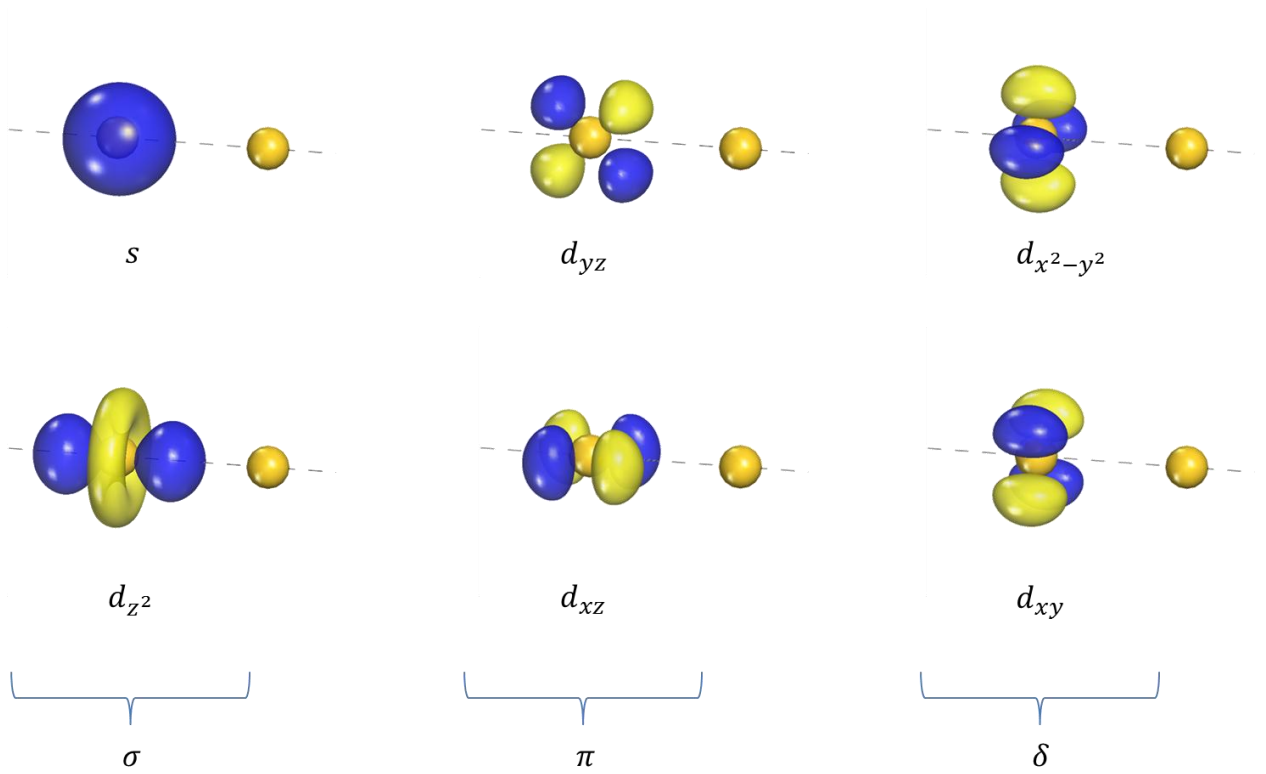


Figure 2.8 Set of atomic orbitals used to generate the conjugative interactions.

2.1.2 Conjugation

We would now like to examine the extent of conjugation in the $5d$ transition metal fcc crystals. As discussed in Chapter 1, these interactions are constructed from sets of occupied and unoccupied fractional atomic orbitals on the two atoms participating in the interaction. The energy $\Delta E_{a \rightarrow r}$ of such an interaction between an occupied orbital a and an unoccupied orbital r is equal to the expression in Equation (1.65), consisting of the energy $\Delta E_{a \rightarrow r}^R$ of the interaction between the normalized real components of a and r scaled by the magnitude of the interaction $F_{a \rightarrow r}$

$$\Delta E_{a \rightarrow r} = \frac{1}{2} F_{a \rightarrow r} \Delta E_{a \rightarrow r}^R = \frac{1}{2} F_{a \rightarrow r} \frac{|\langle a | H | r \rangle^R|^2}{\epsilon_r^R + e_r^R - \epsilon_a^R - e_a^R} \quad (1.65)$$

Before calculating these interactions, we need to specify the sets of occupied and unoccupied atomic orbitals that define these interactions. Consider interactions between orbitals on the two atoms A and B shown in Figure 2.8. Because of the fcc symmetry of the bonding around both atoms, the orbitals in each set generated by Equation (1.62) have zero-valued matrix elements of the electron number operator between them, and thus satisfy the requirements in Equation (1.60) for a set of electron number conserving interactions. The set of atomic orbitals on atom A we use to generate the donor and acceptor sets is aligned with the A-B bond axis as shown in Figure 2.8. A similar set on atom B is used to generate the interaction basis on this atom. This set of orbitals contains the metal s orbital along with five d orbitals, the latter consisting of one d orbital with σ symmetry with respect to the A-B bond (d_{σ}^{AB}), two orbitals with π symmetry ($d_{\pi_x}^{AB}$ and $d_{\pi_y}^{AB}$), and two with δ symmetry ($d_{\delta_1}^{AB}$ and $d_{\delta_2}^{AB}$). The s orbital along with d_{σ}^{AB} on atom A can participate in σ interactions with orbitals on atom B. The other d orbitals can only participate in π and δ interactions, which will be neglected as done previously when discussing the zero order electronic structure.

These atomic orbitals lead to a set of donor orbitals on atom A consisting of the occupied bonding s and d_{σ}^{AB} orbitals \underline{s} and $\underline{d}_{\sigma}^{AB}$ and the nonbonding lone pair orbital \ddot{d}_{σ}^{AB} and a set of acceptor orbitals consisting of the unoccupied bonding s and d_{σ}^{AB} orbitals \bar{s} and \bar{d}_{σ}^{AB} . Similarly, atom B has three donor orbitals \underline{s} , $\underline{d}_{\sigma}^{BA}$, and \ddot{d}_{σ}^{BA} and two acceptor orbitals \bar{s} and \bar{d}_{σ}^{AB} . This leads to a set of twelve possible interactions, six involving electron transfer from atom A to atom B and the other six involving electron transfer from atom B to atom A.

At this point, we would like to determine how the magnitudes of the different conjugative interactions vary with the valence of the metal atom. To do this, we need to know the magnitudes of the donor and acceptor orbitals, which for Au to Re, are equal to

$$\eta(\underline{s}) = \eta(\bar{s}) = \frac{1}{2} \quad (2.13a)$$

$$\eta(\underline{d}_{\sigma}^{AB}) = \eta(\bar{d}_{\sigma}^{AB}) = \frac{1}{2} \times \frac{7}{32} (v - 1) \quad (2.13b)$$

$$\eta(\ddot{d}_{\sigma}^{AB}) = \frac{7}{8} \times \frac{1}{4}(5 - v) + \frac{1}{8} \quad (2.13c)$$

For W, the magnitude of the four bonding orbitals is equal to 1/2 and the magnitude of the nonbonding orbital \ddot{d}_{σ}^{AB} is zero since there are no lone pairs.

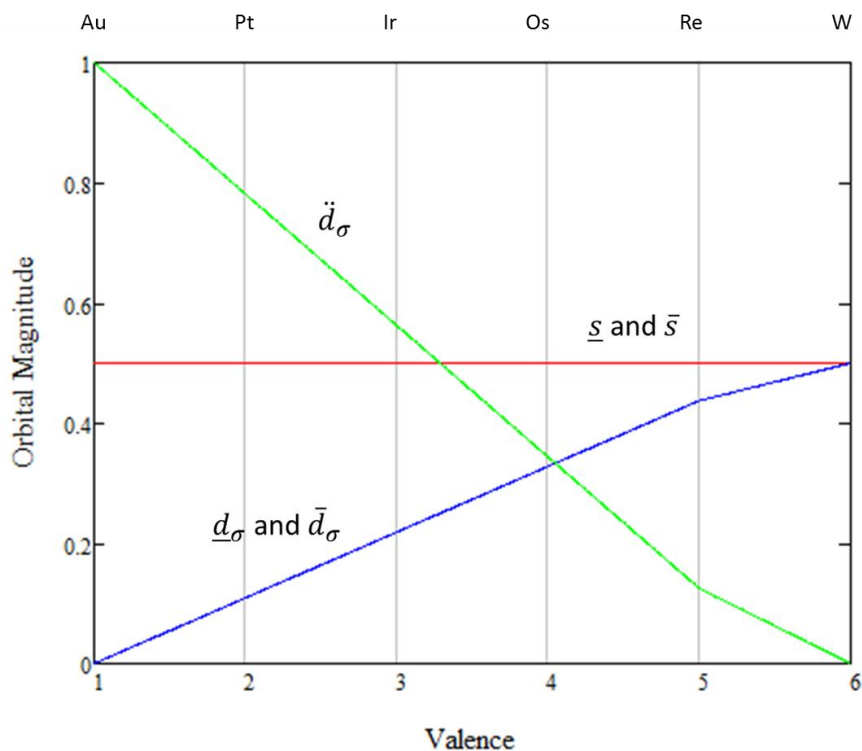


Figure 2.9 Magnitudes of the atomic orbitals used to generate the conjugative interactions given by Equation (2.13)

These magnitudes are plotted with respect to metal atom valence in Figure 2.9. The magnitudes of the \underline{s} and \bar{s} orbitals are constant and equal to 1/2 since the s orbital is always fully participating in covalent bonding and never contains a lone pair, with one half of the orbital being occupied and the other half unoccupied. The magnitudes of the occupied and unoccupied bonding d_{σ}^{AB} orbitals ($\underline{d}_{\sigma}^{AB}$ and \bar{d}_{σ}^{AB}) are proportional to the number of d orbitals participating in covalent bonding ($v - 1$) and thus increase linearly with valence. The magnitude of the lone

pair orbital \ddot{d}_σ is proportional to the number of d_{co} lone pairs on the atom $(5 - v)$ plus a contribution from the d_o lone pair, resulting in a linear decrease with increasing valence.

The magnitudes of the individual interactions between the three donor orbitals $\{\underline{s}, \underline{d}_\sigma, \ddot{d}_\sigma\}$ and two acceptor orbitals $\{\bar{s}, \bar{d}_\sigma\}$ are calculated using Equation (1.76). First, it is necessary to determine the magnitudes of the interactions corresponding for the A-B bond in the zero order structure that was discussed in Chapter 1. To do this, the zero-order bonding interaction $\underline{h}_{AB} \rightarrow \bar{h}_{BA}$ is decomposed into four separate interactions involving the occupied s and d_σ^{AB} orbitals on atom A ($\underline{s}, \underline{d}_\sigma^{AB}$) and the unoccupied s and d_σ orbitals on atom B ($\bar{s}, \bar{d}_\sigma^{AB}$)

$$\underline{h}_{AB} \rightarrow \bar{h}_{BA} = \eta_{AB} \left[\begin{array}{ccc} |\langle s|h_{AB} \rangle^R|^2 & |\langle s|h_{BA} \rangle^R|^2 & [\underline{s} \rightarrow \bar{s}] \\ + |\langle s|h_{AB} \rangle^R|^2 & |\langle d_\sigma^{AB}|h_{BA} \rangle^R|^2 & [\underline{s} \rightarrow \bar{d}_\sigma] \\ + |\langle d_\sigma^{AB}|h_{AB} \rangle^R|^2 & |\langle s|h_{BA} \rangle^R|^2 & [\underline{d}_\sigma \rightarrow \bar{s}] \\ + |\langle d_\sigma^{AB}|h_{AB} \rangle^R|^2 & |\langle d_\sigma^{AB}|h_{BA} \rangle^R|^2 & [\underline{d}_\sigma \rightarrow \bar{d}_\sigma] \end{array} \right] \quad (2.14)$$

We then define the interaction magnitudes $F_{a \rightarrow r}^0$ corresponding to these interactions from Equation (1.75), using expressions for the hybrid orbitals h_{AB} and h_{BA} given by Equation (2.3)

$$F_{\underline{s} \rightarrow \bar{s}}^0 = \frac{1}{12 v} \quad (2.15a)$$

$$F_{\underline{s} \rightarrow \bar{d}_\sigma^{AB}}^0 = F_{\underline{d}_\sigma^{AB} \rightarrow \bar{s}}^0 = \frac{v-1}{12 v} \quad (2.15b)$$

$$F_{\underline{d}_\sigma^{AB} \rightarrow \bar{d}_\sigma^{AB}}^0 = \frac{(v-1)^2}{12 v} \quad (2.15c)$$

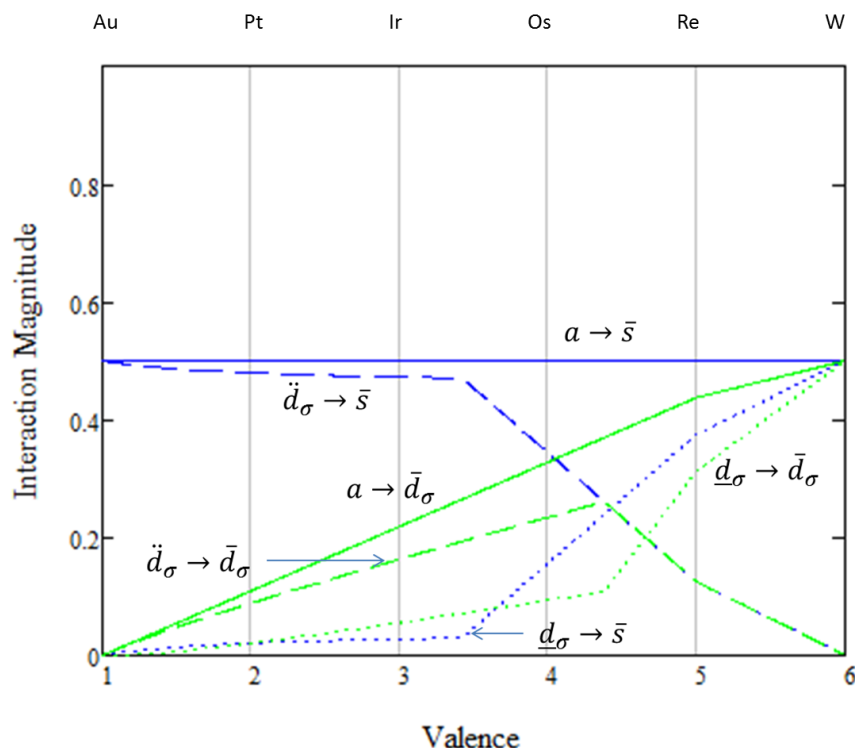


Figure 2.10 Magnitudes of the conjugative interactions between metal atoms. Blue lines correspond to charge transfer into the \bar{s} orbital and green lines correspond to charge transfer into the \bar{d}_σ orbital. Also shown are the individual contributions due to donation \ddot{d}_σ (dashed lines) and \underline{d}_σ (dotted lines).

These zero order interaction magnitudes can then be used along with the orbital magnitudes in Equation (2.13) to calculate the overall conjugative interaction magnitudes using Equation (1.76), the results being plotted in Figure 2.10. The plot also shows the combined magnitude of the $\underline{d}_\sigma^{AB} \rightarrow r$ and $\ddot{d}_\sigma^{AB} \rightarrow r$ interactions ($r = \{\bar{s}, \bar{d}_\sigma^{AB}\}$) given by Equation (1.70). It can be seen that the magnitudes of these two combined interactions and the two $\underline{s} \rightarrow r$ interactions are all limited by the magnitude of the acceptor orbital r . When the acceptor orbital is \bar{s} , these interactions have a constant magnitude of $1/2$ for all metal atom valences since the magnitude of \bar{s} is always equal to this value. In contrast, when the acceptor orbital is \bar{d}_σ^{AB} , the interaction magnitudes increase linearly as the valence of the metal atom increases, reaching maximum magnitude for W. Thus, we can expect there to be two components to the conjugation energy for fcc transition metals – one that is relatively constant for all atoms along a given row of the periodic table and another that increases from right to left, reaching a maximum value for metals in group IV.

If we now look at the $\underline{d}_\sigma^{AB} \rightarrow r$ and $\ddot{d}_\sigma^{AB} \rightarrow r$ interactions separately, we see that at lower metal atom valence, the combined interaction is dominated by donation from the lone pair \ddot{d}_σ^{AB} , with donation from the bonding orbital $\underline{d}_\sigma^{AB}$ occurring only due to the zero order A-B bond as specified in Equation (2.15). As the number of lone pairs on the metal atom decreases with valence, however, a point is reached where the magnitude of the lone pair \ddot{d}_σ^{AB} drops below the magnitude of the acceptor orbital r (minus the magnitude of the $\underline{d}_\sigma^{AB} \rightarrow r$ interaction from the A-B bond), after which, the magnitude of the $\ddot{d}_\sigma^{AB} \rightarrow r$ interaction begins to decrease as the magnitude of the $\underline{d}_\sigma^{AB} \rightarrow r$ increases to take its place. We can see in Figure 2.10 that this occurs between Ir and Os for the $a \rightarrow \bar{s}$ interactions ($a = \{\underline{d}_\sigma^{AB}, \ddot{d}_\sigma^{AB}\}$) and between Os and Re for the $a \rightarrow \bar{d}_\sigma^{AB}$ interactions.

Now that we have the magnitudes of the conjugative interactions, we need to determine the intrinsic interaction energy $\Delta E_{a \rightarrow r}^R$ in Equation (1.65). This term is composed of the square of the resonance integral between the real components of a and r divided by the difference in energy between the two real components

$$\Delta E_{a \rightarrow r}^R = -\frac{1}{2} \frac{|\langle a|H|r \rangle^R|^2}{\varepsilon_r^R + e_r^R - \varepsilon_a^R - e_a^R} \quad (2.16)$$

The resonance integral is simply equal to the resonance integrals between atomic orbitals on atoms A and B, calculated using the σ interaction defined by Equation (2.7)

$$\langle \underline{s}|H|\bar{s} \rangle^R = \langle s|H|s \rangle = b_s^2 V_\sigma \quad (2.17)$$

$$\langle \underline{d}_\sigma|H|\bar{d}_\sigma \rangle^R = \langle \ddot{d}_\sigma|H|\bar{d}_\sigma \rangle^R = \langle d_\sigma|H|d_\sigma \rangle = b_{d^2} V_\sigma \quad (2.18)$$

$$\langle \underline{s}|H|\bar{d}_\sigma \rangle^R = \langle \underline{d}_\sigma|H|\bar{s} \rangle^R = \langle \ddot{d}_\sigma|H|\bar{s} \rangle^R = \langle s|H|d_\sigma \rangle = b_s b_d V_\sigma \quad (2.19)$$

The energies of a and r are determined using Equation (1.66), with the resulting expressions equal to

$$\varepsilon(\underline{s}) = \varepsilon_s + \sqrt{v} b_s V_\sigma \beta(v) \quad (2.20a)$$

$$\varepsilon(\bar{s}) = \varepsilon_s - \sqrt{v} b_s V_\sigma \beta(v) \quad (2.20b)$$

$$\varepsilon(\underline{d}_\sigma) = \varepsilon_d + \sqrt{v} \sqrt{\frac{7}{32}} b_d V_\sigma \beta(v) \quad (2.20c)$$

$$\varepsilon(\bar{d}_\sigma) = \varepsilon_d - \sqrt{v} \sqrt{\frac{7}{32}} b_d V_\sigma \beta(v) \quad (2.20d)$$

$$\varepsilon(\ddot{d}_\sigma) = \varepsilon_d \quad (2.20e)$$

with $\beta(v)$ equal to the energy of the metal-metal bonds in the zero-order structure given by Equation (2.12) normalized by the bond magnitude in Equation (2.2)

$$\beta(v) = \frac{1}{\sqrt{v}} [b_s + (v - 1)b_d] \quad (2.21)$$

As discussed in Chapter 1, these orbital energies are composed of the energy of the original atomic orbital (s or d_σ^{AB}) modified by a term accounting for the bonding in which that orbital participates in the zero order structure. This additional term lowers the energy of the donor bonding orbitals and raises the energy of the acceptor antibonding orbitals, accounting for the fact that these orbitals participate in weaker conjugative interactions because they are already participating in zero order interactions. The energy expression for the lone pair orbital \ddot{d}_σ has no such term because it does not participate in bonding in the zero order structure.

We finally have all of the quantities needed to calculate the energies of the conjugative interactions given by Equation (1.65). As an initial approximation, we use the value of the real orbital interaction energy $\Delta E_{a \rightarrow r}^R$ calculated for Ir as the value for all of the transition metals examined. This way, we can focus solely on the effect of the interaction magnitudes on the

conjugation energy, which is the dominant contribution. The total conjugation energy associated with a single metal-metal bond is equal to the sum of all individual interactions involving electron transfer from orbitals on atom A to atom B ($\Delta E_{A \rightarrow B}^{conj}$) and the analogous sum of interactions involving electron transfer from orbitals on atom B to atom A ($\Delta E_{B \rightarrow A}^{conj}$). Additionally, the zero order A-B bond energy $\Delta E_{\underline{h}_{AB} \rightarrow \bar{h}_{BA}}$ given by Equation (1.73) is subtracted from this value. In a symmetric bond such as the ones in a pure transition metal crystal, these two quantities are equal, giving a total bond conjugation energy of

$$\Delta E_{A-B}^{conj} = \Delta E_{A \rightarrow B}^{conj} + \Delta E_{B \rightarrow A}^{conj} \quad (2.22)$$

$$\Delta E_{A \rightarrow B}^{conj} = \Delta E_{B \rightarrow A}^{conj} = \sum_a \Delta E_{a \rightarrow \bar{s}} + \sum_a \Delta E_{a \rightarrow \bar{d}_\sigma} - \Delta E_{\underline{h}_{AB} \rightarrow \bar{h}_{BA}} \quad (2.23)$$

$$\sum_a \Delta E_{a \rightarrow \bar{s}} = \Delta E_{\underline{s} \rightarrow \bar{s}} + \Delta E_{\underline{d}_\sigma \rightarrow \bar{s}} + \Delta E_{\bar{d}_\sigma \rightarrow \bar{s}} \quad (2.24a)$$

$$\sum_a \Delta E_{a \rightarrow \bar{d}_\sigma} = \Delta E_{\underline{s} \rightarrow \bar{d}_\sigma} + \Delta E_{\underline{d}_\sigma \rightarrow \bar{d}_\sigma} + \Delta E_{\bar{d}_\sigma \rightarrow \bar{d}_\sigma} \quad (2.24b)$$

$$\Delta E_{\underline{h}_{AB} \rightarrow \bar{h}_{BA}} = \frac{1}{4} \times \frac{1}{6} \left[\underbrace{b_s^2}_{s-s} + \underbrace{b_d^2 (v-1)}_{d-d} + 2 \underbrace{b_s b_d \sqrt{v-1}}_{s-d} \right] V_{\sigma_+} \quad (2.24c)$$

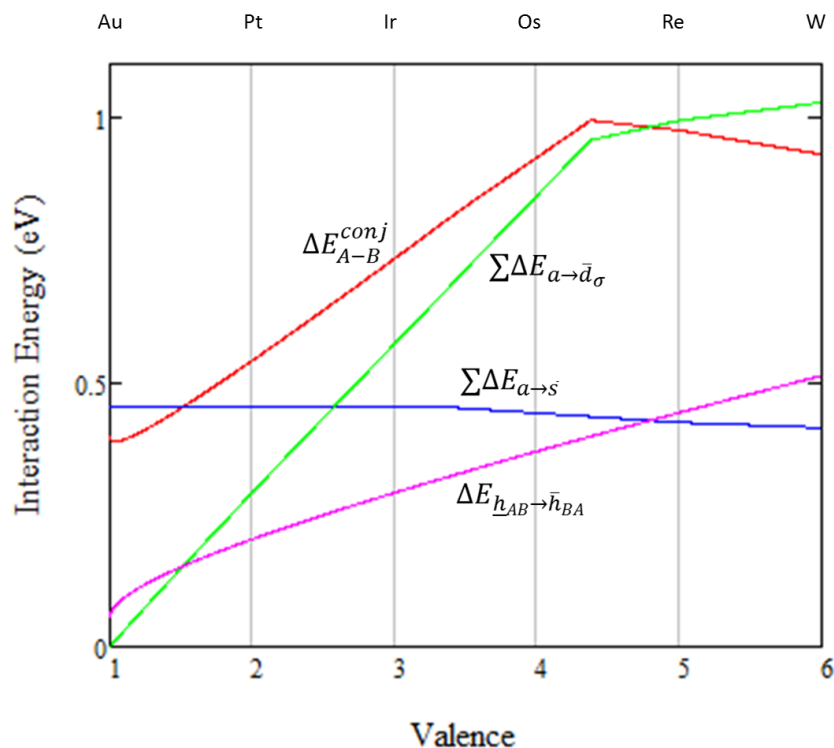


Figure 2.11 Energy of conjugative interactions between metal atoms in the bulk (red). Also shown are the contributions to the total energy in Equation (2.23) involving donation into the s orbital (blue), the d_σ orbital (green), and the zero order term that must be subtracted.

This energy is plotted in Figure 2.11 along with the separate contributions from the interactions involving donation into an \bar{s} orbital and into a \bar{d}_σ orbital as well as the energy subtracted for the zero order A-B bond. The contribution from donation into the \bar{s} orbital is nearly constant for all valences since the magnitude of these interactions is limited by the magnitude of the \bar{s} orbital, which has a constant value of $1/2$. The energy of these interactions does decrease slightly between Ir and W when the magnitude of \bar{d}_σ falls below the magnitude of \bar{s} so that the $\bar{d}_\sigma \rightarrow \bar{s}$ interaction begins to decrease in magnitude with the slightly less stabilizing $\underline{d}_\sigma \rightarrow \bar{s}$ interaction taking its place. The weaker stabilization of the latter interaction is due to the energy of the donor \underline{d}_σ orbital being 2.52 eV lower than the \bar{d}_σ lone pair orbital. The total energy of the interactions involving donation into \bar{d}_σ increases linearly with valence between Au and Os since it is limited by the magnitude of \bar{d}_σ , which was seen to increase linearly with valence in Figure 2.9. Between Os and W, the rate of increase of this interaction energy levels off when the

$\bar{d}_\sigma \rightarrow \bar{d}_\sigma$ interaction begins to decrease in magnitude, being replaced by the weaker $\underline{d}_\sigma \rightarrow \bar{d}_\sigma$ interaction as was seen in Figure 2.10.

As mentioned in Chapter 1, the conjugation energy associated with the zero order A-B bond is equal to half the energy of the zero order bond calculated by Equation (2.12), and thus increases with metal atom valence. Subtracting this quantity from the total conjugation energy cancels some of the increase in energy of the $a \rightarrow \bar{d}_\sigma$ interactions as the metal atom valence increases. This leads to only a 40% increase in the conjugation energy from its minimum value on Au to its maximum value on Os. After reaching its maximum value on Os, the conjugation energy again decreases between Os and W due to the leveling off of the $a \rightarrow \bar{s}$ interaction energy in this region discussed in the previous paragraph.

Comparing Figure 2.11 and Figure 2.7, we see that the conjugation energy varies much less with metal atom valence than the zero order bond energy. This behavior has two causes. The first cause is that as the valence of the metal atom increases, so does the magnitude of the zero order A-B bond. Since the orbitals involved in this zero order bond cannot participate in conjugation (accounted for by subtracting the energy given by Equation (1.73) from the total conjugation energy), there is less available magnitude of the remaining orbitals to participate in conjugation. We saw an extreme example of this for the C-C bond of ethane in Chapter 1 – since the C-C σ bond has a magnitude of unity, there was barely any σ conjugative stabilization, almost all of it coming instead from π interactions (which we have so far ignored in the metal).

The second cause of the relatively small increase in conjugation energy with metal atom valence in Figure 2.11 is that the addition of each d orbital to the bonding space used to form the acceptor orbital \bar{d}_σ from one metal atom to the next has much less of an ability to participate in conjugative interactions than the \bar{s} orbital that is present to the same extent on all metal atoms. This is due to the angular dependence of the amplitude of the d orbital compared to the s orbital, which has no angular dependence. Each increase in the metal atom valence adds almost equally to the magnitudes of the d_σ orbital, the two d_π orbitals, and the two d_δ orbitals in the bonding space, but only the d_σ orbital can participate in strong conjugative interactions with a given neighboring metal atom. Contrast this with the spherically symmetric s orbital, which interacts

equally well with all neighboring atoms. Thus, the increase in conjugation energy due to addition of d orbitals to the bonding space is much less than would be expected if the added d orbitals had spherical symmetry like the s orbital – in that case, the conjugation energy would be nearly proportional to the metal atom valence. We will see in Chapter 3 that this type of behavior plays a very important role in determining the binding energy of adsorbates to a transition metal surface.

Crystal cohesive energy

The total cohesive energy of a transition metal is the sum of the zero order bond energies given by Equation (2.12) and the conjugation energy given by Equation (2.22). Since there are six metal-metal bonds for each metal atom in the crystal, the zero-order cohesive energy of the crystal per atom, referenced to separated atoms in sd^{N-1} ground states, is

$$\Delta E_{crys}^0 = 6 \Delta \varepsilon_{AB} \quad (2.25)$$

where $\Delta \varepsilon_{AB}$ is the zero-order bond energy given by Equation (2.12). Adding to this the conjugation energy for charge transfer across each bond given in Equation (2.22)(1.65) leads to a total cohesive energy of

$$\Delta E_{crys} = 6 [\Delta \varepsilon_{AB} + \Delta E_{M-M}^{conj}] \quad (2.26)$$

It should be noted that this cohesive energy contains only the contribution of covalent bonding and does not include contributions from Pauli repulsion and electrostatic interactions, which will certainly modify the results.³⁹ Figure 2.12 shows how the cohesive energy of the crystal changes between Au and W. It is composed of a zero-order term that increases continuously with valence and a conjugation term that increases between Au and Os and decreases between Os and W. Between Au and Os, both the zero order energy and the conjugation energy increase with valence, leading to a cohesive energy that increases nearly linearly with valence in this region. Between Os and W, the decrease in conjugation energy cancels out much of the increase in zero order energy, resulting in a total cohesive energy that increases more slowly in this region. In

Au, most of the cohesive energy comes from conjugation, but as the valence increases, conjugation contributes an increasingly smaller fraction of the cohesive energy as the zero-order contribution becomes larger, with both contributing approximately equal amounts on Re and W.

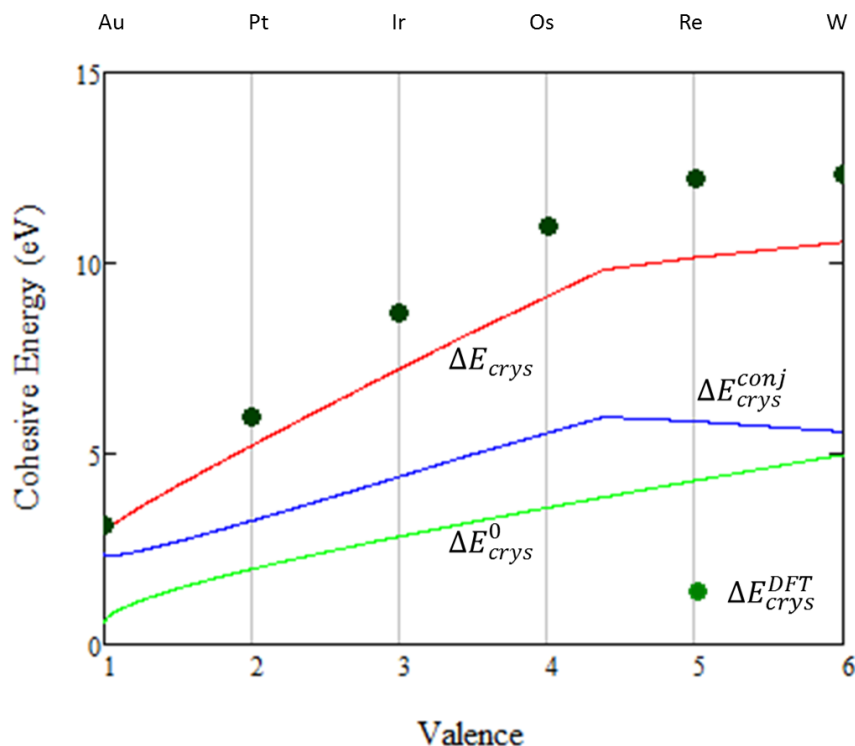


Figure 2.12 Cohesive energy of the fcc transition metal crystals (red) as well as the contributions from the zero order (green) and conjugative (blue) components. Values from DFT calculations (green dots) are shown for comparison.

For comparison, the cohesive energies calculated using DFT with the procedure in Appendix B are shown in Figure 2.12 along with the value calculated from Equation (2.26). The DFT calculated values are slightly higher than the values calculated from the model, although the trend is nearly the same. The discrepancy is likely due to neglect of Pauli repulsion and electrostatic interactions as well as overestimation of the conjugation energy due to the approximations inherent in its calculation using second order perturbation theory. This indicates that our model based on local bonding and semi-local conjugative interactions captures most of the bonding interactions in a metallic system and implies that the interactions that control the chemistry of metals are at most semi-local in nature, not completely nonlocal as previous models

would suggest (although this does not mean that other properties of metals such as electrical conductivity are not dependent on long range interactions).

2.2 Bonding in Surfaces

We now examine the modification of the metal-metal bonding in the bulk upon cleavage of a surface. In this treatment, we ignore the observed relaxation of atoms near the surface from their bulk positions as well as the possibility of complete reconstruction of the surface structure that are known to occur upon surface cleavage.¹² As mentioned at the beginning of this chapter, the fcc symmetry present in the bulk, that we utilized to describe the electronic structure in the previous section, is broken by the cleavage of a surface. This has the potential to make the bonding in surfaces more complicated than in the bulk. The primary effect of this is the breaking of metal-metal bonds upon cleavage of the surface. This is shown in Figure 2.13 for the (111) surface where it can be seen that three bonds are broken to each metal atom in the surface so that these atoms have a coordination number of nine instead of twelve as in the bulk. In order for the surface atoms to remain bond saturated by fulfilling the sum rule in Equation (1.44), the bonds to some or all of the nine remaining ligands must increase in magnitude to compensate for the loss of the other three bonds.

In an accurate electronic structure calculation (performed self-consistently) the orbital energies and resonance integrals associated with atoms in the surface layer (given in Table 2.1 for the bulk) will change when the surface is cleaved. In the Extended Hückel model employed in this work, these changes do not occur since these parameters are independent of the environment surrounding a given atom. While this will lead to additional differences between the model and a full electronic structure calculation, it is likely that this will not affect the qualitative behavior of the trends we are interested in. This approach is taken in other work as well, where it is presumed that the qualitative features of the model are not affected.^{11,12}

one group of three ligands in the subsurface plane. To restore bond saturation of the surface atoms, then, one can either increase the magnitude of the bonds to the surface ligands or increase the magnitude of the bonds to the subsurface ligands, as well as any combination of the two. It turns out that it is much less complicated to increase the magnitude of the bonds to the subsurface ligands. To see why, recall that in the bulk, each pair of collinear ligands forms bonds with a single hybrid on the central metal atom, as was seen in Figure 2.3. Since the subsurface ligands are collinear to the three ligands that were removed when the surface was cleaved, the hybrid on the surface atom that was bound to one of the removed ligands has the same composition as the hybrid bound to one of the subsurface ligands. Therefore, an increase in the magnitude of the bonds to these ligands will not change the composition of any of the hybrids on the surface atoms – we are simply redistributing this hybrid between the two ligands. This is advantageous because most of the results obtained for bonding in the bulk will apply unmodified to the surface. In fact, the zero order binding energy does not even change upon cleavage of the surface – all of the surface energy comes from the loss of conjugative interactions between the two cleaved surface layers.

To restore bond saturation of the surface atoms after surface cleavage, the bonds between the surface and subsurface layers must double in magnitude. This has the negative consequence of bond oversaturating the subsurface atoms. In order to maintain the sum rule, the magnitudes of the other bonds to the subsurface atoms must decrease. If we again constrain these changes to the chains of collinear ligands that were broken when the surface was cleaved, we get the structure shown in Figure 2.13 where the magnitudes of odd bonds along the chain double in magnitude while the magnitudes of the even bonds go to zero. Thus the semi-infinite slab is composed of a stack of non-bonded two-layer slabs. This seems unrealistic because cleavage of a surface should only affect the electronic structure in the first few layers of atoms – it would be unphysical for bonds deep within the bulk to be affected by the presence of a surface. While the conjugative interactions will counteract this and actually restore the original electronic structure of the bulk deep within the surface (although it will be proportioned differently than in the bulk between zero order bonding and conjugative bonding), it is still disconcerting that the zero order electronic structure is so unrealistic.

The issues just discussed pose a major problem with the present scheme for restoring bond saturation after surface cleavage – however, we are not interested in the electronic structure deep within the bulk if we are examining chemisorption to the surface. In fact, almost all ab-initio calculations of chemisorption model the semi-infinite surface as consisting of a few layers of metal atoms surrounded by vacuum on both sides¹. We therefore reconcile with the complications addressed in the previous paragraph by examining adsorption on a two layer slab in the next chapter instead of on a semi-infinite surface. Although the absolute values of the chemisorption energy will likely be different than those on a thicker slab, we would expect that these are only small perturbations and have little impact on periodic trends in chemisorption.¹

On a final note, a more realistic (but less practical) model of the semi-infinite surface would be to restore the bond saturation of the surface atoms by increasing the magnitudes of the bonds between surface atoms. Using this scheme, restoring the bond saturation of one surface atom will not cause any other atoms to become oversaturated – it actually helps the neighboring surface atoms to restore their bond saturation as well. This has the advantage of restricting changes in the zero order electronic structure to the first layer. The disadvantage of this scheme, as mentioned earlier, is that the hybrids forming the new bonds between surface atoms will not have the same composition as they did in the bulk. The modified hybrids would no longer be directed along the bond axes connection pairs of surface atoms, and instead, would be bent out outwards with respect to the plane of the surface. This is not a major problem fundamentally, but it makes the model more cumbersome to describe.

2.2.2 Surface Energy

The zero order surface energy of the two-layer slab can be calculated by envisioning the cleavage of the slab from the bulk as shown in Figure 2.14. Since this process creates two new surfaces, the surface energy is equal to half the energy lost by this cleavage. If the surface contains N atoms, then there will be $3N$ bonds joining each pair of neighboring layers in the bulk. Creating the slab involves making two cuts in the bulk to free the slab which involves breaking $6N$ metal-metal bonds, followed by annealing the two remaining sections of the bulk

back together to restore $3N$ of the metal-metal bonds. Thus, creating the slab requires a net total of $3N$ bonds be broken.

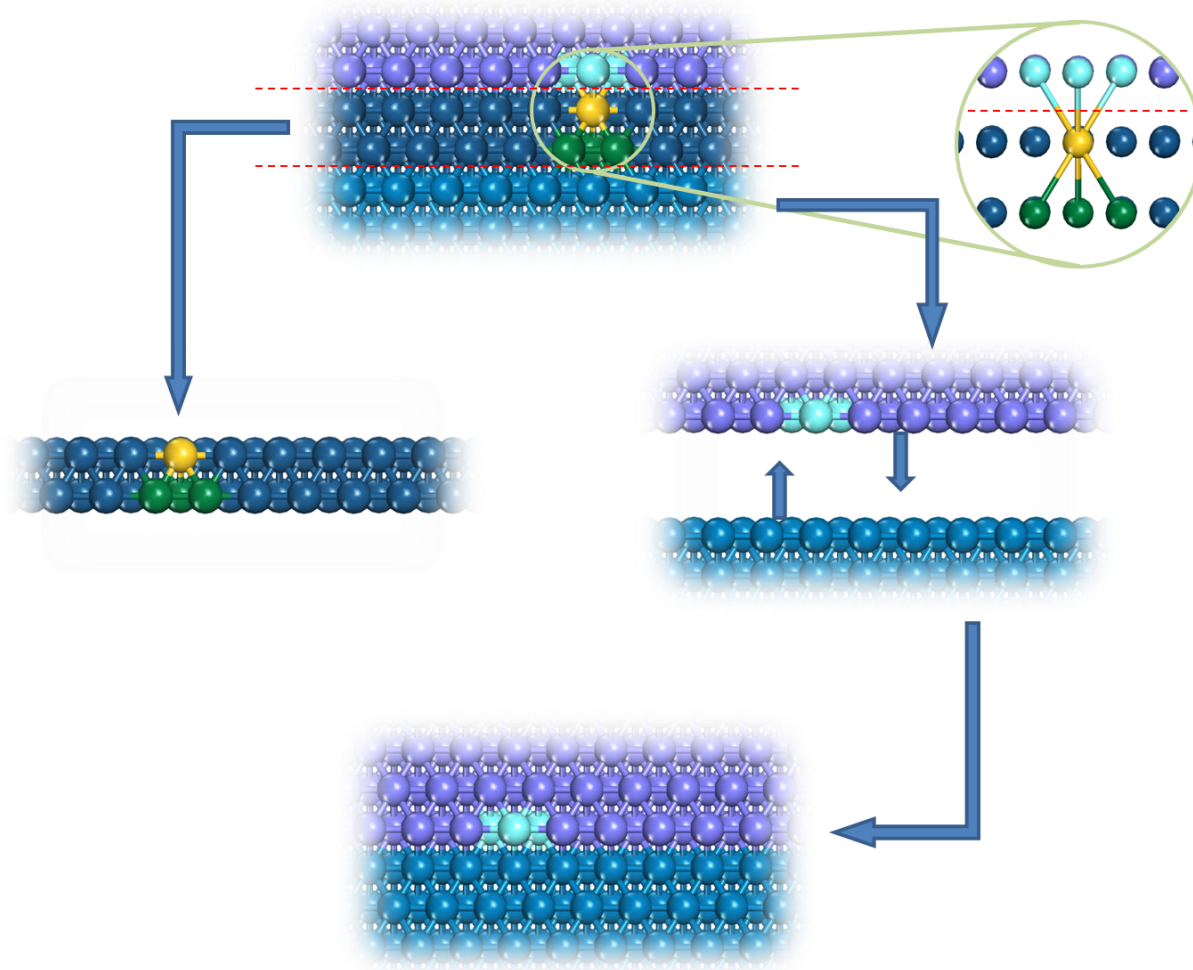


Figure 2.14 Cleavage of a two-layer slab from the bulk occurs in two steps. First, two cuts are made in the bulk to remove the slab, breaking three bonds for every atom in the slab. This leaves a gap in the bulk, which is then annealed, forming three bonds for every pair of atoms in the slab.

As previously discussed, when the two-layer slab is isolated from the bulk, the $3N$ bonds between the two layers double in magnitude to make up for the loss of the bonds between the slab and the remaining bulk. This results in a doubling of the bond energies of these bonds, which exactly cancels out the loss in bond energy from the $3N$ bonds that were broken to create

the slab. Therefore, there is no change in zero-order energy to cut the slab from the surface, and the surface energy is due entirely to a loss of conjugative interactions.

For each of the $3N$ inter-slab bonds that were broken to create the slab, the energy of the conjugative interactions across that bond (ΔE_{M-M}^{conj} , given by Equation (2.22)) will be lost. Since two surface atoms are created for every three of these bonds that are broken, the resulting contribution to the surface energy is

$$\Delta E_{surf}^{inter} = -\frac{3}{2} \Delta E_{M-M}^{conj} \quad (2.27)$$

Recall that this energy increases from Au to a maximum at Os before decreasing from Os to W, as shown in Figure 2.11.

An additional loss of conjugation energy occurs due to the doubling of the magnitude of the zero order bonds between the two surface layers. Since the orbitals participating in zero order bonding cannot participate in conjugation, increasing the magnitude of these bonds leads to a corresponding decrease in the associated conjugation energy. This decrease is equal to the doubling of the zero order bond energy in Equation (2.24c) that is subtracted from the total conjugation energy to account for this effect and increases from Au to W as the zero order bonds become stronger as shown in Figure 2.15

$$\Delta E_{surf}^{intra} = -\frac{3}{2} \Delta E_{\underline{h}_{AB} \rightarrow \bar{h}_{BA}} \quad (2.28)$$

On W, these bonds have magnitudes of unity so that the conjugation energy is particularly weak, similar to what was seen for ethane in Chapter 1.

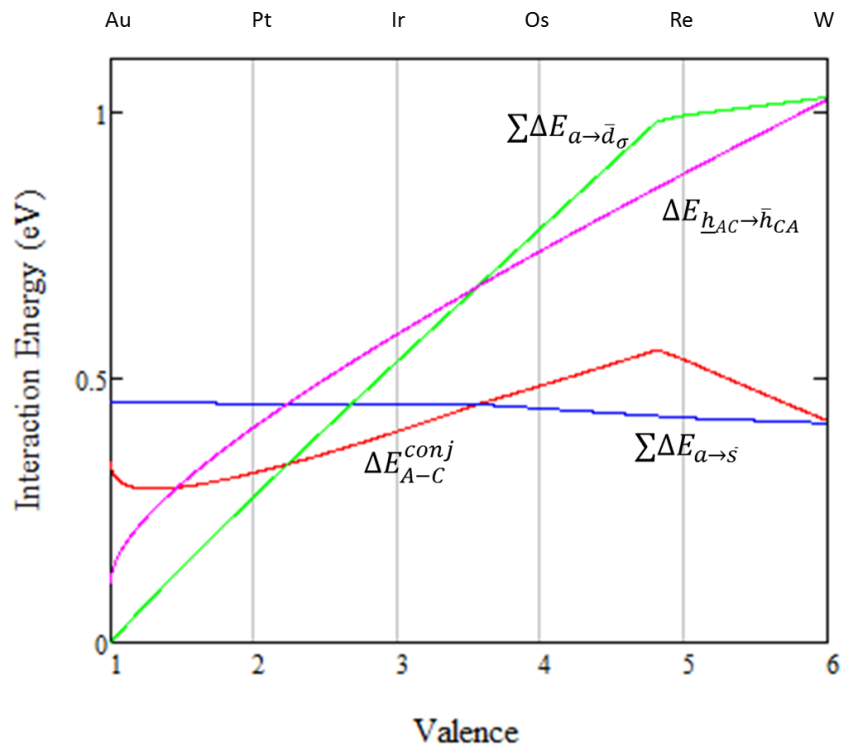


Figure 2.15 Energies of conjugative interactions between a surface atom and a neighboring subsurface atom (red). Also shown are the contributions to the total energy in Equation (2.23) involving donation into the s orbital (blue), the d_{σ} orbital (green), and the zero order term that must be subtracted.

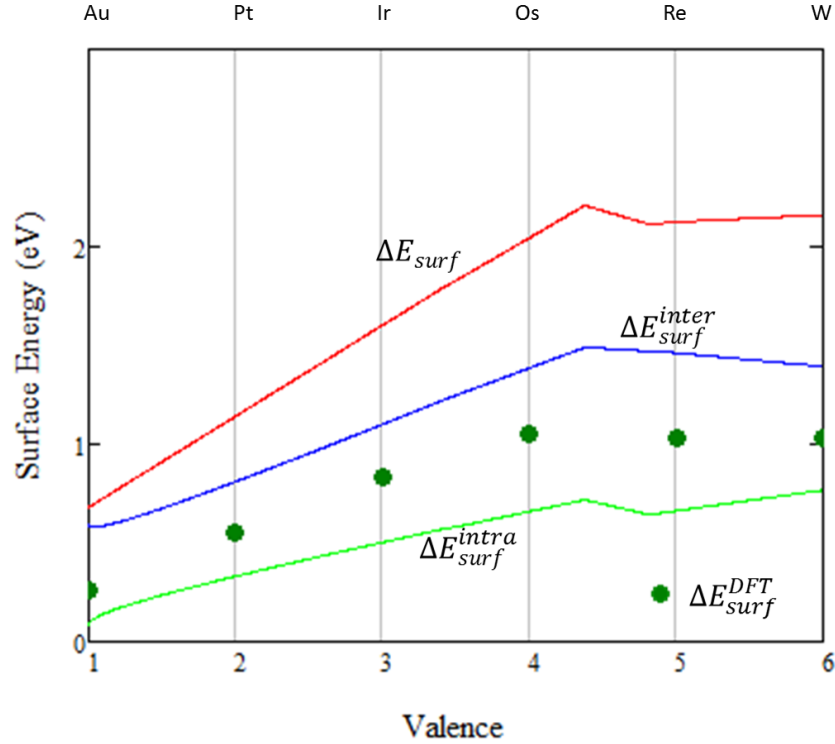


Figure 2.16 Loss of bond energy due to surface formation (red) with contributions from breakage of inter-slab bonds (blue) and reduction of conjugation in intra-slab bonds (green). DFT values (green dots) are shown for comparison.

Combining the two contributions to the surface energy from Equations (2.27) and (2.28) leads to a total surface energy of

$$\Delta E_{surf} = -\frac{3}{2}(\Delta E_{M-M}^{conj} + \Delta E_{\underline{h}_{AB} \rightarrow \bar{h}_{BA}}) \quad (2.29)$$

As seen in Figure 2.16, this energy increases from Au to Os and then levels out and remains nearly constant between Os and W. The increase between Au and Os is due to increases in both the conjugation energy of the broken inter-slab bonds and the decrease in conjugation energy of the intra-slab bonds upon surface formation. The surface energy is constant between Os and W because the decrease in conjugation energy of the broken inter-slab bonds cancels out the increase in conjugation energy lost from the intra-slab bonds. Fundamentally, the leveling out of the surface energy between Os and W, as well as the leveling out of the cohesive energy seen in

the last section, is due to the reduction in magnitude of the lone pair donor orbitals below the point where they are able to saturate the acceptor orbitals, which occurs between Os and Re. Figure 2.16 also shows the DFT values of the surface energy calculated using the procedure in Appendix B. These values are considerably smaller than the values calculated by the model, and also only increase in magnitude from Au to Os by about half as much. The shape of the trend, however, is still the same as the trend for the model, indicating that the model captures the qualitative features that control the metal-metal bonding. As with the cohesive energy, the discrepancy between the model and DFT values of the surface energy may be due to neglect of Pauli repulsion and electrostatic interactions as well as an overestimation of the conjugation energy since it was calculated only to second order in perturbation theory.

Chapter 3 – Local Bonding Description of Chemisorption on 5d Transition Metal Surfaces

Now that we have an understanding of the bonding within a transition metal crystal in both the bulk and at the surface, we would like to use the local bonding formalism we have developed to study how adsorbates bind to transition metal surfaces. As seen in Figure 3.1, the adsorption energies calculated by DFT have very different behavior for different species. The binding energy of atomic hydrogen is seen to strengthen significantly between Au and Pt, level out between Pt and Os, and then weaken going from Os to Re. Other species such as atomic oxygen and hydroxyl have very different behavior in which the adsorption energy strengthens continuously between Au and Re. These different qualitative behaviors of different adsorbates cannot be explained by employing the commonly used d-band center model of Hammer and Nørskov.^{7,8} This is due to the fact that this model predicts that the binding energies of all adsorbates should scale linearly with the energy of the center of the d-band with respect to the Fermi level. This implies that the binding energies of two different adsorbates should qualitatively behave the same way as the composition of the metal surface changes, which is shown in Figure 3.1 to be clearly not the case. We would ultimately like to see if we can rationalize these different behavior using the bonding model we have developed.

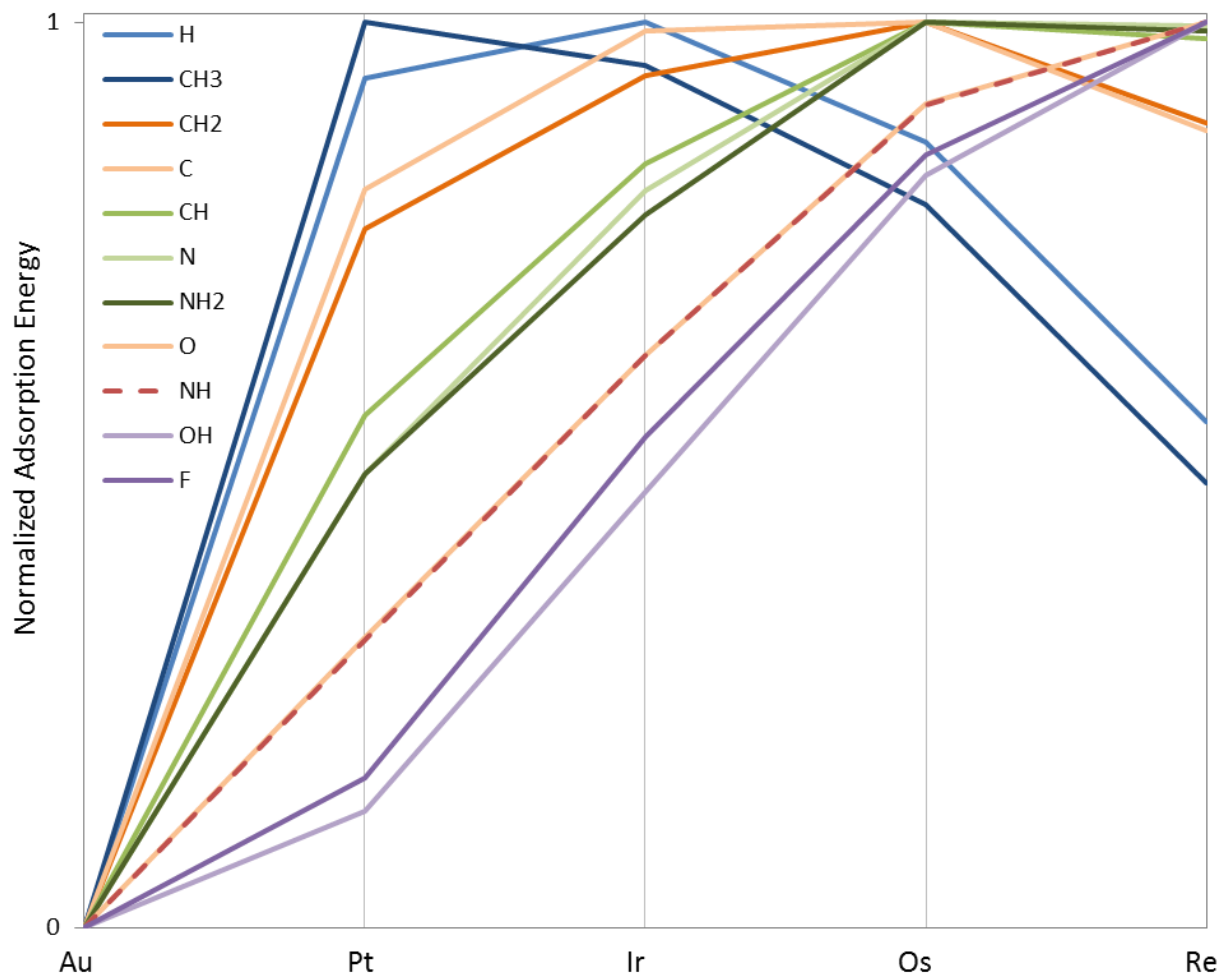


Figure 3.1 Adsorption energies of different species on the (111) surface of fcc 5d transition metals calculated with DFT using the method in Appendix B. Values for a given adsorbate have been normalized to the maximum adsorption energy for that adsorbate across all five metal atoms. The structures of these adsorbates are shown in Appendix C. NH_2 is constrained to have planar geometry while NH and OH are constrained to have linear geometry. Note that the lines for O and NH are nearly identical.

3.1 Chemisorption of Atomic Hydrogen

Atomic hydrogen, with its single unpaired electron in an s orbital, is the simplest of the adsorbates that fall into the category of strong chemisorption. It therefore serves as a good starting point for understanding strong chemisorption to transition metal surfaces using the

concepts of local bonding. After examining atomic hydrogen, we will apply the insights we have gained towards the chemisorption of more complicated adsorbates in section 3.2.

3.1.1 Zero order bonding

Since the hydrogen atom has one unpaired electron, it is bond saturated by forming a full σ bond with a surface metal atom in the zero order electronic structure, leading to an increase in the total binding energy of the system due to the formation of this new bond. At this point, the metal atom bound to the hydrogen is bond oversaturated so in order to maintain the sum relation in Equation (1.44), the magnitudes of the bonds it forms with its neighbors must decrease by a total of one unit, leading to a decrease in binding energy that partially offsets the increase due to formation of the metal-hydrogen bond. This reduction in metal-metal bonding then leads to bond undersaturation of the metal atoms surrounding the adsorption site, requiring that the magnitudes of other nearby bond be adjusted to maintain bond saturation for all metal atoms, partially cancelling out the loss in binding energy due to the original reduction in metal-metal bonding.

If instead of using a model where one hydrogen atom is adsorbed on an infinite two-layer slab, we use a model where both sides of the slab are covered with a monolayer of hydrogen as shown in Figure 3.2, the translational and inversion symmetry of the clean two-layer slab is retained and the complications due to bond undersaturation in the metal atoms surrounding the adsorption site do not occur since the loss in metal-metal bonding is made up by the formation of bonds to hydrogen for all the metal atoms. We will therefore use this simpler model for the remainder of this chapter. The adsorption energy predicted by this model will differ from the value for a single hydrogen atom on an infinite surface because we are implicitly including through-surface interactions between the neighboring adsorbates (although through-space interactions are not included). However, through-surface interactions between adsorbates bound to neighboring metal atoms are known to be weak (as long as the each metal atom is bound to at most one adsorbate) compared to the magnitude of the adsorption energy¹ so it is expected that the removal of these interactions would not change the qualitative nature of the bonding structure

around the adsorption site and we can still gain important insights that are relevant to adsorption at any coverage.

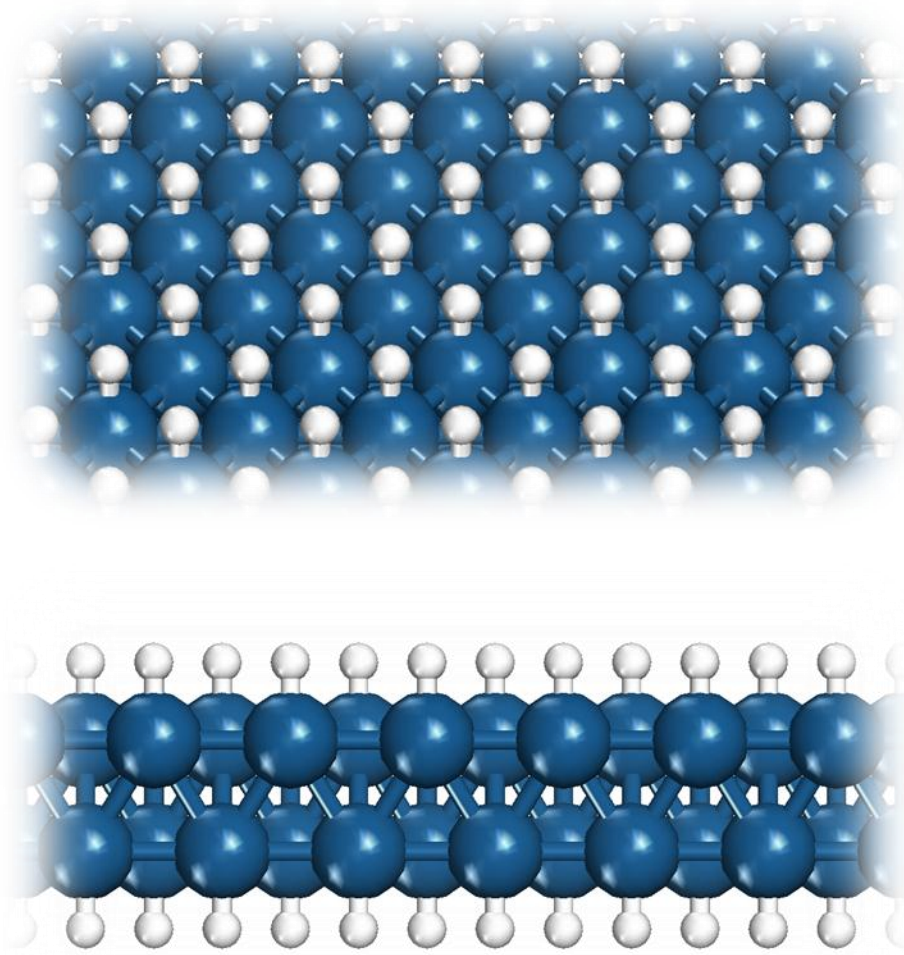


Figure 3.2 Two-layer infinite slab with a monolayer of hydrogen adsorbed on each side

Adsorption energy in the surface-molecule limit

In the surface molecule limit, the chemisorption process can be broken down into the three steps shown in Figure 3.3. The first process involves the decomposition of the two-layer slab into the constituent metal atoms. This results in an increase in total energy equal to the cohesive energy of the slab, ΔE_{slab} , due to breaking of the metal-metal bonds. The second process involves formation of one or more bonds between each adsorbate and metal atom to form a surface

molecule, leading to a decrease in total energy equal to ΔE_{M-A} . Finally, the slab is rebuilt from the surface molecules, resulting in the formation of metal-metal bonds and a decrease in total energy equal to $\Delta E'_{slab}$. This allows us to express the adsorption energy of a fragment as

$$\Delta E_{ads} = \Delta E_{M-A} + \Delta E'_{slab} - \Delta E_{slab} = \Delta E_{M-A} + \Delta \Delta E_{slab} \quad (3.1)$$

Thus, the adsorption energy is equal to the formation energy ΔE_{M-A} of the surface molecule between the adsorbate and a single metal atom in isolation plus the change in cohesive energy of the metal slab $\Delta \Delta E_{slab}$. We will begin by examining the surface molecule formation energy and then turn to the more complicated change in cohesive energy in the remainder of this section.

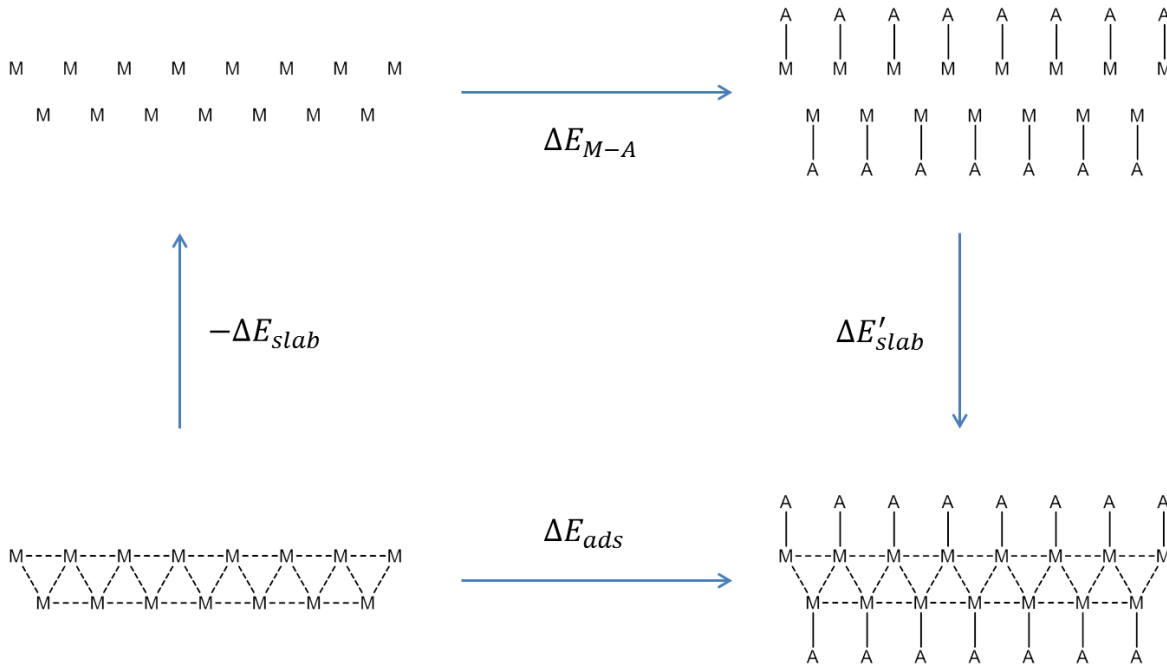


Figure 3.3 The chemisorption process can be broken down into three steps – first the slab is separated into its constituent metal atoms accompanied by a loss of binding energy equal to ΔE_{slab} ; then each metal atom bonds to an adsorbate to form a metal-adsorbate “molecule”, resulting in an increase in binding energy of ΔE_{M-A} ; finally the metal-adsorbate molecules are brought back together to reform the slab, leading to an increase in binding energy of $\Delta E'_{slab}$. This leads to the adsorption energy ΔE_{ads} given by Equation (3.1).

Formation of the surface molecule

In the surface molecule, the s orbital on the hydrogen atom forms a bond with an sd hybrid h_a on the single metal atom. This hybrid orbital is formed from the metal s orbital and a d orbital oriented towards the hydrogen that will be called d_a

$$h_a = a_s s + a_d d_a \quad (3.2a)$$

A second hybrid h_n is also formed from the metal s and d_a orbitals that does not form any bond with the hydrogen atom

$$h_n = a_d s - a_s d_a \quad (3.2b)$$

Both of these hybrid orbitals are shown in Figure 3.4 where it can be seen that h_a is concentrated along M-H bond axis while h_n is concentrated in a ring in the plane of the surface. These orbitals have energies given by Equation (1.2) of

$$\varepsilon(h_a) = a_s^2 \varepsilon_s + a_d^2 \varepsilon_d = \varepsilon_d + a_s^2 \Delta \varepsilon_{sd} \quad (3.3a)$$

$$\varepsilon(h_n) = a_d^2 \varepsilon_s + a_s^2 \varepsilon_d = \varepsilon_d + a_d^2 \Delta \varepsilon_{sd} \quad (3.3b)$$

where ε_s and ε_d are the energies of the metal s and d orbitals, with $\Delta \varepsilon_{sd} = \varepsilon_s - \varepsilon_d$. The metal-hydrogen bonding orbital is then formed from h_a and the s orbital on the hydrogen as shown in Figure 3.5 and has the form

$$\sigma_{MH} = c_M h_a + c_H s_H \quad (3.4)$$

while the corresponding antibonding orbital has the form

$$\sigma_{MH}^* = c_H h_a - c_M s_H \quad (3.5)$$

where c_M and c_H are the polarization coefficients that determine the electron distribution between the metal orbital and the hydrogen atom.

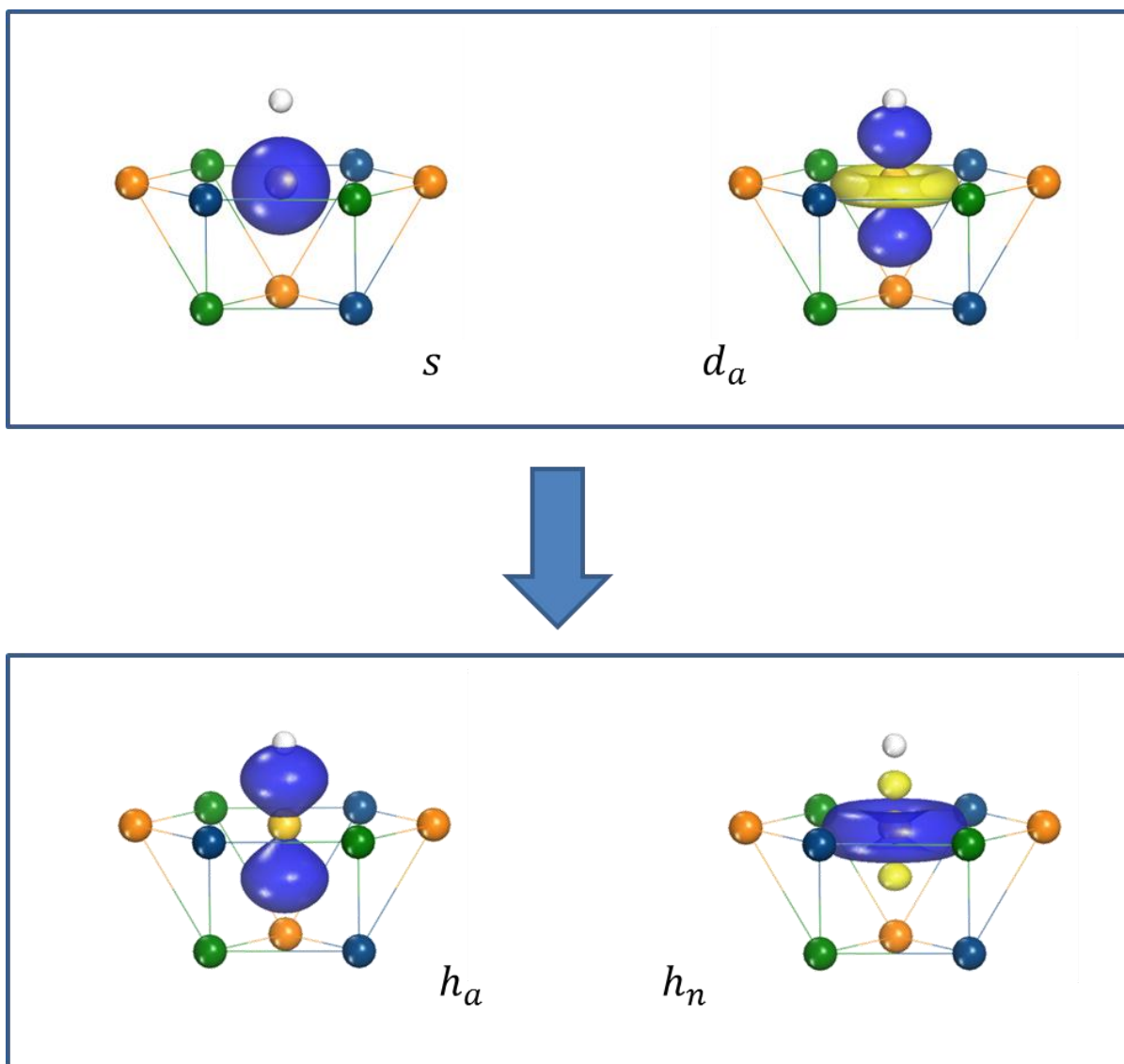


Figure 3.4 The s orbital and a d orbital aligned with the metal-hydrogen bond axis, called d_a , combined to form two new orthogonal orbitals, h_a and h_n . The orbital h_a is used to form a bond with hydrogen while h_n participates in metal-metal bonding.

The total change in binding energy due to formation of the metal-hydrogen bond is equal to the sum of the bond formation energy $\Delta\epsilon_{MH}$ and the hybridization energy of the metal atom $\Delta\epsilon_M$ (Equation (1.14))

$$\Delta E = \Delta \varepsilon_{MH} + \Delta \varepsilon_M \quad (3.6)$$

The bond formation energy is given by Equation (1.11) and is equal to the sum of a covalent term and an ionic term

$$\Delta \varepsilon_{MH} = - \underbrace{\overbrace{(c_M^2 - c_H^2)}^{\text{ionicity}} [\varepsilon(h_a) - \varepsilon_{s_H}]}_{\text{ionic}} - \underbrace{\overbrace{2 c_M c_A}_{\text{covalency}} 2 V_{MA}}_{\text{covalent}} \quad (1.11)$$

where ε_{s_H} is the energy of the hydrogen s orbital and V_{MA} is the resonance integral between h_a and the hydrogen s orbital given by

$$V_{MA} = a_s \langle s|H|s_H \rangle + a_d \langle d|H|s_H \rangle \quad (3.7)$$

which is determined by Equations (1.10) and (3.2).

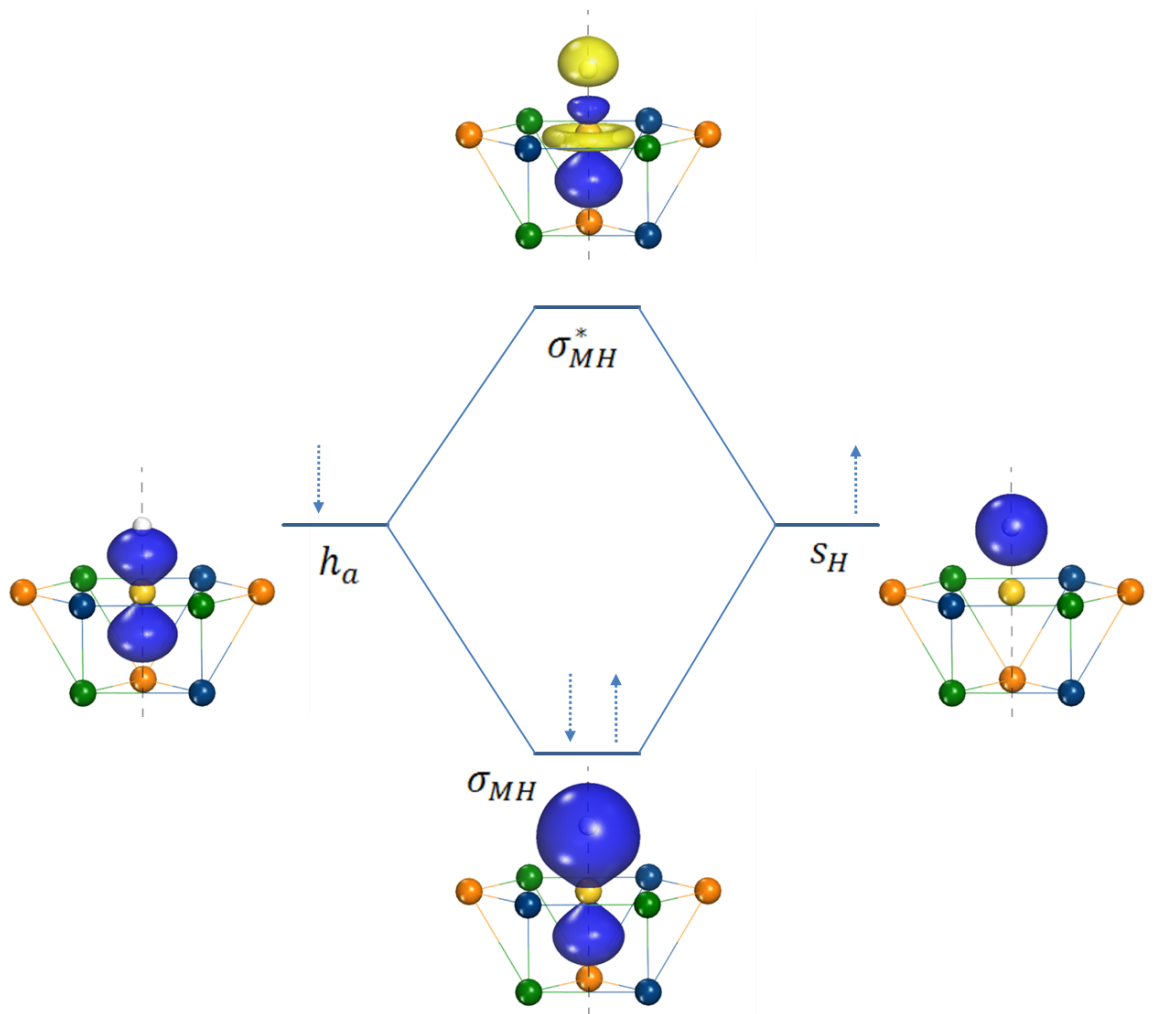


Figure 3.5 The metal-hydrogen bond is formed from an sd^n hybrid h_a on the metal atom interacting with the s orbital on the hydrogen atom.

The hybridization energy of the metal atom is given by Equation (1.15)

$$\Delta\varepsilon_M = \varepsilon_s - \varepsilon(h_a) + f_n[\varepsilon_d - \varepsilon(h_n)] \quad (3.8)$$

where f_n is the occupancy of h_n in the hybridized atom. The reference electron configuration of the metal atom used to define the hybridization energy is sd^{v-1} . Following hybridization, the electron configuration becomes $h_a h_n^{f_n} d^{v-1-f_n}$. One electron occupies h_n for all transition metal atoms except for the coinage metals – in these atoms, the four unhybridized d orbitals are

completely filled with eight of the eleven valence electrons so that h_n must contain two electrons. Using the energies of h_a and h_n in Equation (3.3) gives

$$\Delta\varepsilon_M = a_d^2(1 - f_n)\Delta\varepsilon_{sd} \quad (3.9)$$

We can see that for all transition metal atoms other than the coinage metals, the hybridization energy is zero since $f_n = 1$; for the coinage metals it is equal to

$$\Delta\varepsilon_M = -a_d^2\Delta\varepsilon_{sd} \quad (3.10)$$

As the d character of h_a increases, the d character of h_n decreases and the s character increases, leading to an increase in binding energy since the energy of the s orbital is higher than the energy of the d orbitals. Therefore, any d character in the metal-hydrogen bond will lead to a decrease in binding energy.

The forms of the metal atom hybrids h_a and h_n along with the polarization coefficients of the metal-hydrogen bonding orbital are determined by maximizing the binding energy of the system in Equation (3.6). The resonance integrals and orbital energies that appear in this equation are shown in Table 2.1. If we ignore for the moment the variation in these parameters between the different metals, there is no change in the expression for the metal-adsorbate bond energy in Equation (1.11) from one metal to the next. The only part of the total binding energy that changes between different metals is the hybridization energy in Equation (3.9) which is given by Equation (3.10) for the coinage metals and is zero for the other metals. We therefore obtain two solutions for σ_{MH} – one for the coinage metals and one for the others. Using the parameters for Ir in Table 2.1 for all the metals, the change in binding energy upon formation of the metal-hydrogen bond is -6.03 eV for the coinage metals and -7.08 eV for the other metals. The bonding orbital is moderately polarized towards the metal atom, with a charge transfer of 0.23 electrons from the hydrogen atom to the metal atom for the non-coinage metals and a charge transfer of 0.15 electrons for the coinage metals.

The metal hybrid h_a has greater d character (67%) than s character for the non-coinage metals, which can be attributed to the greater value individual resonance integral between the hydrogen s orbital and the metal d orbital (-2.69 eV) compared to the resonance integral with the metal s orbital (-2.16 eV). The composition of h_a on the coinage metals is richer in s character (64%) than d character due to the energy required to promote part of an electron from d_a to the metal s orbital so that d_a can participate in bonding. This leads to a less favorable interaction between h_a and the hydrogen s orbital since the hybrid does not have the optimal composition of the hybrids in the non-coinage metals. The reduction in this interaction along with the hybridization energy leads to the lower surface molecule formation energy to coinage metal atoms compared to the non-coinage metal atoms.

Adsorption induced changes in metal atom hybridization

The formation of a full bond between the metal hybrid h_a and the hydrogen s orbital removes h_a from participating in metal-metal bonding, causing a change in the composition, shape, and magnitude of the metal-metal bonding hybrids that were previously used in the bulk. To discuss hybridization in the presence of the adsorbate layer, it is convenient to use a different basis of atomic orbitals than those presented in Figure 2.2 for the bulk metal and metal slab. In this new basis set, shown in Figure 3.6, the z axis used to define the canonical set of d orbitals is oriented along the metal-hydrogen bond so the d_{z^2} orbital corresponds to the d orbital that bonds with hydrogen, d_a . Two other atomic d orbitals, d_{xz} and d_{yz} , have π symmetry with respect to the M-H bond while the remaining two, d_{xy} and $d_{x^2-y^2}$, have δ symmetry. As discussed in the previous section, d_a and the metal s orbital combine to form h_a and h_n , of which only the latter participates in metal-metal bonding. This leaves us with the orbital set $\{h_n, d_{xz}, d_{yz}, d_{xy}, d_{x^2-y^2}\}$ for forming metal-metal bonds.

The hybrids used for forming metal-metal bonds in the bulk shown in Figure 2.3 cannot be constructed from the present set, due to the removal of h_a . The formation of the metal-hydrogen bond breaks the fcc symmetry around the metal atom so that it is no longer possible to form equivalent surface and subsurface hybrids. By comparing the shapes of the new orbital set in Figure 3.6 with the positions of the metal atoms, we can see that h_n , d_{xy} , and $d_{x^2-y^2}$ are mainly

oriented towards atoms in the surface layer while d_{xz} and d_{yz} are oriented towards atoms in the subsurface layer. We will therefore use the first three orbitals to form metal-metal bonds within the surface layer and the last two orbitals to form metal-metal bonds between the surface layer and the subsurface layer.

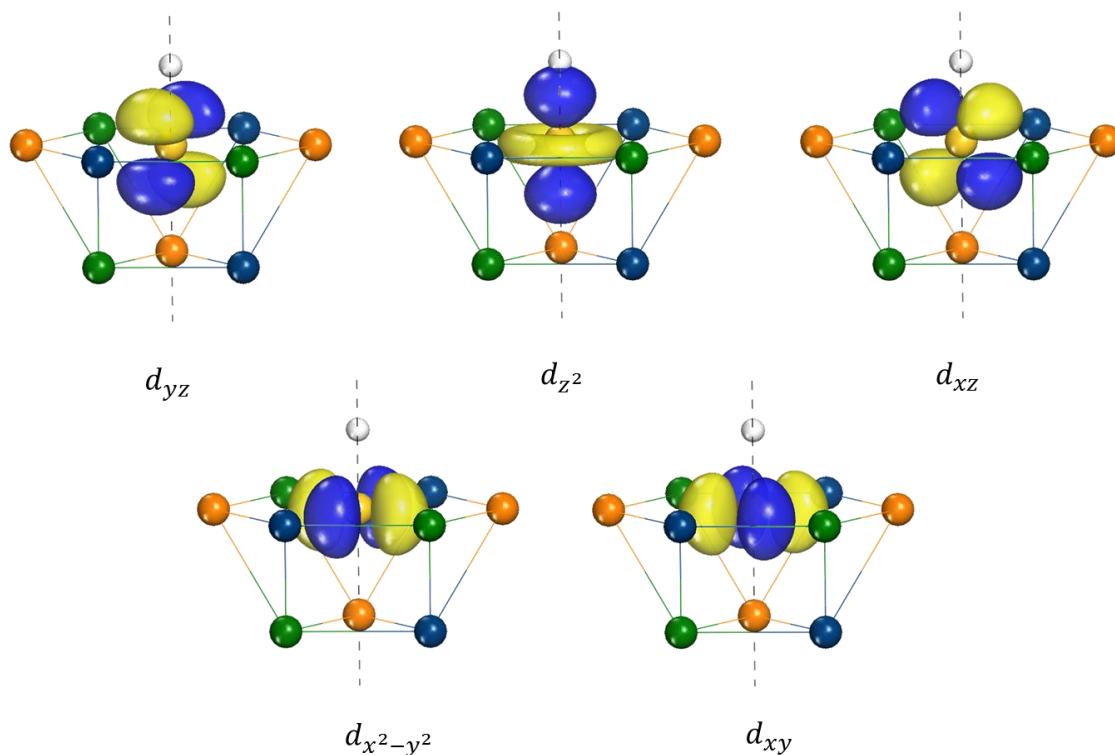


Figure 3.6 Atomic d orbitals used to construct hybrid orbitals in the adsorbate covered surface

As shown in Figure 3.7, the d_{xy} and $d_{x^2-y^2}$ orbitals can be transformed into a fractional set of three orbitals, each having magnitude of $2/3$. Each of the orbitals in this set is oriented towards a pair of collinear surface ligands. It should be noted that even though these orbitals have the same magnitude as the d_{co} orbitals in the bulk, they do not have the same shape, leading to lower concentration along the bond axis. Similarly, the d_{xz} and d_{yz} orbitals can also be transformed into a fractional set of three orbitals of magnitude $2/3$, each being oriented towards one of the three subsurface ligands. The positive lobes of these orbitals are not even oriented along the metal-metal bond axis as the surface orbitals were, being offset by about 10 degrees. The first

set of fractional orbitals will be referred to as the d_{surf}^2 set while the second will be referred to as the d_{sub}^2 set. Together with h_n , this forms the $h_n d_{surf}^2 d_{sub}^2$ representation of the orbital space available for metal-metal bonding.

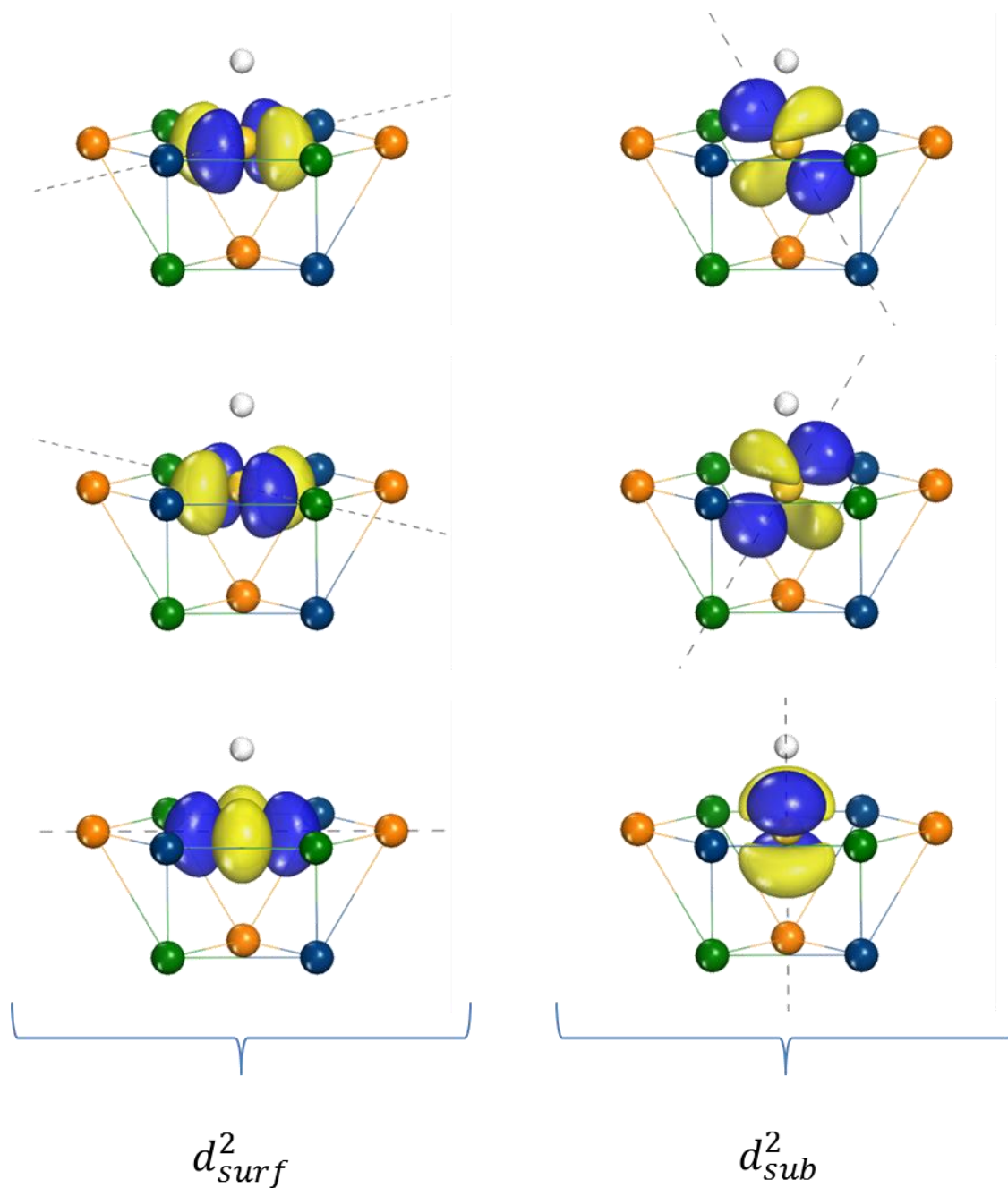


Figure 3.7 Fractional d orbitals used to construct hybrids in the adsorbate covered surface

Metal-metal bonding in W-H

Tungsten atoms have no lone pairs so the entire $h_n d_{surf}^2 d_{sub}^2$ orbital space on the atom can be used to form metal-metal bonds. As discussed previously, the $h_n d_{surf}^2$ set will be used to form hybrid orbitals to bond with the surface metal atoms while the d_{sub}^2 set will be used to form hybrids to bond with the subsurface metal atoms. This leads to a set of six hybrids of magnitude 1/2 to form bonds with the six surface ligands and a set of three hybrids of magnitude 2/3 to form bonds with the three subsurface ligands. The resulting hybrids on atom A forming a bond with surface atom B have the form

$$h_{AB} = \frac{1}{\sqrt{6}} [h_n + \sqrt{2} d_{AB}^{surf}] \quad (3.11a)$$

where d_{AB}^{surf} is a d_{surf} orbital with the positive lobe oriented towards atom B. These hybrids have the same magnitude as those in the absence of the adsorbate layer but have a different shape as we will see shortly. A hybrid on atom A forming a bond with subsurface atom C has the form

$$h_{AC} = \sqrt{\frac{2}{3}} d_{AC}^{sub} \quad (3.11b)$$

being composed entirely of a d_{sub} orbital with the positive lobe positioned as close as possible to atom C. These hybrids only have 2/3 the magnitude on the clean surface and have a significantly different shape, being much less concentrated along the metal-metal bond axis.

Metal-metal bonding in Re-H to Au-H

The lone pairs on atoms of Re to Au can go into three different sets of orbitals that maintain the symmetry of the surface as shown in Figure 3.8. Placing 1/2 of a lone pair into each of the two d_{surf} orbitals leads to a charge distribution concentrated in a ring around the metal-hydrogen bond axis in the plane of the surface. Alternatively, 1/2 of a lone pair can be placed into each of the two d_{sub} orbitals, leading to a charge distribution concentrated in two parallel rings around

the metal-hydrogen bond axis, one above and one below the plane of the surface. Up to two lone pairs can be placed into each of these two sets, for a total of four lone pairs. Finally, a lone pair can be placed in the h_n orbital, leading to a charge distribution concentrated in a narrow ring around the metal atom in the plane of the surface.

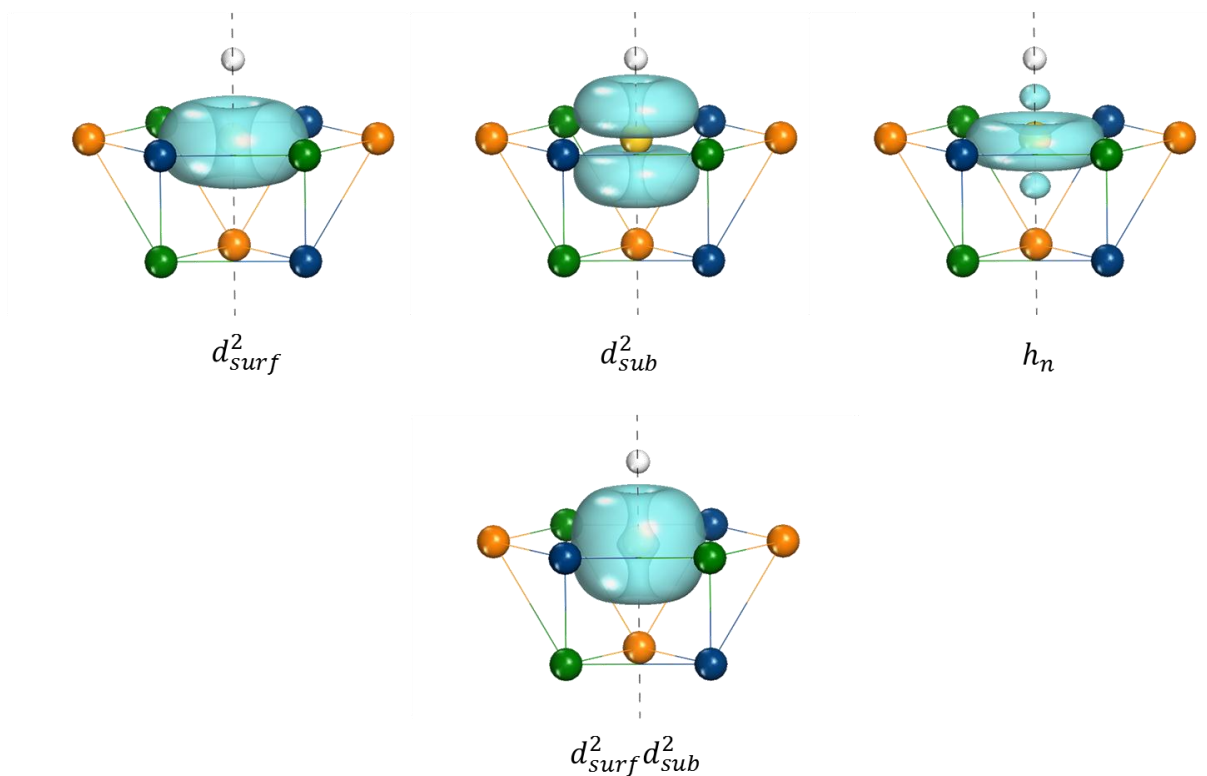


Figure 3.8 Charge distributions from placing a lone pair into a certain set of orbitals on the adsorbate covered surface

Since there is no obvious reason to place lone pairs in one of the sets of d orbitals over the other, each lone pair will be distributed equally between the two in a $d_{surf}^2 d_{sub}^2$ set that can contain up to four lone pairs and has the charge distribution shown in Figure 3.8. Each lone pair added to this set removes $1/2$ each of a d_{surf} orbital and a d_{sub} orbital from those available to form metal-metal bonds. This leads to surface and subsurface hybrids having forms given by

$$h_{AB} = \frac{1}{\sqrt{6}} \left[h_n + \sqrt{\frac{v-2}{2}} d_{AB}^{surf} \right] \quad (3.12a)$$

and

$$h_{AC} = \frac{1}{\sqrt{3}} \sqrt{\frac{v-2}{2}} d_{AC}^{sub} \quad (3.12b)$$

for a metal atom of valence v having $n = 6 - v$ lone pairs. As with the hybrids on W, the surface hybrids have the same magnitude but different shape than on the clean surface while the subsurface hybrids have $2/3$ of the magnitude of those on the clean surface. This leads to a sum of metal-metal bond orders to a given metal atom equal to $v - 1$, which is one unit less than the sum of bond orders to a metal atom in the clean surface. This satisfies the sum rule in Equation (1.44) which states that the formation of the metal-hydrogen bond must lead to a decrease in total metal-metal bond order of one unit. Interestingly, we see that all of this decrease occurs in bonds to metal atoms in the subsurface layer. This seems reasonable because the h_a orbital used to form the metal-hydrogen bond is oriented along the M-H bond axis and thus has high concentration towards the subsurface ligands and low concentration towards the surface ligands. It makes sense, then, that taking this orbital away from metal-metal bonding should predominantly affect the bonds to subsurface ligands.

On Pt, the four lone pairs occupy the entire $d_{surf}^2 d_{sub}^2$ orbital space leaving only the h_n orbital to form zero order bonds with the surface metal atoms and no ability to form zero order bonds to subsurface metal atoms (although conjugative interactions will still occur). Additionally, the h_n orbital is much less concentrated along the metal-metal bond axes than the hybrid orbitals on Ir to W, much like the s orbital in bulk Au compared to the sd hybrids on Pt to W for forming metal-metal bonds. The fifth lone pair on Au must go into the h_n orbital, leaving no orbitals to form metal-metal bonds in the zero order electronic structure. As we will see later, these behaviors will cause the adsorption energies to Au and Pt to differ significantly from the adsorption energies to the other $5d$ transition metals.

Metal-metal bond energy

The energies of the metal-metal bonds in the metal slab in the presence of an adsorbate layer can be calculated in a manner similar to those in the bulk in Chapter 2. In that case, the bond energy due to the σ interaction between atoms A and B is calculated from Equation (2.6)

$$\Delta\varepsilon_{AB} = 2 \langle h_{AB} | h_{\sigma_+}^A \rangle \langle h_{\sigma_+}^B | h_{BA} \rangle V_{\sigma_+} \quad (3.13)$$

where V_{σ_+} is the resonance integral associated with the σ_+ interaction and $h_{\sigma_+}^A$ and $h_{\sigma_+}^B$ are the hybrid orbital that defines this interaction given in Equation (2.7)

$$h_{\sigma_+}^A = b_s s + b_d d_{AB} \quad (3.14a)$$

$$h_{\sigma_+}^B = b_s s + b_d d_{BA} \quad (3.14b)$$

with d_{AB} being a d orbital on atom A oriented along the A-B having the shape of the canonical d_{z^2} orbital and d_{BA} being the same for atom B.

The overlap integrals $\langle h_{AB} | h_{\sigma_+}^A \rangle$ and $\langle h_{\sigma_+}^B | h_{BA} \rangle$ can be written in terms of integrals involving the h_n , and d_{surf} components of the bonding hybrids h_{AB} and h_{BA} for bonds to surface atoms

$$\langle h_{AB} | h_{\sigma_+}^A \rangle = \langle h_{AB} | h_n \rangle \langle h_n | h_{\sigma_+}^A \rangle + \langle h_{AB} | d_{AB}^{surf} \rangle \langle d_{AB}^{surf} | h_{\sigma_+}^A \rangle \quad (3.15a)$$

$$\langle h_{\sigma_+}^B | h_{BA} \rangle = \langle h_{\sigma_+}^B | h_n \rangle \langle h_n | h_{BA} \rangle + \langle h_{\sigma_+}^B | d_{AB}^{surf} \rangle \langle d_{AB}^{surf} | h_{BA} \rangle \quad (3.15b)$$

Using the forms of the hybrid orbitals in Equations (3.2b), the overlap integrals in these expressions are found to be

$$\langle h_{AB} | h_n \rangle = \langle h_n | h_{BA} \rangle = \frac{1}{\sqrt{6}} \quad (3.16a)$$

$$\langle h_{AB} | d_{AB}^{surf} \rangle = \langle d_{AB}^{surf} | h_{BA} \rangle = \frac{1}{\sqrt{6}} \sqrt{\frac{v-2}{2}} \quad (3.16b)$$

$$\langle h_n | h_{\sigma_+}^A \rangle = \langle h_{\sigma_+}^B | h_n \rangle = b_s a_d - b_d a_s \langle d_a | d_{AB} \rangle = b_s a_d + \frac{1}{2} b_d a_s \quad (3.17a)$$

$$\langle d_{AB}^{surf} | h_{\sigma_+}^A \rangle = \langle h_{\sigma_+}^B | d_{BA}^{surf} \rangle = b_d \langle d_{AB}^{surf} | d_{AB} \rangle = \frac{\sqrt{3}}{2} b_d \quad (3.17b)$$

so that the bond energy can be written in terms of interactions between these components

$$\Delta \varepsilon_{AB} = \frac{1}{6} \left[\underbrace{2 \alpha^2}_{h_n-h_n} + \underbrace{\frac{3}{4} b_d^2 (v-2)}_{d-d} + 2 \underbrace{\sqrt{\frac{3}{2}} \alpha b_d \sqrt{v-2}}_{h_n-d} \right] V_{\sigma_+} \quad (3.18)$$

$$\alpha = \langle h_n | h_{\sigma_+}^A \rangle = \langle h_{\sigma_+}^B | h_n \rangle = b_s a_d + \frac{1}{2} b_d a_s \quad (3.19)$$

As with the bond energy in the bulk and the clean surface, this bond energy contains three terms, shown in Figure 3.9, that account for the three different types of interactions between the orbitals on A and B. The first term is due to interactions between the h_n components of the bonding hybrid orbitals on A and B and, like the $s-s$ term in Equation (2.12) for the bulk, is independent of the metal atom valence. As seen in the figure, this interaction contributes the same amount to the bond energy for Pt to W. The second term is due to interactions between the d_{surf} components of the hybrids on A and B and, like the corresponding $d-d$ term for the bulk, is proportional to the number of d_{surf} orbitals participating in metal-metal bonding ($v-2$), leading to a linear increase in the bond energy with increasing metal atom valence. The last term is due to the interaction between the h_n component of the hybrid on one metal atom and the d_{surf} component of the hybrid on the other atom. Analogous to the corresponding $s-d$ term in the bulk, it is proportional to the square root of the number of d_{surf} orbitals participating in metal-metal bonding. As in the bulk and the clean surface, this term accounts for a large

portion of the total bond energy in Ir to W and causes a larger increase in bond energy between Pt and Ir than between other pairs of metals differing in valence by one unit. The surface bond energy on Au is zero since, as discussed before, Au has no orbitals to participate in metal-metal bonding.

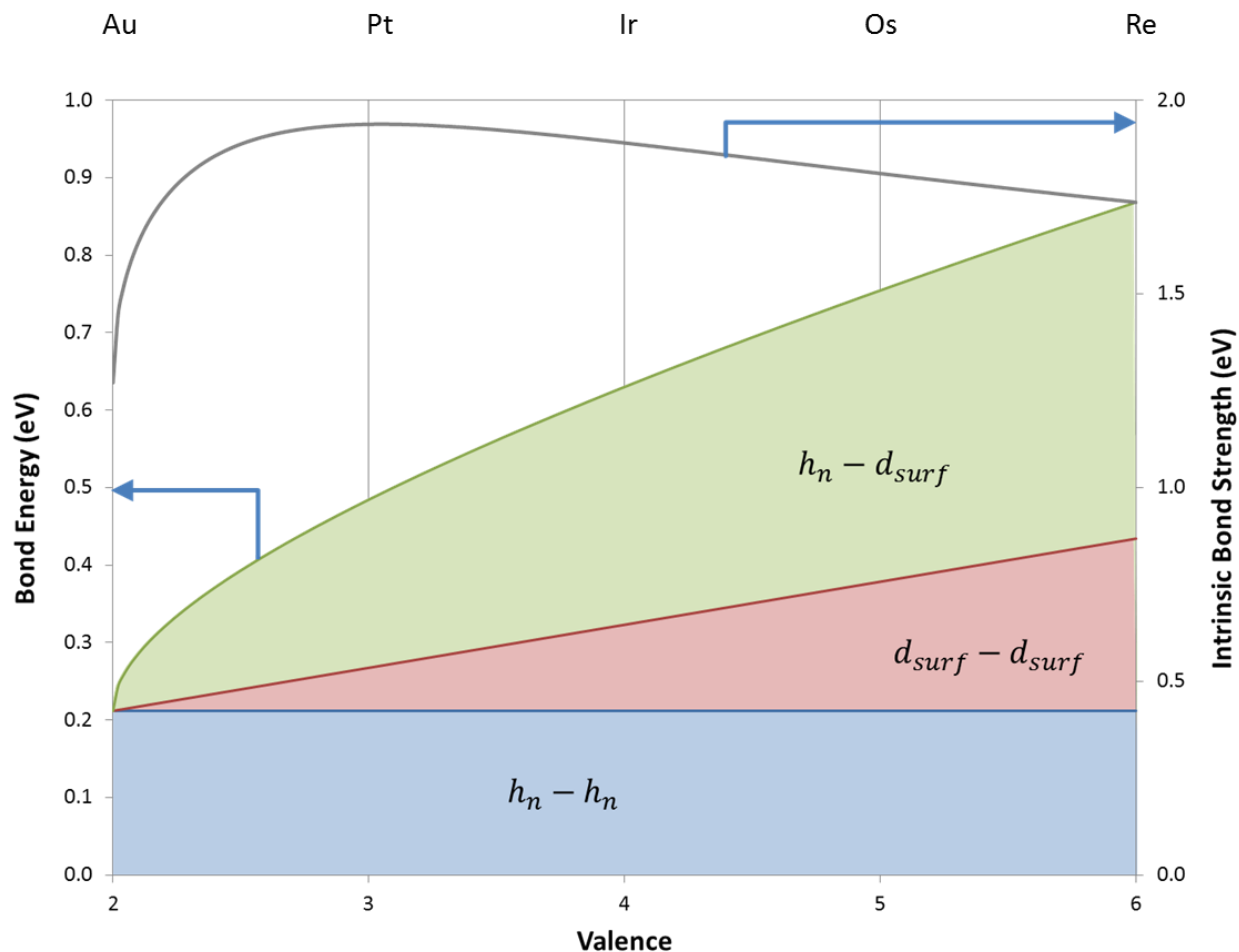


Figure 3.9 Decomposition of the zero order energy of surface bonds in the presence of an adsorbate layer of atomic hydrogen

The bond energy of the bonds to subsurface atoms is due only to the interaction between d_{sub} components of the hybrid orbitals forming the bond since h_n does not participate in these bonds. The overlap integrals in Equation (3.15) corresponding to the d_{AB}^{sub} components are equal to

$$\langle h_{AB} | d_{AC}^{sub} \rangle = \langle d_{AC}^{sub} | h_{CA} \rangle = \frac{1}{\sqrt{3}} \sqrt{\frac{v-2}{2}} \quad (3.20)$$

$$\langle d_{AC}^{sub} | h_{\sigma_+}^A \rangle = \langle h_{\sigma_+}^C | d_{CA}^{sub} \rangle = b_d \langle d_{AC}^{sub} | d_{AC} \rangle = \sqrt{\frac{2}{3}} b_d \quad (3.21)$$

so that the total bond energy in Equation (3.13) is

$$\Delta \varepsilon_{AC} = \frac{2}{3} \left[\underbrace{\frac{1}{3} b_d^2 (v-2)}_{d-d} \right] V_{\sigma_+} \quad (3.22)$$

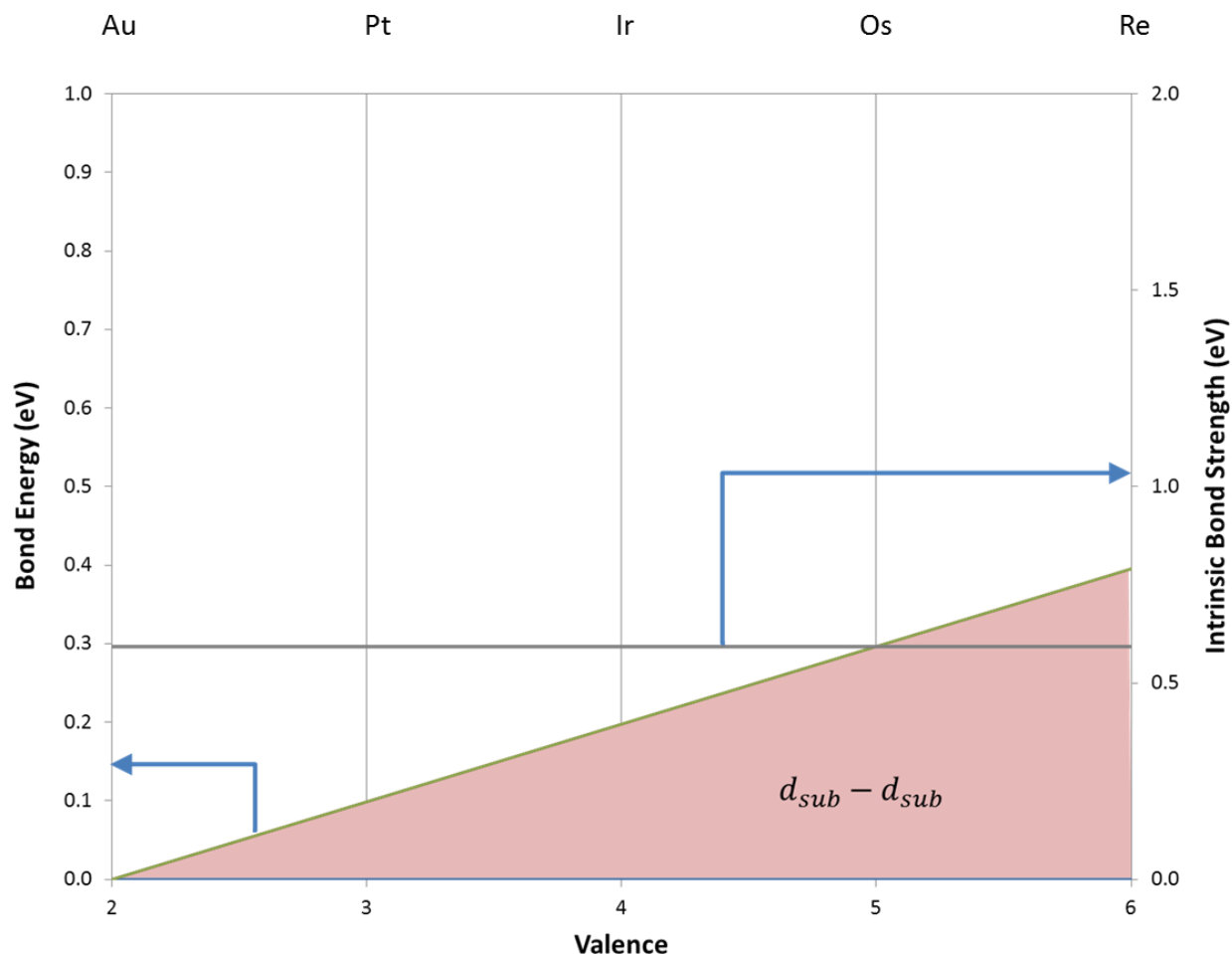


Figure 3.10 Decomposition of the zero order energy of subsurface bonds in the presence of adsorbate layer of atomic hydrogen

This bond energy expression for the bonds to subsurface atoms contains only one term which accounts for the interaction between the d_{sub} components of the hybrids forming the bond and is proportional to the number of d_{sub} orbitals participating in bonding ($v - 2$) as shown in Figure 3.10. Thus, the bond energy is zero for Pt and increases linear with metal atom valence from Pt to W. As with the surface bonds, these bonds are absent on Au due the absence of orbitals containing unpaired electrons.

Reduction in metal-metal bonding due to addition of a hydrogen adsorbate layer

Using the bond energies in Equations (3.18) and (3.22) for the slab in presence of the adsorbate layer just discussed along with the bond energies in the clean surface, we can calculate the reduction in metal-metal bonding energy resulting from adsorption of the adsorbate layer. Recall from Chapter 2 that these bond energies are given by

$$\Delta\varepsilon_{AB}^{clean} = \frac{1}{6} \left[\underbrace{b_s^2}_{s-s} + \underbrace{b_d^2 (v-1)}_{d-d} + 2 \underbrace{b_s b_d \sqrt{v-1}}_{s-d} \right] V_{\sigma_+} \quad (3.23a)$$

$$\Delta\varepsilon_{AC}^{clean} = \frac{1}{3} \left[\underbrace{b_s^2}_{s-s} + \underbrace{b_d^2 (v-1)}_{d-d} + 2 \underbrace{b_s b_d \sqrt{v-1}}_{s-d} \right] V_{\sigma_+} \quad (3.23b)$$

for surface and subsurface bonds in the clean surface and by

$$\Delta\varepsilon_{AB}^{ads} = \frac{1}{6} \left[\underbrace{2 \alpha^2}_{h_n-h_n} + \underbrace{\frac{3}{4} b_d^2 (v-2)}_{d-d} + 2 \underbrace{\sqrt{\frac{3}{2}} \alpha b_d \sqrt{v-2}}_{h_n-d} \right] V_{\sigma_+} \quad (3.24a)$$

$$\Delta\varepsilon_{AC}^{ads} = \frac{1}{3} \left[\underbrace{\frac{2}{3} b_d^2 (v-2)}_{d-d} \right] V_{\sigma_+} \quad (3.24b)$$

for surface and subsurface bonds in the surface with an adsorbate layer (from Equations (3.18) and (3.22)). Combining like terms in these expressions gives the following for the loss of metal-metal bond energy upon adsorption in surface bonds

$$\Delta\Delta\varepsilon_{AB} = -\frac{1}{6} \left[\begin{aligned} & (1 + 2 b_s b_d - 2 \alpha^2) + \frac{1}{4} b_d^2 (v-2) \\ & + 2 b_d \left[b_s (\sqrt{v-1} - 1) - \sqrt{\frac{3}{2}} \alpha \sqrt{v-2} \right] \end{aligned} \right] V_{\sigma_+} \quad (3.25a)$$

and in subsurface bonds

$$\Delta\Delta\varepsilon_{AC} = -\frac{1}{3}\left[(1 + 2 b_s b_d) + \frac{1}{3} b_d^2 (v - 2) + 2 b_s b_d (\sqrt{v - 1} - 1)\right] V_{\sigma_+} \quad (3.25b)$$

These losses in bond energy are shown in Figure 3.11 where it can be seen that, with the exception of Pt, the surface bonds actually increase in strength upon addition of the adsorbate layer. To understand why these bonds increase in strength, it is useful to write the surface hybrids in terms of the metal s orbital and a canonical d orbital basis with the d_{z^2} orbital (now d_{AB}) lying along the A-B bond.

$$h_{AB} = \frac{1}{\sqrt{6}} \left[a_d s + \frac{1}{2} \left[a_s + \sqrt{3} \sqrt{\frac{v-2}{2}} \right] d_{AB} + \frac{1}{2} \left[\sqrt{\frac{v-2}{2}} - \sqrt{3} a_s \right] d_{AB}^\delta \right] \quad (3.26)$$

As seen in this expression, the hybrid also has a component d_{AB}^δ having δ symmetry with respect to the A-B bond that does not participate in formation of the σ metal-metal bond. Using the values of a_s and a_d listed earlier for Pt to W, we can see that the magnitude of the s component is 36% larger than it is in the bulk and the clean surface. Since the magnitude of the s component in the bulk hybrids is below the optimal value of b_s^2 , increasing the magnitude of this component in the presence of the adsorbate leads to an increase in bond energy. Furthermore, we can see that the shape of the d component of h_{AB} stays very similar to the optimal d_{AB} shape by calculating the normalized overlap with d_{AB} , which is equal to

$$\frac{\langle d_{AB} | h_{AB} \rangle}{\sqrt{|\langle d_{AB} | h_{AB} \rangle|^2 + |\langle d_{AB}^\delta | h_{AB} \rangle|^2}} = \frac{a_s + \sqrt{3} \sqrt{\frac{v-2}{2}}}{2 \sqrt{a_s^2 + \frac{v-2}{2}}} \quad (3.27)$$

For Ir to W, this value is greater than 0.99, indicating that the shape of the d component of h_{AB} deviates very little from the optimal d_{AB} shape. Therefore, the d component of h_{AB} participates just as effectively in the σ interaction with h_{BA} on atom B as it did in clean surface.

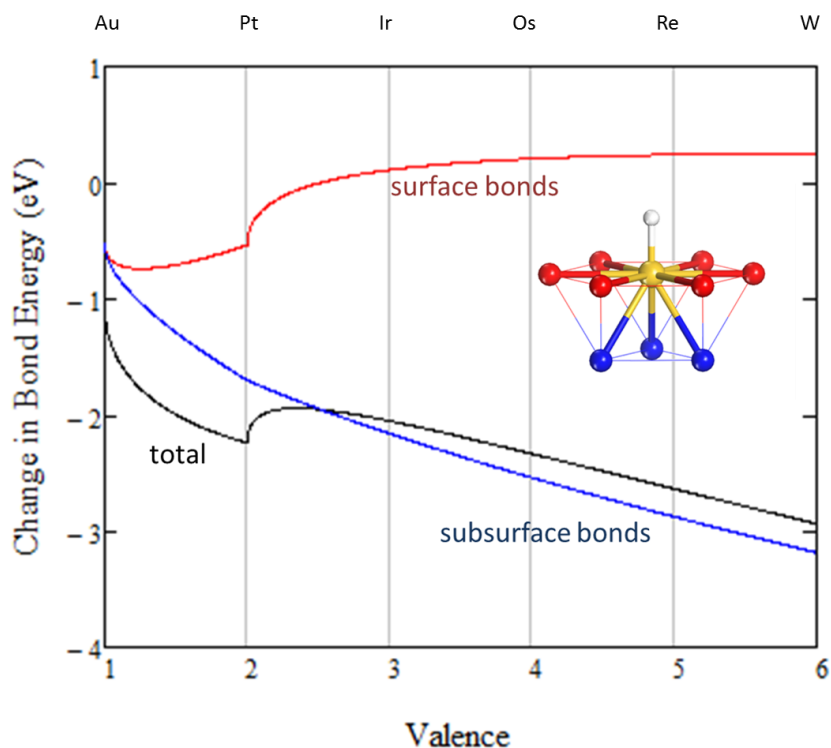


Figure 3.11 Change in zero order metal-metal bond energy upon adsorption (black) with contributions from surface (red) and subsurface (blue) bonds

On Pt, however, the shape of the d component of h_{AB} differs significantly from the shape in the clean surface. This is due to the complete filling of the d_{surf}^2 shell with lone pairs so that only the d_a orbital can participate in forming surface metal-metal bonds. The overlap of this component with d_{AB} drops to 0.5 and the bond energy decreases significantly upon adsorption as was seen in Figure 3.11. This leads to a larger decrease in metal-metal bond energy due to formation of the metal-hydrogen bond for Pt than for Ir to W.

In contrast to the surface bonds, the subsurface bonds weaken significantly due to hydrogen adsorption as seen in Figure 3.11. This is related to the reduction in bond magnitude by 1/3 of a unit compared to the magnitude on the clean surface as well as the complete removal of the s orbital from participating in subsurface bonding. As discussed earlier, the subsurface bonds are completely broken in Pt as the d_{sub}^2 shell becomes completely filled with two lone pairs leading to a complete loss of subsurface metal-metal bond energy. As the valence increases from Pt to

W, the subsurface bonds in the clean surface increase in strength faster than they do in the presence of the adsorbate layer, causing the loss of subsurface bond energy to increase.

The total decrease in zero-order metal-metal bond energy per metal atom upon adsorption, $\Delta\Delta E_{slab}$, is equal to the sum of the losses over all six surface bonds and all three subsurface bonds

$$\Delta\Delta E_{slab}^0 = \frac{1}{2} (6 \Delta\epsilon_{AB} + 3 \Delta\epsilon_{AC}) \quad (3.28)$$

This quantity is shown in Figure 3.11 for Au to W where it can be seen to increase over this range as the metal atom valence increases, with the exception of Pt. The anomalously high loss in metal-metal bond energy for Pt is due to the loss in the surface bonds discussed earlier due to changes in hybridization. The general increase in this quantity from Au to W is due to the increase in the loss of subsurface bond energy as these bonds become stronger in the clean surface from Au to W.

Trends in zero-order adsorption energy

Figure 3.12 shows how the zero order adsorption energy of the hydrogen atom depends on the metal it is adsorbed to. This adsorption energy ΔE_{ads} can be broken down into contributions from formation of the metal-hydrogen bond energy (ΔE_{M-H}) and the resulting weakening of metal-metal bond energy (ΔE_{M-M}).

$$\Delta E_{ads}^0 = \Delta E_{M-H} + \Delta\Delta E_{M-M}^0 \quad (3.29)$$

The adsorption energy increases almost linearly from Re to Ir. This increase is due to the increase in the loss of metal-metal bond energy upon adsorption from Ir to Re as the strength of the bonds in the clean surface increases – therefore, weakening these bonds by addition of an adsorbate costs more energy. The adsorption energy decreases from Ir to Pt due to the weakening of the surface bonds upon adsorption that is specific to Pt that we discussed earlier. The adsorption energy decreases further on Au due to the lower formation energy of the surface

molecule resulting from the energy cost of promoting an electron from the filled d shell to the half filled s orbital to form an sd hybrid that bonds to the hydrogen.

Also shown in the figure is the DFT calculated adsorption energy of hydrogen for each metal. It can be seen that, although the absolute value is off, the behavior between Re and Pt is quite similar between these values and those calculated from Equation (3.29). The difference in adsorption energy between Au and Pt (0.76 eV), however, is underestimated by the zero order model, which predicts Au to bind hydrogen only 0.18 eV weaker than Pt. We will see next that this additional decrease in adsorption energy on Au is due to the loss of conjugative interactions upon adsorption.

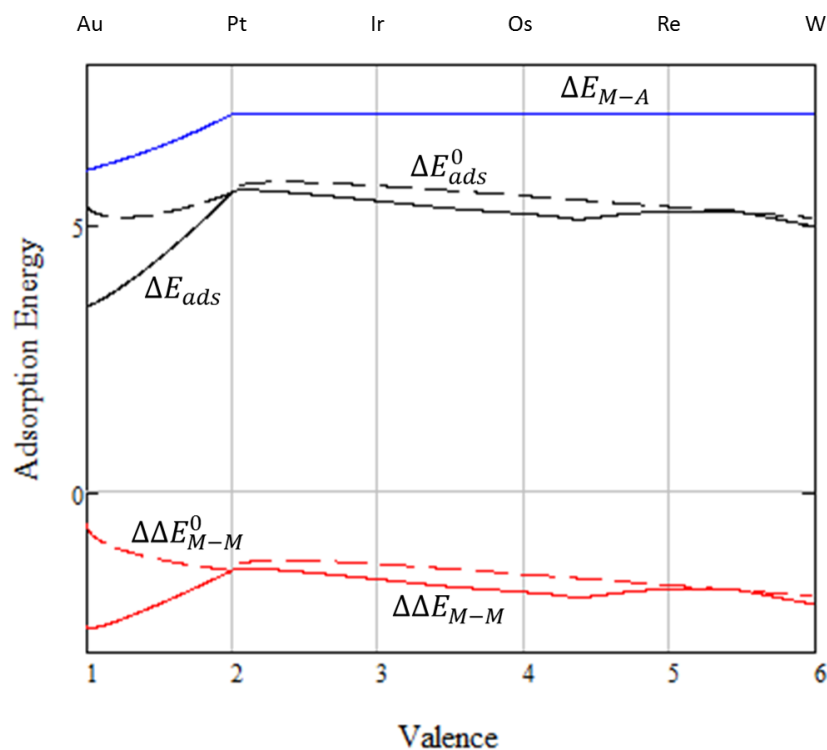


Figure 3.12 Hydrogen adsorption energy on (111) fcc metal surfaces (black) along with the individual components in Equation (3.29) due to formation of the bond between hydrogen and a single isolated metal atom (blue) and the loss of metal-metal bond energy upon adsorption (red). Contributions from zero order bonding are also shown (dashed lines).

3.1.2 Conjugation

In addition to changing the zero-order metal-metal bond energies, adsorption of hydrogen also changes the energies for conjugative interactions involving charge transfer across metal-metal bonds. Determination of the conjugation energy for the adsorbate covered slab is similar to the calculation for the bulk and the clean slab in Chapter 2 except that the orbital basis used to define the individual charge transfer interactions is different due to the presence of the metal-hydrogen bond. Although the fcc symmetry that simplified determination of this orbital basis is broken by the metal-hydrogen bond, there is still symmetry between the surface bonds and between the subsurface bonds – the addition of hydrogen only breaks the symmetry between the surface and subsurface bonds. Since we use different sets of real atomic orbitals to form the surface and subsurface bonds, the occupied and unoccupied fractional orbitals generated by Equation (1.62) still obey the constraints in Equation (1.60) for a set of electron conserving interactions.

For each bond between surface atoms A and B, conjugative interactions can be generated by a set of occupied and unoccupied fractional orbitals derived from h_n , two d_{surf} orbitals, and two d_{sub} orbitals. Out of these five orbitals, only h_n and the d_{surf} orbital aligned with the A-B bond, d_{surf}^{AB} , can participate in interactions with non-zero σ components. The other d_{surf} orbital and one of the d_{sub} orbitals can only participate in π interactions and the remaining d_{sub} orbital can only participate in a δ interaction. Since we are ignoring the π and δ interactions, we will only consider interactions involving h_n and d_{surf}^{AB} . This leads to a set of donor orbitals on atom A consisting of the occupied bonding h_n and d_{surf}^{AB} orbitals \underline{h}_n and $\underline{d}_{surf}^{AB}$ and the nonbonding lone pair orbital \ddot{d}_{surf}^{AB} . The acceptor orbitals consist of the unoccupied bonding orbitals \bar{h}_n and \bar{d}_{surf}^{AB} . A similar set exists on atom B. As with the bulk, these orbitals form twelve conjugative interactions, six involving electron transfer from A to B and the other six involving transfer from B to A.

The conjugative interactions between a surface atom A and a subsurface atom C can be generated by the set of occupied and unoccupied fractional orbitals derived from the atomic orbitals in Figure 3.9. These consist of h_n , a d_{sub} orbital aligned with the A-C bond, d_{sub}^{AC} , a

d_{surf} orbital with one lobe in the vertical plane passing through the A-C bond, d_{surf}^{AC} , and an additional d_{sub} and d_{surf} orbital that only participate in π and δ interactions with orbitals on atom C. Interactions involving d_{surf}^{AC} are much weaker than the others since the σ interactions between this orbital and orbitals on atom C are very weak, so we will not consider these interactions. This leaves us with three donor orbitals \underline{h}_n , \underline{d}_{sub}^{AC} , and \ddot{d}_{sub}^{AC} and two acceptor orbitals \bar{h}_n and \bar{d}_{sub}^{AC} . A similar set exists on atom C, leading to twelve conjugative interactions, as with interactions between surface atoms.

The magnitudes of the basis orbitals for the conjugative interactions are equal to

$$\eta(\underline{h}_n) = \eta(\bar{h}_n) = \frac{1}{2} \quad (3.30a)$$

$$\eta(\underline{d}_{surf}^{AB}) = \eta(\bar{d}_{surf}^{AB}) = \eta(\underline{d}_{sub}^{AC}) = \eta(\bar{d}_{sub}^{AC}) = \frac{1}{2} \times \frac{1}{4}(v - 2) \quad (3.30b)$$

$$\eta(\ddot{d}_{surf}^{AB}) = \eta(\ddot{d}_{sub}^{AC}) = \frac{1}{4}(6 - v) \quad (3.30c)$$

These orbital magnitudes are plotted in Figure 3.13. Based on the way that the orbital magnitude changes with metal atom valence, the orbitals derived from \underline{h}_n are analogous to those derived from the s orbital in the bulk, both having constant magnitudes of $1/2$. Likewise, the orbitals derived from $\underline{d}_{surf}^{AB}$ and \underline{d}_{sub}^{AC} are analogous to those derived from d_{σ}^{AB} in the bulk, with the magnitude of the bonding orbitals being proportional to the number of d orbitals participating in metal-metal bonding ($v - 1$ in the bulk and $v - 2$ in the adsorbate covered surface) and the magnitude of the lone pair orbitals being proportional to the number of lone pairs ($6 - v$ in both systems).

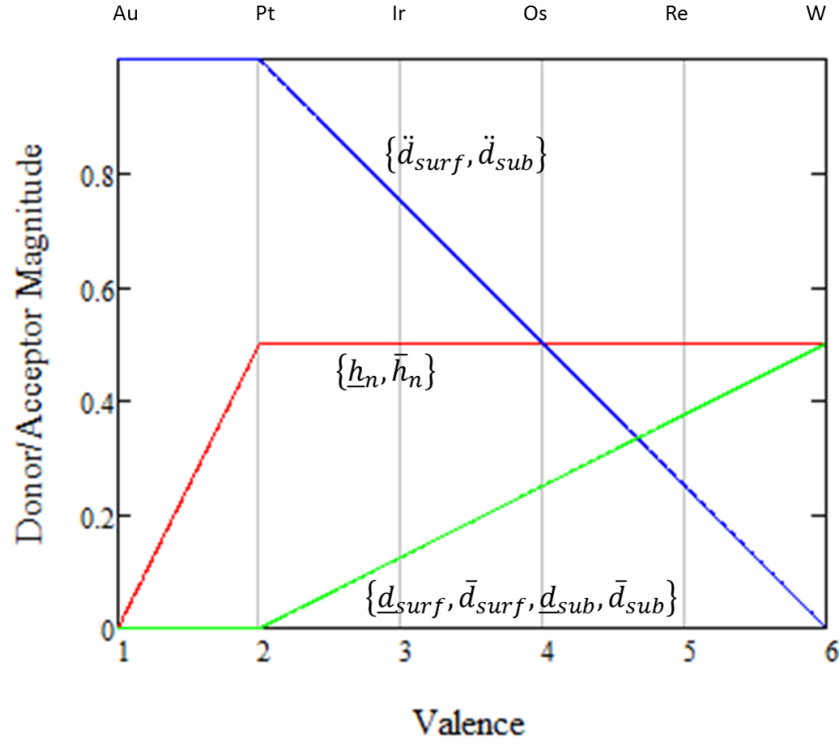


Figure 3.13 Magnitudes of orbitals used to generate conjugative interactions given by Equation (3.30)

The interaction magnitudes arising from the zero order A-B bond are calculated in a similar way to those in the bulk in Equation (2.15) using Equation (3.12a) for the hybrids forming this bond. These are equal to

$$F_{\underline{h}_n \rightarrow \bar{h}_n}^0 = \frac{1}{3v} \quad (3.31a)$$

$$F_{\underline{h}_n \rightarrow \bar{d}_{surf}^{BA}}^0 = F_{\underline{d}_{surf}^{AB} \rightarrow \bar{h}_n}^0 = \frac{v-2}{6v} \quad (3.31b)$$

$$F_{\underline{d}_{surf}^{AB} \rightarrow \bar{d}_{surf}^{BA}}^0 = \frac{(v-2)^2}{12v} \quad (3.31c)$$

Similarly, the interaction magnitude arising from the zero order A-C bond are equal to

$$F_{\underline{d}_{sub}^{AC} \rightarrow \bar{d}_{surf}^{CA}}^0 = \frac{1}{2} \times \frac{v-2}{6} \quad (3.32)$$

since only the \underline{d}_{sub}^{AC} orbital participates in this interaction.

The magnitudes of the six conjugative interactions involving electron transfer from atom A to atom B can now be calculated using Equation (1.73). The interaction magnitudes are plotted in Figure 3.14a and bare a strong resemblance to those in the clean surface in Figure 2.10. The interactions involving electron transfer into \bar{h}_n are limited by the magnitude of \bar{h}_n to a magnitude of 1/2 as were the interactions in the bulk transferring electrons into \bar{s} . As with the interactions in the bulk having \bar{d}_σ^{AB} as the acceptor orbital, those in the adsorbate covered surface with \bar{d}_{surf}^{AB} as the acceptor orbital are limited by the magnitude of \bar{d}_{surf}^{AB} and thus increase in magnitude linearly with valence. We can see that the interactions for Pt in the adsorbate covered surface are similar to the interactions for Au in the bulk – effectively, the formation of the M-H bond has lowered the valence of the metal atom by one for forming metal-metal bonds so that Pt-H only has interactions where \bar{h}_n is the acceptor orbital and Au-H has no available acceptor orbitals. This is similar to what we saw for the zero order metal-metal bonding where bonds between two Pt-H involved only the h_n orbitals on both Pt atoms while there was no metal-metal bonding between two Au-H. Similar behavior is seen for the magnitudes of the six conjugative interactions involving electron transfer from surface atom A to subsurface atom C shown in Figure 3.14b.

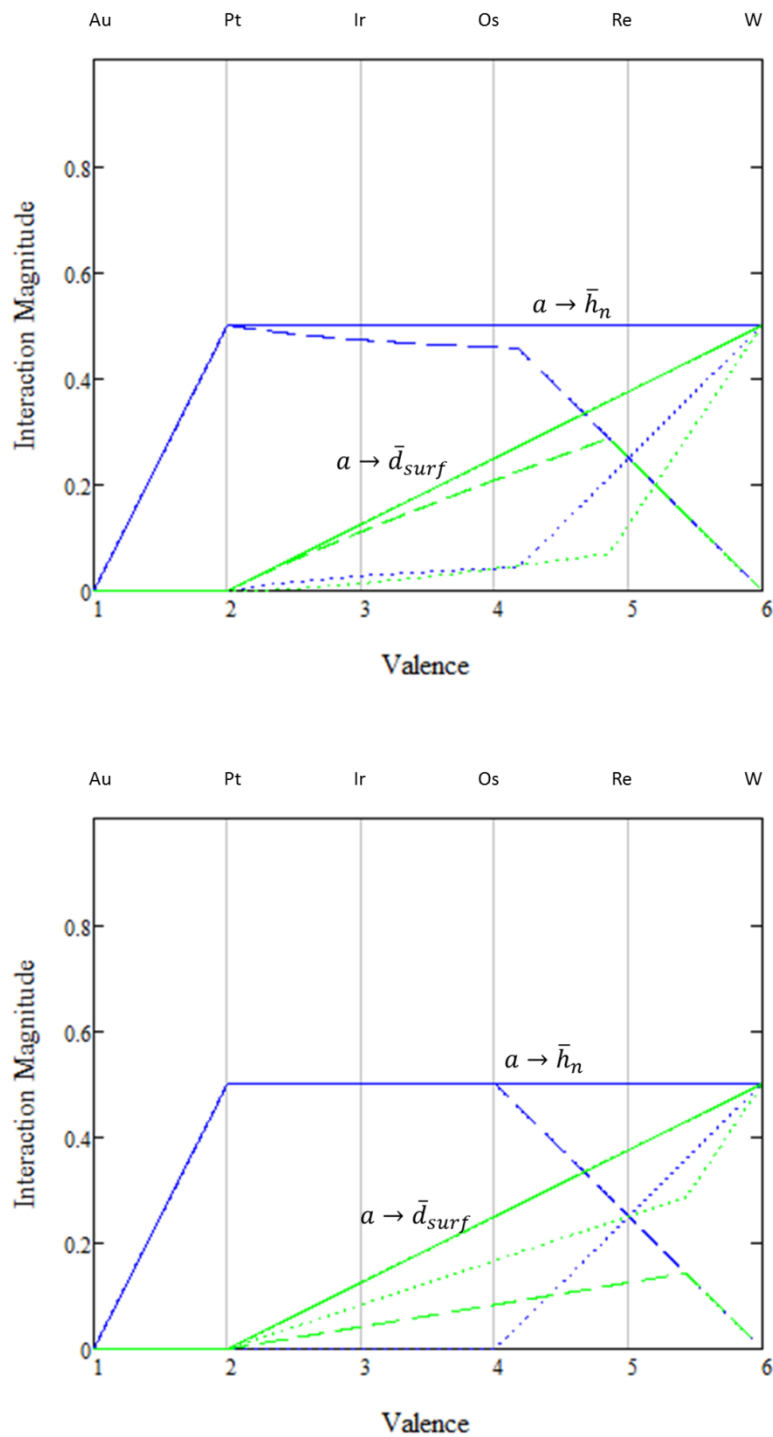


Figure 3.14 Magnitudes of surface (top) and subsurface (bottom) conjugative interactions. Blue lines correspond to charge transfer into the \bar{s} orbital and green lines correspond to charge transfer into the \bar{d}_σ orbital. Also shown are the individual contributions due to donation \bar{d}_σ (dashed lines) and \underline{d}_σ (dotted lines).

The resonance integrals needed to calculate the intrinsic interaction energy $\Delta E_{a \rightarrow r}^R$ in Equation (1.65) for surface interactions are equal to

$$\langle \underline{h}_n | H | \bar{h}_n \rangle^R = \langle h_n | H | h_n \rangle = \left(a_d b_s + \frac{1}{2} a_s b_d \right)^2 V_\sigma \quad (3.33a)$$

$$\langle \underline{d}_{surf} | H | \bar{d}_{surf} \rangle^R = \langle \ddot{d}_{surf} | H | \bar{d}_{surf} \rangle = \frac{3}{4} b_d^2 V_\sigma \quad (3.33b)$$

$$\begin{aligned} \langle \underline{h}_n | H | \bar{d}_{surf} \rangle^R &= \langle \underline{d}_{surf} | H | \bar{h}_n \rangle^R = \langle \ddot{d}_{surf} | H | \bar{h}_n \rangle^R = \langle h_n | H | d_{surf} \rangle \\ &= \frac{\sqrt{3}}{2} b_d \left(a_d b_s + \frac{1}{2} a_s b_d \right) V_\sigma \end{aligned} \quad (3.33c)$$

while those for subsurface interactions are equal to

$$\langle \underline{h}_n | H | \bar{h}_n \rangle^R = \langle h_n | H | h_n \rangle = \left(a_d b_s - \frac{1}{2} a_s b_d \right)^2 V_\sigma \quad (3.34)$$

$$\langle \underline{d}_{sub} | H | \bar{d}_{sub} \rangle^R = \langle \ddot{d}_{sub} | H | \bar{d}_{sub} \rangle = \frac{2}{3} b_d^2 V_\sigma \quad (3.35)$$

$$\begin{aligned} \langle \underline{h}_n | H | \bar{d}_{sub} \rangle^R &= \langle \underline{d}_{sub} | H | \bar{h}_n \rangle^R = \langle \ddot{d}_{sub} | H | \bar{h}_n \rangle^R = \langle h_n | H | d_{sub} \rangle \\ &= \frac{2}{3} b_d \left(a_d b_s - \frac{1}{2} a_s b_d \right) V_\sigma \end{aligned} \quad (3.36)$$

The effective energies in the denominator of $\Delta E_{a \rightarrow r}^R$ are equal to

$$\varepsilon(\underline{h}_n) = \varepsilon(h_n) + \sqrt{\frac{v}{2}} \left(a_d b_s + \frac{1}{2} a_s b_d \right) V_\sigma \beta_{surf}(v) \quad (3.37a)$$

$$\varepsilon(\bar{h}_n) = \varepsilon(h_n) - \sqrt{\frac{v}{2}} \left(a_d b_s + \frac{1}{2} a_s b_d \right) V_\sigma \beta_{surf}(v) \quad (3.37b)$$

$$\varepsilon(\underline{d}_{surf}) = \varepsilon_d + \sqrt{\frac{v}{2}} \sqrt{\frac{3}{2}} b_d V_\sigma \beta_{surf}(v) \quad (3.37c)$$

$$\varepsilon(\bar{\underline{d}}_{surf}) = \varepsilon_d - \sqrt{\frac{v}{2}} \sqrt{\frac{3}{2}} b_d V_\sigma \beta_{surf}(v) \quad (3.37d)$$

$$\varepsilon(\underline{d}_{surf}) = \varepsilon_d + \frac{1}{\sqrt{3}} \sqrt{\frac{v-2}{2}} b_d V_\sigma \beta_{sub}(v) \quad (3.38)$$

$$(\bar{\underline{d}}_{surf}) = \varepsilon_d - \frac{1}{\sqrt{3}} \sqrt{\frac{v-2}{2}} b_d V_\sigma \beta_{sub}(v) \quad (3.39)$$

$$\varepsilon(\ddot{\underline{d}}_{surf}) = \varepsilon(\ddot{\underline{d}}_{sub}) = \varepsilon_d \quad (3.39a)$$

where $\varepsilon(h_n)$, $\beta_{surf}(v)$, and $\beta_{sub}(v)$ are given by

$$\varepsilon(h_n) = a_d^2 \varepsilon_s + a_s^2 \varepsilon_d \quad (3.40)$$

$$\beta_{surf}(v) = \left(\frac{v}{2}\right)^{-\frac{1}{2}} \left(b_s a_d + \frac{1}{2} b_d a_s + \frac{\sqrt{3}}{2} b_d \frac{1}{\sqrt{2}} \sqrt{v-2} \right) \quad (3.41)$$

$$\beta_{sub}(v) = \sqrt{\frac{2}{3}} b_d \quad (3.42)$$

Finally, the total conjugation energy associated with a bond between two surface atoms A and B in the adsorbate covered slab can be calculated to be sum of all interactions in which charge is transferred from A to B $\Delta E_{A \rightarrow B}$ and all interactions in which charge is transferred from B to A $\Delta E_{B \rightarrow A}$

$$\Delta E_{A-B}^{conj} = \Delta E_{A \rightarrow B} + \Delta E_{B \rightarrow A} \quad (3.43)$$

where $\Delta E_{A \rightarrow B}$ and $\Delta E_{B \rightarrow A}$ are equal to the sum of all interactions transferring charge into \bar{h}_n and all interactions transferring charge into \bar{d}_{surf} , with the energy associated with the zero order A-B bond $\Delta E_{\underline{h}_{AB} \rightarrow \bar{h}_{BA}}$ subtracted

$$\Delta E_{A \rightarrow B} = \Delta E_{B \rightarrow A} = \sum_a \Delta E_{a \rightarrow \bar{h}_n} + \sum_a \Delta E_{a \rightarrow \bar{d}_{surf}} - \Delta E_{\underline{h}_{AB} \rightarrow \bar{h}_{BA}} \quad (3.44)$$

$$\sum_a \Delta E_{a \rightarrow \bar{h}_n} = \Delta E_{\underline{h}_n \rightarrow \bar{h}_n} + \Delta E_{\underline{d}_{surf} \rightarrow \bar{h}_n} + \Delta E_{\bar{d}_{surf} \rightarrow \bar{h}_n} \quad (3.45a)$$

$$\sum_a \Delta E_{a \rightarrow \bar{d}_{surf}} = \Delta E_{\underline{h}_n \rightarrow \bar{d}_{surf}} + \Delta E_{\underline{d}_{surf} \rightarrow \bar{d}_{surf}} + \Delta E_{\bar{d}_{surf} \rightarrow \bar{d}_{surf}} \quad (3.45b)$$

$$\Delta E_{\underline{h}_{AB} \rightarrow \bar{h}_{BA}} = \frac{1}{4} \times \frac{1}{6} \left[\underbrace{2\alpha^2}_{h_n - h_n} + \underbrace{\frac{3}{4}b_d^2(v-2)}_{d-d} + 2 \underbrace{\sqrt{\frac{3}{2}}\alpha b_d \sqrt{v-2}}_{h_n - d} \right] V_{\sigma_+} \quad (3.45c)$$

Similarly, the total conjugation energy associated with a bond between surface atom A and subsurface atom C is given by

$$\Delta E_{A-C}^{conj} = \Delta E_{A \rightarrow C} + \Delta E_{C \rightarrow A} \quad (3.46)$$

with

$$\Delta E_{A \rightarrow C} = \Delta E_{C \rightarrow A} = \sum_a \Delta E_{a \rightarrow \bar{h}_n} + \sum_a \Delta E_{a \rightarrow \bar{d}_{sub}} - \Delta E_{\underline{h}_{AC} \rightarrow \bar{h}_{CA}} \quad (3.47)$$

$$\sum_a \Delta E_{a \rightarrow \bar{h}_n} = \Delta E_{\underline{h}_n \rightarrow \bar{h}_n} + \Delta E_{\underline{d}_{sub} \rightarrow \bar{h}_n} + \Delta E_{\bar{d}_{sub} \rightarrow \bar{h}_n} \quad (3.48a)$$

$$\sum_a \Delta E_{a \rightarrow \bar{d}_{sub}} = \Delta E_{\underline{h}_n \rightarrow \bar{d}_{sub}} + \Delta E_{\underline{d}_{sub} \rightarrow \bar{d}_{sub}} + \Delta E_{\ddot{d}_{sub} \rightarrow \bar{d}_{sub}} \quad (3.48b)$$

$$\Delta E_{\underline{h}_{AC} \rightarrow \bar{h}_{CA}} = \frac{1}{4} \times \frac{1}{3} \left[\underbrace{\frac{2}{3} b_d^2 (v-2)}_{d-d} \right] V_{\sigma_+} \quad (3.48c)$$

The total conjugation energy for a surface bond is plotted in Figure 3.15 with respect to metal atom valence, along with the three components that make up the three terms in Equation (3.44). As with bonds in the clean surface, the total energy of all interactions donating charge into \bar{h}_n is nearly constant with metal atom valence, although it does decrease somewhat between Os and W as the intrinsically weaker $\underline{d}_{surf} \rightarrow \bar{h}_n$ interaction begins to replace the $\ddot{d}_{surf} \rightarrow \bar{h}_n$ interaction after the latter becomes limited by the decreasing magnitude of \ddot{d}_{surf} , as was seen in Figure 3.14. As was also the case with bonds in the clean surface, the total energy of the interactions donating charge into \bar{d}_{surf} increases linearly with metal atom valence between Pt and Re since the magnitudes of these interactions are limited by the linearly increasing magnitude of \bar{d}_{surf} . Between Re and W, this interaction levels off as the intrinsically weaker $\underline{d}_{surf} \rightarrow \bar{d}_{surf}$ interaction replaces the \ddot{d}_{surf} interactions.

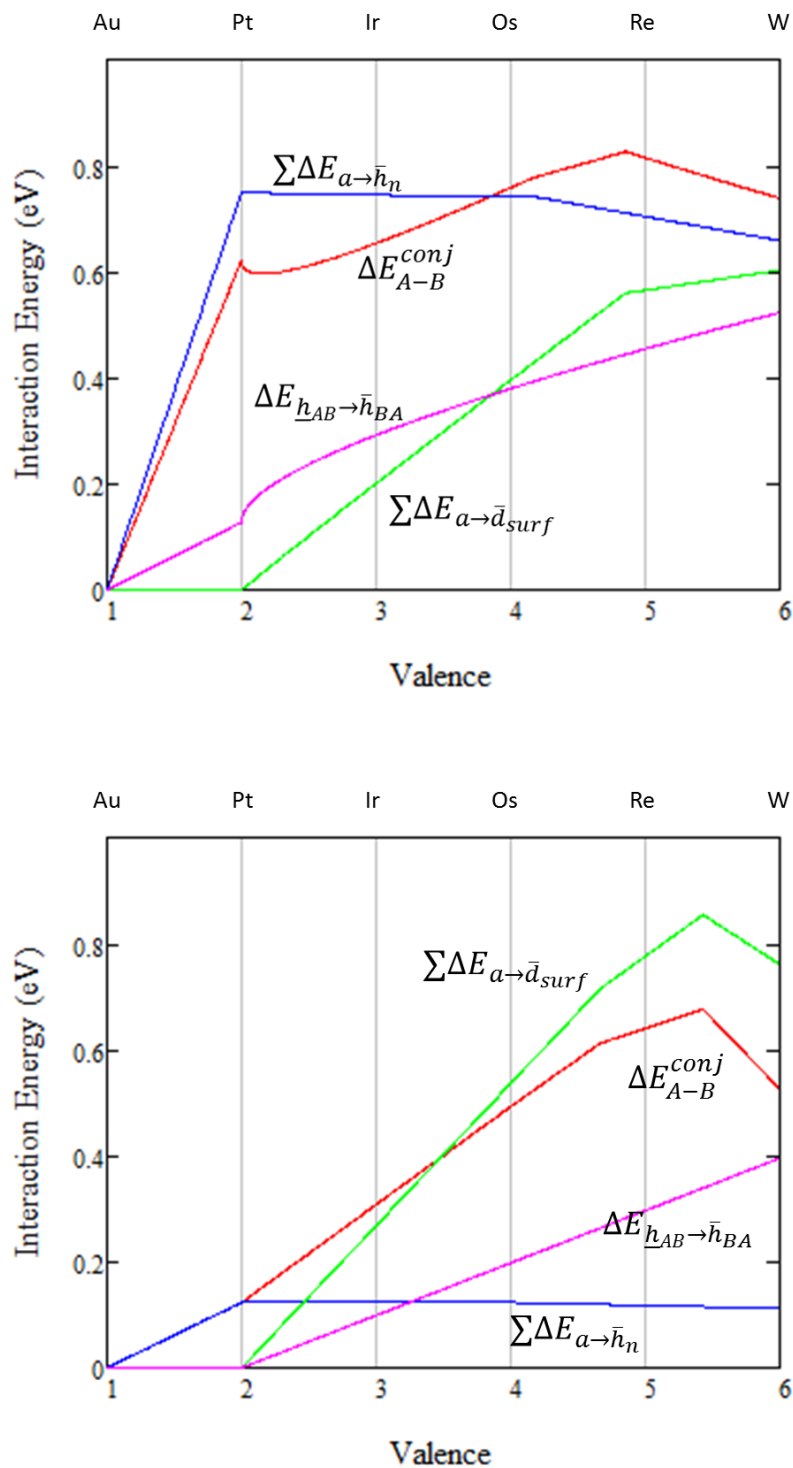


Figure 3.15 Energies of surface (top) and subsurface (bottom) conjugative interactions (red). Also shown are the contributions to the total energy in Equations (3.44) and (3.47) involving donation into the s orbital (blue), the d_{σ} orbital (green), and the zero order term that must be subtracted.

Figure 3.15 plots the total conjugation energy for subsurface bonds along with the three components that contribute to it in Equation (3.47). As with the analogous quantities for surface bonds, the energy of interactions donating into \bar{h}_n is nearly constant with metal atom valence while the energy of interactions donating into \bar{d}_{sub} increases between Pt and Re and then levels out between Re and W once donation from \bar{d}_{sub} start to be replaced by weaker donation from \underline{d}_{sub} . Combined, the three components lead to a total conjugation energy for subsurface bonds that increases between Pt and Re and decreases slightly between Re and W.

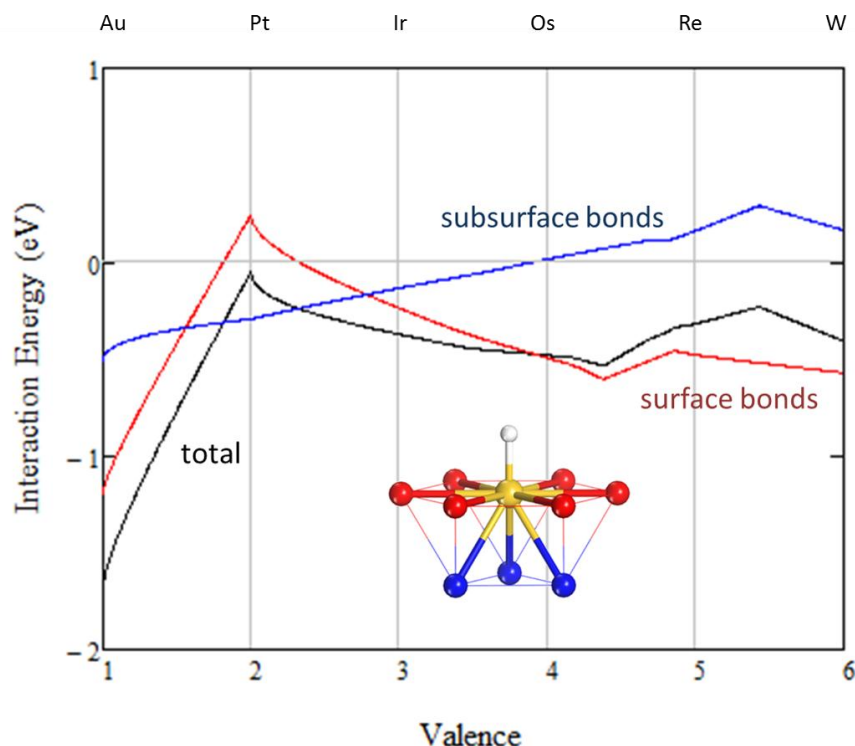


Figure 3.16 Change in conjugation energy upon adsorption of hydrogen with contributions from surface (red) and subsurface (blue) bonds

The total loss in conjugation energy upon adsorption of hydrogen is equal to the energy lost by the six surface bonds and the three subsurface bonds and is shown in Figure 3.16 with the breakdown between surface and subsurface bonds.

The adsorption energy of hydrogen on the metal surface including the change in conjugation energy is shown in Figure 3.12. Here, we can see that the addition of conjugation to the model

results in a very large decrease in adsorption energy between Pt and Au of 2.10 eV. This is more than twice the value predicted by DFT of 0.78 eV, and is likely due to the over-prediction of conjugation by second order perturbation theory.

Based on the discussion in the last two paragraphs, we can conclude that adsorption of hydrogen on slabs of Pt to Re has only a small effect on the conjugation energy calculated by this model associated with metal-metal bonds in the slab, and the loss of bond energy in the slab upon adsorption is almost entirely due to changes in the zero-order structure. This is not the case for Au, however. Looking at Figure 3.16, we can see that the conjugation energy completely vanishes for both surface and subsurface bonds when a monolayer of hydrogen is adsorbed on each side of the slab. This results in a large decrease in metal-metal bond energy from the zero-order value and accounts for the large decrease in adsorption energy that was seen in the DFT calculations between Pt and Au. The reason for this is that there are no metal-metal bonds in the zero-order structure of the slab since each Au-H “molecule” it is composed of is completely bond saturated. Therefore, there are also no conjugative interactions involving charge transfer to or from metal-metal bonds. There will be interactions involving charge transfer between metal-hydrogen bonds, but these interactions are much weaker due to the large energy difference between the Au-H bonding and antibonding orbitals.

3.2 Chemisorption Involving Multiple Interactions

As was seen in Figure 3.1 at the beginning of the chapter (reproduced below), the trends in normalized adsorption energies of different adsorbates on the (111) surfaces of fcc Au to Re exhibit very different behavior. Looking at the figure, it is apparent that the adsorbates fall into five different groups. The first group contains atomic hydrogen and methyl (CH_3) and exhibits an increase in adsorption energy from Au to Pt, which then levels out and decreases between Pt and Re. The second group contains atomic carbon and methylene (CH_2) which have an adsorption energy that increases between Au and Ir before leveling out and decreasing between Ir and Re. Similarly, the adsorption energies of the third group containing atomic nitrogen, methyldiyne (CH), and planar NH_2 increase between Au and Os and are constant between Os and Re. The species in the fourth group, atomic oxygen and linear NH , and the fifth group,

atomic fluorine and linear hydroxyl (OH), all have adsorption energies that increase over all the metals from Au to Re, although the distribution of this increase between different metals is different for the two groups.

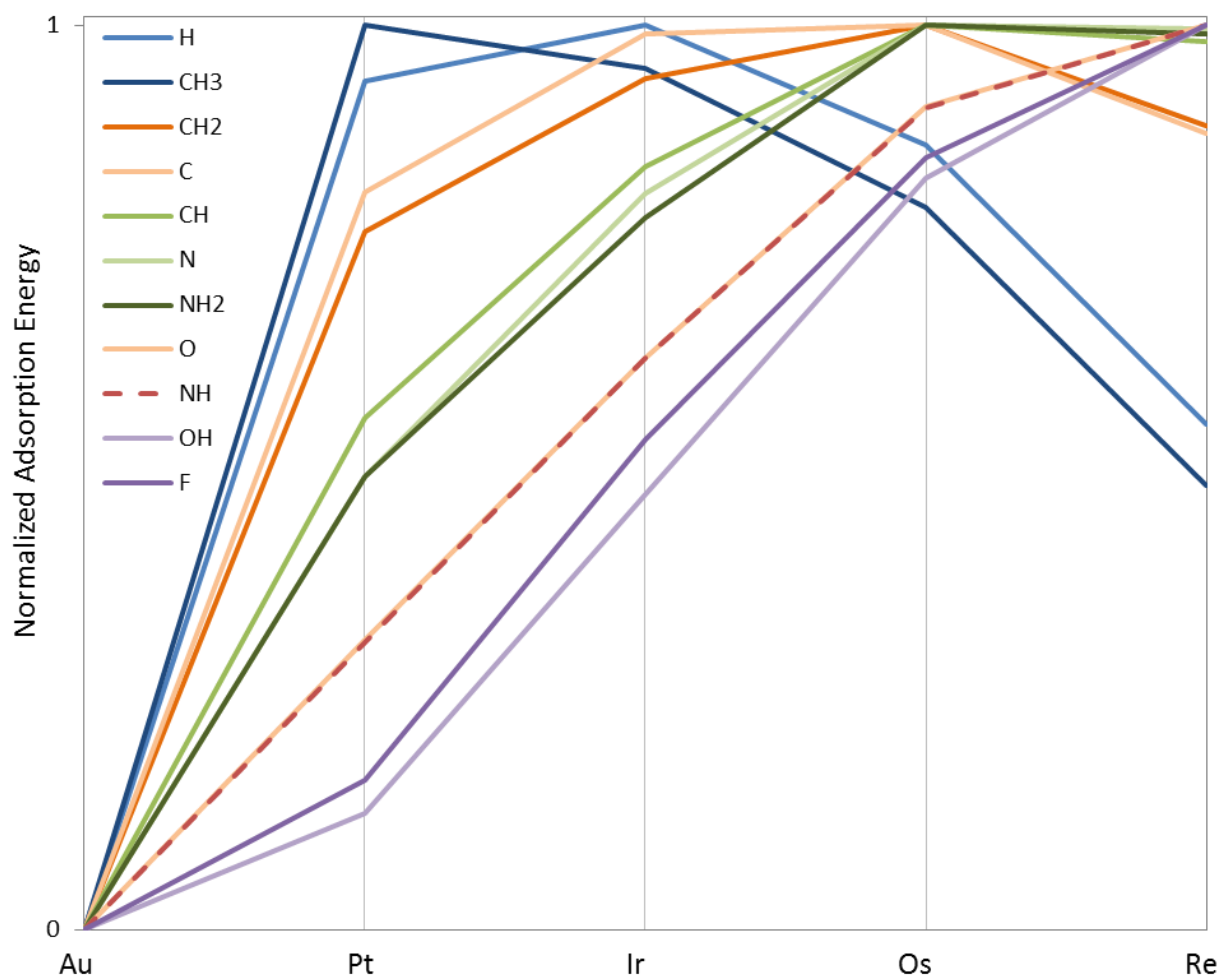


Figure 3.1 (reproduced)

In the previous section, we concluded that the behavior of the adsorption energy of atomic hydrogen is due to a combination of changes in both the zero-order structure and the conjugative interactions upon adsorption. The decrease in adsorption energy between Pt and Re was attributed to the increase in metal-metal bond strength in the clean slab, making it more energetically costly to form the metal-hydrogen bond, while the decrease in adsorption energy between Pt and Au was attributed to the elimination of strong conjugative interactions in the slab

upon adsorption of hydrogen on Au due to the formation of the bond saturated Au-H “molecule” as well as the energy needed to promote part of an electron from the filled *d* shell to the higher energy *s* orbital in order to form the metal-hydrogen bond. Since the adsorption energy of CH₃ follows a similar trend and is isovalent to atomic hydrogen, we conclude that a similar electronic structure is present for both adsorbates.

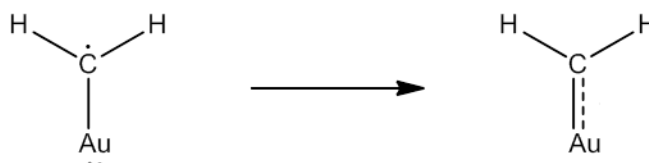


Figure 3.17 After one of the unpaired electrons on CH₂ forms a σ bond with the unpaired electron on Au, the remaining unpaired electron on CH₂ can form a three electron π bond (dashed bond) with one of the lone pairs on Au, leading to a total Au-C bond order of 1.5

The adsorption energy of CH₂ is seen to increase between Au and Ir before leveling out and decreasing slightly between Ir and Re. To understand this behavior, we first contemplate how CH₂ should bond to an Au atom. The unpaired electron on Au can form a σ bond with one of the unpaired electrons on the carbon to form the structure shown in Figure 3.17. The unpaired electron on carbon can still interact with the one of the lone pairs on Au to form a three electron bond. This bond consists of a doubly occupied bonding orbital and a singly occupied antibonding orbital, leading to a total bond order of one half. Therefore, the total Au-C bond order is 1.5. Since the Au atom in this “molecule” is bond saturated, the Au atom is expected to interact only weakly with the neighboring metal atoms, similar to the Au-H and Au-CH₃ molecules. Since the cohesive energy in the slab after adsorption is very weak, due to bond saturation of the Au-CH₂ surface molecule, the total binding energy can be approximated by

$$\Delta E_{ads}(Au) = \Delta E_{Au-C} - \Delta E_{slab}(Au) \quad (3.49)$$

When CH₂ adsorbs on Pt, its two unpaired electrons can form a σ bond and one π bond with the two unpaired electrons on Pt. This forms to the bond saturated Pt=CH₂ “molecule”, which has a larger bond formation energy than Au-CH₂ due to the increase of the metal-carbon bond order from 1.5 to 2. Since this molecule is also bond saturated, it interacts only weakly with the

neighboring metal atoms in the slab so that $\Delta E'_{slab} \cong 0$ and the total binding energy is approximated by

$$\Delta E_{ads}(Pt) = \Delta E_{Pt-C} - \Delta E_{slab}(Pt) \quad (3.50)$$

Both terms in this equation are larger than the corresponding terms in Equation (3.49) for Au, but the increase in ΔE_{M-C} should be greater than the increase in ΔE_{slab} so that the adsorption energy increases from Au to Pt as shown by the DFT calculations. It can therefore be concluded that the increase in adsorption energy of CH_2 between Au and Pt is due to the increase in metal-carbon bond order – a very different mechanism than the one behind the increase in adsorption energy of H and CH_3 between Au and Pt that was solely due to changes in metal-metal bonding.

The increase in CH_2 adsorption energy between Pt and Ir, however, is due to this same mechanism. On Pt, the CH_2 is completely bond saturated so that the bond order of the metal-adsorbate bond cannot increase any more going from Pt to Ir – therefore, the $\text{Ir}=\text{CH}_2$ molecule is left with one unpaired electron. As with hydrogen and CH_3 on Pt, this unpaired electron can form strong bonds with the neighboring metal atoms in the slab. Therefore, the large decrease in metal-metal bond energy observed for adsorption on Au and Pt is not seen on Ir since the metal-metal bonds are not almost completely eliminated after adsorption. The metal-carbon bond energy does not significantly increase between Pt and Ir but the loss of metal-metal bond energy from adsorption becomes much smaller, leading to the increase in adsorption energy seen in Figure 3.1. Between Ir and Re, both ΔE_{M-A} and ΔE_{M-M} are relatively constant for the same reason they were for hydrogen between Pt and Re – therefore, the adsorption energy of CH_2 does not change much in this region.

A similar argument can be used to rationalize the behavior of all the other adsorbates. Over a certain range, the adsorption energy increases continuously due to an increase in the metal-adsorbate bond order by increments of one half, while the metal-metal bonds in the slab are nearly eliminated in the final state due to bond saturation of the metal by the adsorbate. Once the adsorbate is bond saturated, the metal-adsorbate bond energy remains constant, however, one further increase in adsorption energy occurs due to the ability of the metal atoms to form strong

metal-metal bonds following adsorption. After this, all terms in Figure 3.3 remain constant and the adsorption energy does not change significantly anymore. Looking at the structure of the metal-adsorbate bond across the different metals shown in Figure 3.18, it is seen that this explanation is easily applied to CH, and atomic nitrogen, which go from having a double bond with Au (a σ bond and a coordinative π bond involving donation of a lone pair from Au to the adsorbate) to a triple bond with Ir, leading to a continuous increase in adsorption energy between Au and Os.

$\begin{array}{c} \text{CH}_3 \\ \\ \text{Au} \end{array}$	$\begin{array}{c} \text{CH}_3 \\ \\ \text{Pt} \\ \cdot \end{array}$				
$\begin{array}{c} \text{CH}_2 \\ \vdots \\ \text{Au} \end{array}$	$\begin{array}{c} \text{CH}_2 \\ \equiv \\ \text{Pt} \end{array}$	$\begin{array}{c} \text{CH}_2 \\ \equiv \\ \text{Ir} \\ \cdot \end{array}$			
$\begin{array}{c} \text{CH} \\ \equiv \\ \text{Au} \end{array}$	$\begin{array}{c} \text{CH} \\ \equiv \\ \text{Pt} \end{array}$	$\begin{array}{c} \text{CH} \\ \equiv \\ \text{Ir} \end{array}$	$\begin{array}{c} \text{CH} \\ \equiv \\ \text{Os} \\ \cdot \end{array}$		
$\begin{array}{c} \cdot\cdot \\ \vdots \\ \text{C}^- \\ \vdots \\ \text{Au}^+ \end{array}$	$\begin{array}{c} \cdot\cdot \\ \vdots \\ \text{C}^- \\ \vdots \\ \text{Pt}^+ \end{array}$	$\begin{array}{c} \cdot\cdot \\ \vdots \\ \text{C}^- \\ \vdots \\ \text{Ir}^+ \\ \cdot \end{array}$			
$\begin{array}{c} \text{:NH}_2 \\ \\ \text{Au} \end{array}$	$\begin{array}{c} \text{NH}_2 \\ \vdots \\ \text{Pt} \end{array}$	$\begin{array}{c} \text{NH}_2 \\ \equiv \\ \text{Ir} \end{array}$	$\begin{array}{c} \text{NH}_2 \\ \equiv \\ \text{Os} \\ \cdot \end{array}$		
$\begin{array}{c} \text{:NH} \\ \vdots \\ \text{Au} \end{array}$	$\begin{array}{c} \text{:NH} \\ \equiv \\ \text{Pt} \end{array}$	$\begin{array}{c} \text{NH} \\ \equiv \\ \text{Ir} \end{array}$	$\begin{array}{c} \text{NH} \\ \equiv \\ \text{Os} \end{array}$	$\begin{array}{c} \text{NH} \\ \equiv \\ \text{Re} \\ \cdot \end{array}$	
$\begin{array}{c} \cdot\cdot \\ \vdots \\ \text{N} \\ \vdots \\ \text{Au} \end{array}$	$\begin{array}{c} \cdot\cdot \\ \vdots \\ \text{N} \\ \vdots \\ \text{Pt} \end{array}$	$\begin{array}{c} \cdot\cdot \\ \vdots \\ \text{N} \\ \vdots \\ \text{Ir} \end{array}$	$\begin{array}{c} \cdot\cdot \\ \vdots \\ \text{N} \\ \vdots \\ \text{Os} \\ \cdot \end{array}$		
$\begin{array}{c} \text{:OH} \\ \\ \text{Au} \end{array}$	$\begin{array}{c} \text{:OH} \\ \vdots \\ \text{Pt} \end{array}$	$\begin{array}{c} \text{:OH} \\ \equiv \\ \text{Ir} \end{array}$	$\begin{array}{c} \text{OH} \\ \equiv \\ \text{Os} \end{array}$	$\begin{array}{c} \text{OH} \\ \equiv \\ \text{Re} \end{array}$	$\begin{array}{c} \text{OH} \\ \equiv \\ \text{W} \\ \cdot \end{array}$
$\begin{array}{c} \cdot\cdot \\ \vdots \\ \text{O} \cdot \\ \vdots \\ \text{Au} \end{array}$	$\begin{array}{c} \cdot\cdot \\ \vdots \\ \text{O} \cdot \\ \vdots \\ \text{Pt} \end{array}$	$\begin{array}{c} \cdot\cdot \\ \vdots \\ \text{O} \cdot \\ \vdots \\ \text{Ir} \end{array}$	$\begin{array}{c} \cdot\cdot \\ \vdots \\ \text{O} \\ \vdots \\ \text{Os} \end{array}$	$\begin{array}{c} \cdot\cdot \\ \vdots \\ \text{O} \\ \vdots \\ \text{Re} \\ \cdot \end{array}$	
$\begin{array}{c} \cdot\cdot \\ \vdots \\ \text{F} \cdot \\ \vdots \\ \text{Au} \end{array}$	$\begin{array}{c} \cdot\cdot \\ \vdots \\ \text{F} \cdot \\ \vdots \\ \text{Pt} \end{array}$	$\begin{array}{c} \cdot\cdot \\ \vdots \\ \text{F} \cdot \\ \vdots \\ \text{Ir} \end{array}$	$\begin{array}{c} \cdot\cdot \\ \vdots \\ \text{F} \\ \vdots \\ \text{Os} \end{array}$	$\begin{array}{c} \cdot\cdot \\ \vdots \\ \text{F} \\ \vdots \\ \text{Re} \end{array}$	$\begin{array}{c} \cdot\cdot \\ \vdots \\ \text{F} \\ \vdots \\ \text{W} \\ \cdot \end{array}$

Figure 3.18 Bonding in the metal-adsorbate “molecule” formed between a single metal atom and each adsorbate. Dashed bonds indicate a three electron bond of order one half. The structure furthest to the right for each adsorbate has a metal atom with a leftover unpaired electron that can form bonds with the other metal atoms in the surface.

The way that atomic carbon bonds to metal atoms is somewhat different compared to the other adsorbates examined so far. Before atomic carbon adsorbs on Au, it abstracts one electron from the Au atom so that the anionic carbon has three unpaired electrons and the cationic Au has two unpaired electrons. This allows the formation of a σ bond and one π bond along with a three electron bond containing the third lone pair of the anionic carbon and a lone pair from Au – therefore, the Au-C bond order is 2.5 as shown in Figure 3.18. Similarly, carbon abstracts one electron from Pt and forms a triple bond using the three unpaired electrons on each ion. At this point, the carbon atom is bond saturated so that all of the other metals form a triple bond with it after first transferring one electron. Thus, like CH₂, atomic carbon is bond saturated at Pt and exhibits the same variation of binding energy across the different metals.

The remaining adsorbates follow a similar pattern as the ones previously discussed (excluding atomic carbon). The metal-adsorbate bond order continuously increases in increments of one half, along with a corresponding increase in adsorption energy, until the adsorbate is bond saturated. At this point, these adsorbates behave differently because they all contain lone pairs that can further interact with any unpaired electrons on the metal atom. Consider as an example the adsorption of NH₂. As shown in Figure 3.18, this species is bond saturated after forming a single σ bond with Au. In the Pt-NH₂ molecule, the Pt has one unpaired electron that can form a three electron bond with the lone pair on the nitrogen atom, leading to a bond order of 1.5 and an increase in adsorption energy between Au and Pt. Since Ir contains one less electron than Pt, the three electron bond is converted into a two electron bond, leading to an increase in M-N bond order to two and a further increase in adsorption energy. At this point, the adsorbate along with its lone pairs, is bond saturated so the metal-adsorbate bond order can no longer increase. The adsorption energy increases once again between Pt and Ir due to the ability of the Ir-NH₂ molecule to form metal-metal bonds. After this, the adsorption energy remains constant for the same reason that was given for the adsorbates previously discussed.

The same explanation applies to adsorption of atomic oxygen, OH, NH, and atomic fluorine. Although atomic oxygen has two lone pairs and fluorine has three, one of these cannot participate in bonding with the metal because they are contained in *sp* orbitals oriented away from the metal atom. The same is true for the lone pairs in atomic nitrogen and carbon.

At this point, we have rationalized the periodic trends in bonding energy for all of the adsorbates in Figure 3.1 based on our understanding of the chemisorption of hydrogen. While the model developed in this work has not been applied numerically to these other adsorbates, it is still very satisfying to see that we can use it to qualitatively explain the very different trends in adsorption energy that are observed for many characteristically different adsorbates. We can see that the structure of the metal-adsorbate bond is quite similar to the bonding expected in an analogous organometallic complex, with the metal atom ligands taking the place of the organic ligands. The main difference is that the metal atom in the slab is over-coordinated prior to (and after) adsorption while the organometallic complex is not. This leads to the additional increase in adsorption energy that occurs after the adsorbate is already bond saturated once the metal-adsorbate “molecule” gains the ability to form metal-metal bonds.

Summary

In this dissertation, a framework has been developed for describing the bonding within transition metals and between a transition metal surface and an adsorbate in terms of fractional diatomic covalent bonds and the conjugative interactions between these bonds. Using this framework, we were able to semi-quantitatively describe trends in bulk cohesive energies of transition metal crystals, surface formation energies, and energies of hydrogen adsorption on transition metal surfaces. The values calculated in this way reproduce the qualitative features of trends obtained from full DFT calculations, indicating that the model developed here is capable of describing the most important features of metal-metal and metal-adsorbate bonding, even though it ignores the long range interactions between non-neighboring atoms that are known to be present in the metallic state. Additionally, we were able to apply the qualitative aspects obtained from studying hydrogen adsorption to the study of more complicated adsorbates. By doing this, it was possible to qualitatively rationalize the adsorption energy trends of most common adsorbates in the atop binding site, indicating that this model is applicable to most chemisorption phenomena.

In the first chapter, a framework was proposed for describing local bonding in transition metal crystals. The difficulty of constructing this lies in the fact that the number of metal-metal bonds each metal atom forms in a crystal far exceeds the number of unpaired electrons available for forming these bonds, meaning that these atoms are extremely hypervalent. This hypervalency, along with the inflexibility of the coordination environment of a metal atom in the crystal, makes common methods of quantitatively describing localized bonding in molecules and transition metal complexes unsuitable for describing bonding in transition metal crystals.

We find that in order to describe bonding in transition metal crystals in a similar way, it is necessary to introduce the concept of fractional bonds and fractional orbitals. By eliminating the constraint that bonds must have integer bond order, it is possible to describe the bonding in transition metal crystals in terms of Lewis-like structures consisting of fractional bonds and lone pairs. In classical Valence Bond Theory, each bond in a Lewis structure corresponds to a pair of electrons occupying a bonding molecule orbital composed of a linear superposition of two atomic hybrid orbital. When fractional bonds are allowed, each fractional bond in a Lewis

structure corresponds to a fraction of an electron pair occupying a fractional bonding molecular orbital composed of fractional atomic hybrid orbitals. A fractional orbital is an orbital whose wavefunction is normalized to a value (magnitude) less than unity. The magnitude of a fractional bonding orbital is set equal to the bond order (magnitude) of the fractional bond it describes. Furthermore, each fractional bonding orbital is constructed as a linear superposition of two fractional atomic hybrid orbitals, both having magnitudes equal to the magnitude of the bond. In a more mathematically rigorous approach, each fractional orbital is constructed of a real component having a magnitude equal to the bond magnitude and a virtual component that normalizes the orbital to a value of unity. The rules for determining Lewis structures in classical Valence Bond Theory can be seamlessly modified to accommodate fractional bonding by constraining the sum of the bond orders of all fractional bonds to a given atom to equal the valence of that atom.

In addition to the fractional bonds formed in the zero order electronic structure of a transition metal crystal, there are conjugative interactions between these bonds and with lone pairs that involve electron transfer from an occupied bonding orbital or lone pair into a neighboring unoccupied antibonding orbital. These conjugative interactions have only a secondary effect on the electronic structures of molecules that can be described by a single classical Lewis structure. In most transition metal complexes and crystals, however, these interactions make up a large part of the total binding energy due to the hypervalency of the metal atoms in these systems. In current quantitative models of localized bonding, such as the Natural Bond Orbital Theory of Weinhold and Landis, the energies of these interactions are calculated using second order perturbation theory. Adapting this procedure to systems with fractional orbitals is troublesome because electron transfer between two orbitals with different magnitudes leads to a change in the total number of electrons in the system. Furthermore, even if all interactions occur between donor and acceptor orbitals with equal magnitudes, coupling between multiple interactions can also lead to changes in the total number of electrons.

To get around this problem, we introduce an alternative way of describing conjugative interactions. Instead of basing these interactions off of electron transfer from bonding orbitals and lone pairs into antibonding orbitals, we base them off of electron transfer between *s* and *d*

atomic orbitals on neighboring atoms. This results in a set of decoupled interactions that can be easily made to individually conserve the total number of electrons. Basing the conjugative interactions off of atomic orbitals requires a few modifications to the formulae for calculating the energies of these interactions in order to take into account the bonding between atomic orbitals in the zero order electronic structure. After making these modifications, this framework for describing conjugative interactions can be applied universally to any system with fractional orbitals.

In Chapter 2, we applied the local fractional bonding formalism to describe the bonding in $5d$ transition metal fcc crystals. Each atom in an fcc crystal is coordinated by twelve other metal atoms. Therefore, a metal with a valence v will form a fractional bond of magnitude $v/12$ with each of its twelve neighbors. As with the transition metal complexes, each metal atom will have $n = 6 - v$ lone pairs that are contained in nonbonding fractional hybrid orbitals of d character so that the bonding hybrid orbitals will have sd^{v-1} composition. On Au, the d shell is completely filled with lone pairs so that metal-metal bonding occurs only through the s orbital, while on W, there are no lone pairs so that the s orbital and the entire d shell is involved in bonding. This hybridization is the same observed in transition metal complexes, so even though we are describing hypervalent atoms with fractional bonds, the hybrids will still have the same composition as they do in molecular systems although their arrangement and orientation will be different.

The zero-order cohesive energy (not including conjugation) of the metal crystal is found to increase from Au to W as the hybrids forming the metal-metal bonds increase in magnitude, being nearly proportional to the metal atom valence. The contribution to the cohesive energy from interactions between the s components of the hybrids is the same for all metals examined since the s orbital is fully involved in bonding for all of these metals as it does not contain any lone pairs. As the valence increases from Au to W, the number of lone pairs decreases, freeing up d orbitals to participate in bonding. As a result, the cohesive energy from interactions involving the d orbitals steadily increases. It is found that the interactions between a d orbital on one metal atom and the s orbital on the other metal atom of a bond make a significant contribution to the cohesive energy, especially for the higher valent metals. This contradicts the

popular qualitative model of transition metal electronic structure that separates the bands into independent *s* states and *d* states, suggesting instead that the *s* and *d* orbitals are hybridized to the same extent that the *s* and *p* orbitals are hybridized in compounds involving 2*p* elements.

In addition to the zero-order cohesive energy, there is also a component arising from conjugative interactions involving charge transfer from occupied bonding and nonbonding atomic orbitals to unoccupied bonding atomic orbitals on a neighboring atom. The total conjugation energy between two metal atoms can be decomposed into a component due to donation into the *s* orbital and another component due to donation into a *d* orbital. The first of these components is limited by the occupancy of the *s* orbital, which is half filled for all transition metal atoms studied. Since the occupancy of the *s* orbital is constant, the sum of the energies of interactions donating into this orbital is nearly constant from Au to W. The second component, corresponding to interactions donating into a *d* orbital, is limited by the occupancy of the *d* orbital. As the occupancy of the *d* orbital decreases from Au to W, these interactions become stronger since their magnitude is proportional to the fraction of the *d* orbital that is unoccupied – this is because the interactions transfer charge into the *d* orbital, so the less occupied it is, the more charge it can accept.

The interactions donating charge into *d* orbitals lead to a nearly linear increase in the total conjugation energy between Au and Os. Unlike the zero order bond energy, which increases nearly six-fold between Au and Os, the conjugation energy only increases by 65% of its value on Au. The relatively small increase in the conjugation energy over this range is due to the large contribution from interactions donating into the *s* orbital, which is nearly constant for all metals examined. The addition of each *d* orbital to metal-metal bonding that occurs with each increase in metal atom valence makes a much smaller contribution to the conjugation energy than the *s* orbital since only a fraction of the added orbital can participate in σ interactions with a given atom due to the oscillation of the angular part of the wave function. The *s* orbital, on the other hand, is spherically symmetric and interacts equally with all neighboring atoms. An additional factor leading to the relatively small increase in conjugation energy between Au and Os is that the part of an atomic orbital participating in the zero order bond between two atoms cannot also participate in conjugation between those same two atoms. As the zero order bond magnitude

increases with valence, a larger fraction of each orbital is involved in zero order bonding, leaving less to participate in conjugation.

After Os, an additional effect comes into play related to whether charge is donated from the component of the *d* orbital involved in zero order bonding or the nonbonding component that forms the lone pairs. Interactions involving the latter are stronger because any bonding involving the donor orbital in the zero order structure reduces its effective energy so that it is a weaker donor in conjugative interactions. Between Au and Os, the component of the *d* orbital that does not participate in bonding is sufficient to saturate the acceptor orbital so that the interactions involve only the nonbonding component of the *d* orbital. As the metal atom valence increases, a greater fraction of the *d* orbital becomes involved in metal-metal bonding in the zero order structure until W where the entire *d* orbital is involved in metal-metal bonding as there are no lone pairs. Between Os and Re, the nonbonding component of the *d* orbital decreases to a point where it is unable to saturate the acceptor orbital, so part of the bonding component of the *d* orbital takes its place as the donor. Since the bonding component is a weaker donor, the conjugation energy levels off between Os and Re and decreases between Re and W.

Combining the zero order and conjugation energies leads to a crystal cohesive energy that increases by a factor of nearly 2.5 between Au and Os due to increases in both the zero order energy and the conjugation energy in this region. Unlike the zero order bond energy, the cohesive energy in this region is far from being proportional to the metal atom valence due to the relatively small change in the conjugation energy over this region. Between Os and W, the cohesive energy only increases by 10% due to the decrease in conjugation energy over this region.

When a two-layer (111) slab is cleaved from the bulk, changes in zero-order bonding must occur to keep the metal atoms bond saturated, a result of the fact that each metal atom loses three of its neighbors during cleavage. The simplest way to restore the bond saturation of the metal atoms is to double the magnitudes of the bonds between metal atoms on opposite sides of the slab. There is no change in the shape of the bonding hybrids, only a change in magnitude of the bonds – as a

result, the zero-order cohesive energy lost from cleavage of the surface is regained by the increase in magnitude of the bonds within the slab.

Since the zero-order surface energy is zero, all of the surface energy must come from reduction in conjugative interactions. The most obvious loss of conjugation is those interactions occurring between the slab and the bulk it was cleaved from. This energy is equal to the conjugative bond energy across a metal-metal bond in the bulk. The conjugative interactions involving charge transfer across bonds within the slab decrease as well upon cleavage of the slab. This is due to the doubling in magnitude of these bonds in the zero order structure to compensate for the bonds that were broken during surface cleavage. Any increase in the zero order bond magnitude leads to an increase in the fraction of the atomic orbitals on each atom that participate in this bond. Since any fraction of an orbital cannot participate in conjugation between two atoms if it is involved in zero order bonding between those same atoms, this leads to a decrease in the intra-slab conjugation energy.

In Chapter 3, we applied the local bonding formalism for transition metal crystals to study how adsorbates bind to transition metal surfaces. First, the adsorption of atomic hydrogen in the atop site was examined on the (111) surface of the $5d$ transition metals in the limit that the metal-hydrogen bond is much stronger than the metal-metal bonds, leading to formation of a surface molecule between a metal atom and the adsorbate. In this limit, the total binding energy is decomposed into three terms corresponding to removal of a metal atom from the surface, formation of the surface molecule between that metal atom and the adsorbate, and placement of the surface molecule back into the surface. The combination of the first and last terms accounts for the reduction in metal-metal bond energy upon formation of the metal-adsorbate bond. The formation energy of the surface molecule has a constant value for Pt to W if we ignore variations in the resonance integrals and atomic orbital energies between these metals. This energy is lower (weaker) on Au because the d shell is completely filled with five lone pairs, so in order to form an sd^n hybrid orbital to bond to hydrogen, part of an electron pair must be promoted from the d shell into the higher energy s orbital.

Since the formation energy of the surface molecule is the same for Pt to W, any variation in adsorption energy between these elements must come from variations in the reduction of metal-metal bond energy upon formation of the metal-adsorbate bond. We first examined the changes in bonding in the zero order structure induced by adsorption. Formation of the metal-hydrogen bond removes the sd^n hybrid used to form this bond from participating in metal-metal bonding. This orbital is primarily involved in bonds between the surface layer and the subsurface layer in the clean surface, so it is these bonds that are primarily affected by adsorption. In order to form a full M-H bond, the three subsurface bonds must decrease in magnitude by 1/3 of a unit, leading to a large decrease in the zero order energy associated with these bonds. The metal-metal bonds between surface atoms in Ir to W are hardly affected by removal of metal orbital forming the M-H bond and actually increase slightly in energy to make up for some of the decrease in subsurface bonding. In Pt, changes in hybridization introduced by formation of the M-H bond lead to a decrease in energy of the surface bonds. The subsurface bonds are completely broken in the Pt surface in the zero order structure. In Au, all of the orbitals not involved in the M-H bond are filled with lone pairs so that no metal-metal bonding can occur.

The change in zero order energy of the subsurface bonds is positively correlated with the strength of those bonds in the clean surface. Since these bonds increase in strength from Au to W, the zero order subsurface bond energy lost upon adsorption is greatest for W and least for Au. Adding to this the change in surface bonding energy upon adsorption leads to a total loss in metal-metal bond energy that increase from Au to W, except for Pt which has an anomalously large decrease due to the loss in surface bonding upon adsorption that was discussed.

The change in conjugation energy upon formation of the M-H has a minimal effect between Pt and Os, with the absolute value being less than 0.14 eV. For Re and W, however, formation of the M-H bond results in an increase (strengthening) in conjugation energy of 0.56 eV. This occurs because the fraction of each d orbital that does not participate in zero order metal-metal bonding is higher in the presence of the adsorbate, so the point where it is no longer able to saturate the acceptor orbital shifts to higher valences. In the region between the point where this happens on the clean surface and the point where this happens on the adsorbate covered surface, the interactions donating into d orbitals increase in energy for the latter relative to the former.

After this region, the interaction energies of the two systems change at about the same rate. This region occurs between Os and Re, leading to the abrupt change in the difference in conjugation energy between the two adsorbate covered and clean surfaces observed in this region. The reason that a greater fraction of each *d* orbital does not participate in zero order metal-metal bonding in the adsorbate covered surface is that about half of a *d* orbital has been removed from metal-metal bonding in order to form the M-H bond – this makes the lone pairs more concentrated in the remaining *d* orbitals.

The total loss in metal-metal bond energy caused by hydrogen adsorption increases slightly between Pt and Os due to an increasing loss in zero-order bond energy. It then decreases slightly between Os and Re due to an increase in the conjugation energy in the adsorbate covered surface relative to the clean surface resulting from the greater availability of the lone pairs as electron donors when the adsorbate is present. Finally, the loss in metal-metal bond energy increases again from Re to W due to the increasing loss in zero order bond energy. Since the surface molecule formation energy is constant over all of these metals, the hydrogen adsorption energy is controlled solely by the loss in metal-metal bond energy. These trends match some of the qualitative behavior of the DFT calculated hydrogen adsorption energy, which decreases slightly between Ir and Re before leveling out between Re and W.

Unlike the other metals studied, where the conjugation energy increases or remains about the same upon adsorption of hydrogen, the situation for adsorption on Au is very different. Since all of the orbitals on Au not involved in forming the Au-H bond contain lone pairs, there are no acceptor orbitals capable of participating in conjugation – therefore, the conjugation energy drops to zero, leading to a much larger decrease in metal-metal bond energy upon adsorption than the other metals. Essentially, the formation of the Au-H bond leads to a saturated surface molecule that cannot participate in strong interactions when placed back into the surface. In combination with the energy penalty for promoting electrons from a *d* orbital to the higher energy *s* orbital to form the Au-H bond, this leads to the much lower adsorption energies observed in both DFT and experiment for adsorbates on the coinage metals.

Finally, we take what we have learned about chemisorption of hydrogen and apply it qualitatively to other common adsorbates, first to the CH_x series with $x = \{0,1,2,3\}$. Methyl (CH_3), is similar to hydrogen in that it has one unpaired electron and therefore displays the same adsorption energy trends over the $5d$ metals. Methylidene (CH_2) has an additional unpaired electron that can form a π bond with a metal atom in addition to the σ bond present in CH_3 and H. This leads to an increase in adsorption energy between Au and Pt due to the ability of Pt to form a full π bond with CH_2 while Au can only form half of one. The adsorption energy increases again between Pt and Ir as the surface molecule becomes unsaturated and can thus form strong bonds with the other metal atoms upon reinsertion into the surface. The situation is similar for methylidyne (CH), except two π bonds can be formed with the metal atom, leading to an increase in adsorption energy between Au and Os, before leveling off and decreasing. Atomic nitrogen has the same electron configuration as CH and thus displays very similar adsorption energy trends.

When atomic carbon bonds to a metal atom, it abstracts an electron from the metal so that it has the same electron configuration as CH with three unpaired electrons. Since it lost one electron to the carbon atom, an Au atom has two unpaired electrons that can form a σ bond and two half π bonds with the carbon atom. The additional unpaired electron on Pt converts the half π bonds into full π bonds and the left over unpaired electron on Ir can form strong metal-metal bonds. This leads to an increase in adsorption energy from Au to Ir, before leveling off and decreasing.

The adsorbates NH_2 and NH have one and two unpaired electrons and bind similarly to CH_3 and CH_2 between Au and Pt (NH_2) or Ir (NH). On Ir (NH_2) and Os (NH), a half filled d orbital becomes available with which half of the nitrogen lone pair can donate into, forming a half π bond which leads to further stabilization. Upon moving one column more to the left on the row of $5d$ transition metals, the d orbital becomes fully unoccupied so that the nitrogen lone pair can donate into it to form a full π bond, leading to even further stabilization. After this point, no further metal-nitrogen bonds can form and the adsorption energy stops increasing out. Hydroxyl (OH), atomic oxygen, and atomic fluorine also have lone pairs that can donate into empty or partially empty d orbitals on the metal atom. Donation of these lone pairs into the metal forms π

bonds that further stabilize the surface molecule and increase the adsorption energy until all of the lone pairs that can do so have formed coordinative π bonds with the metal atom.

Appendix A – Determination of Tight Binding Parameters

Tight binding parameters were extracted from the periodic DFT calculations (described in Appendix B) using the Quasiatomic Orbital (QO) method⁴² implemented by the author in the Vienna Ab initio Simulation Package.^{43,44} This method generates a tight binding minimal atomic basis set that is able to exactly reproduce the ground state electronic structure of a plane wave calculation. By expressing the Hamiltonian in this basis set, the tight binding orbital energies and resonance (hopping) integrals can be extracted. This procedure was used to determine the parameters in Table 2.1.

The determination of $V_{\sigma+}$, b_s , and b_d in Table 2.1 requires some additional explanation. For a pair of atoms A and B, there are $m \times n$ resonance integrals between the m atomic orbitals of A and the n atomic orbitals of B. These can be represented as an $m \times n$ matrix with the rows corresponding to the atomic orbitals of A and the columns corresponding to the atomic orbitals of B. This matrix H_{AB} can be converted into a diagonal form h_{AB} by means of a singular value decomposition so that

$$H_{AB} = U h_{AB} V^T \quad (\text{A.1})$$

where U is an orthogonal $m \times m$ matrix and V is an orthogonal $n \times n$ matrix. The n hybrid orbitals on A defined by the first n columns of U and the n hybrid orbitals on B defined by the columns of V define a set of characteristic interactions with resonance integrals given by the singular values contained in h_{AB} . For two transition metal atoms, this decomposition will correspond to the characteristic interactions in Equation (2.5). The resonance integrals ($V_{\sigma+}$, $V_{\sigma-}$, V_{π} , and V_{δ}) are given by the singular values in h_{AB} , the hybrids on atom A ($h_{\sigma+}^A$, $h_{\sigma-}^A$, $h_{\pi_x}^A$, $h_{\pi_y}^A$, $h_{\delta_x}^A$, and $h_{\delta_y}^A$) are given by the columns of U , and the hybrids on atom B ($h_{\sigma+}^B$, $h_{\sigma-}^B$, $h_{\pi_x}^B$, $h_{\pi_y}^B$, $h_{\delta_x}^B$, and $h_{\delta_y}^B$) are given by the columns of V . If A and B are chemically equivalent, then $U = V$. Thus, $V_{\sigma+}$ in Table 2.1 was taken directly from h_{AB} , while b_s and b_d were determined from the columns of U and V corresponding to the σ_+ interaction, using Equation (2.7).

Appendix B – Method for DFT Calculations

First principle periodic density functional theory (DFT) calculations were carried out using the Vienna Ab-initio Simulation Package (VASP).^{43,44} The wavefunction was constructed from plane waves with an energy cutoff of 396 eV. Vanderbilt ultrasoft pseudopotentials¹⁷ with real space projection operators were used to describe the sharp features of the wavefunctions in the core region. The Perdew-Wang 91 form of the Generalized Gradient Approximation (GGA)⁴⁵ was used to model the gradient corrections to the correlation and exchange energies. All calculations were performed non-spin polarized.

Both bulk and surface calculations were carried out. The bulk calculations were run on a single fcc unit cell containing four atoms using the experimental lattice constant. For elements that do not occur naturally in the fcc structure (Os, Re, W), the lattice constant was optimized during the calculation. Since lattice constants calculated using DFT are generally larger than the experimental values, the following linear relationship was developed to relate the DFT lattice constants of the naturally occurring fcc metals (Au, Pt, Ir) to the experimental values.

$$a_{exp} = 0.83 a_{DFT} + 0.61 \quad (B.1)$$

This relationship was then used to estimate an effective experimental lattice constant from the DFT optimized lattice constant for those metals that do not naturally occur in the fcc structure.

The (111) surfaces were constructed using four layers cut from the bulk, each with a 3×3 array of metal atoms. The successive slabs were separated by 10 Å of vacuum. In all calculations, the metal atoms were frozen in their corresponding bulk positions. In calculations involving adsorbates, the adsorbates were placed on one side of the slab at a coverage of 1/9 monolayer in the orientations shown in Appendix C.

Each geometry optimization was performed in three steps. First, the geometry was roughly optimized until the force on each atom was less than 0.10 eV/Å. During these runs, a finite Fourier transform (FFT) grid with a cutoff 1.5 times the plane wave cutoff was used and the

wave functions and charge density were converged to within 1×10^{-4} eV. Next, the geometry was refined until the forces less than 0.05 eV/Å. For these runs, an FFT grid with a cutoff of two times the plane wave cutoff was used to eliminate wrap-around errors and the wave functions and charge density were converged to within 1×10^{-6} eV. This was done to ensure that the forces were accurate enough for this level of geometry optimization. These first two geometry optimizations were optimized using a $3 \times 3 \times 1$ k-point mesh ($5 \times 5 \times 5$ for bulk calculations) to sample the first Brillouin zone and a second order Methfessel-Paxton occupation scheme⁴⁶ with smearing of 0.20 eV to determine the occupancy of each band. In the final step, the energies of the optimized structures were calculated with a $6 \times 6 \times 1$ k-point mesh ($11 \times 11 \times 11$ for bulk calculations), using the linear tetrahedron method with Blöchl corrections⁴⁷ to integrate over the first Brillouin zone. The wavefunctions and charge density were converged to within 1×10^{-4} eV and the same FFT grid used in the first run was used since accurate forces were not needed. In all steps, the metal atoms in the surface were frozen in their corresponding bulk position.

Appendix C – Structures of Adsorbates on the (111) Surface

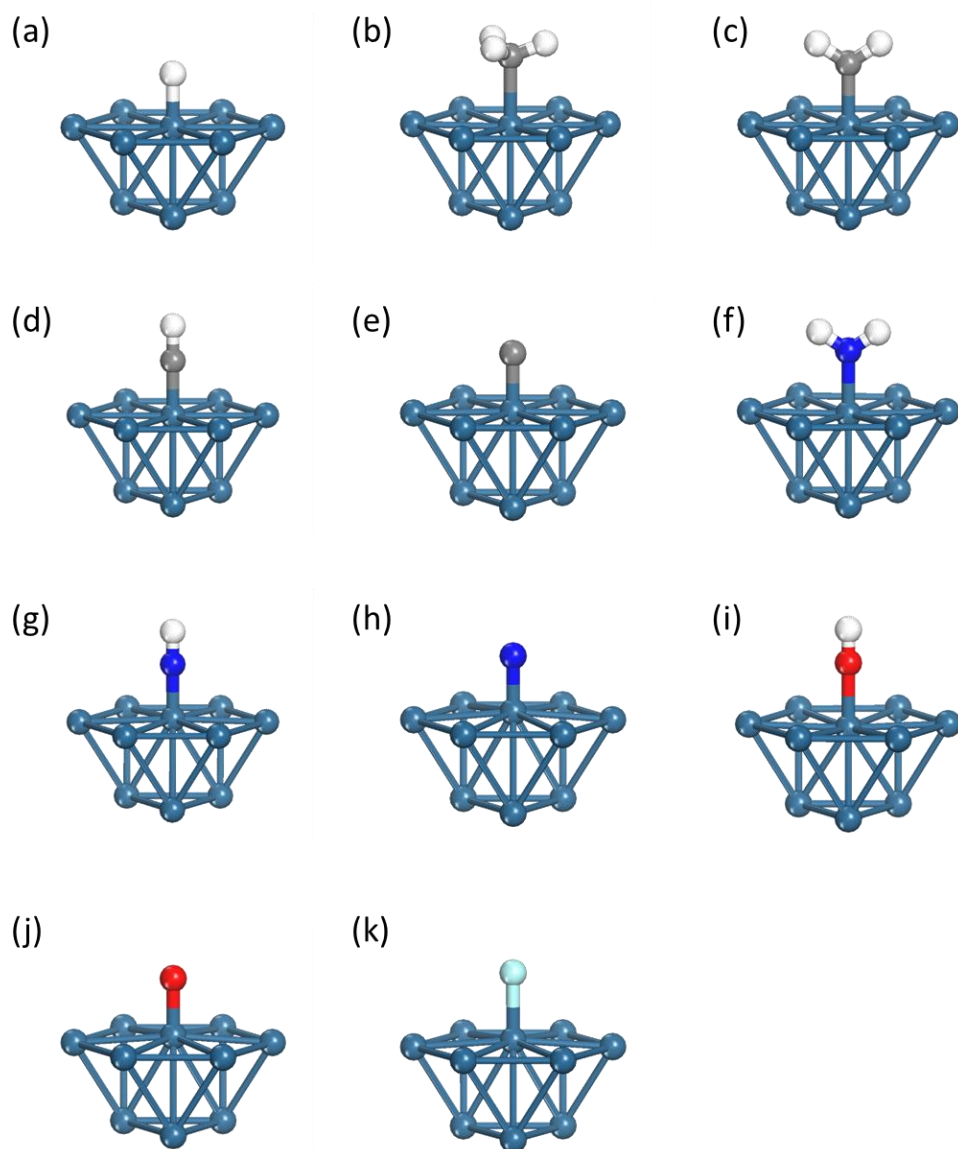


Figure D.1 Adsorption structures used in DFT calculations for (a) H, (b) CH₃, (c) CH₂, (d) CH, (e) C, (f) NH₂, (g) NH, (h) N, (i) OH, (j) O, and (k) F

References

- (1) Santen, R. A. V.; Neurock, M. *Molecular Heterogeneous Catalysis: A Conceptual and Computational Approach*; John Wiley & Sons Inc (E), 2009.
- (2) Pauling, L. *The Nature of the Chemical Bond*; Cornell University Press: Ithaca, 1960.
- (3) Weinhold, F.; Landis, C. R. *Valency and Bonding: A Natural Bond Orbital Donor-Acceptor Perspective*; Cambridge University Press, 2005; p. 760.
- (4) Ashcroft, N. W.; Mermin, N. D. *Solid State Physics*; Brooks Cole, 1976; p. 848.
- (5) Newns, D. *Physical Review* **1969**, *178*, 1123-1135.
- (6) Grimley, T. *Advances in Catalysis* **1960**, *12*, 1–30.
- (7) Hammer, B.; Norskov, J. K.; Nørskov, J. K. *Nature* **1995**, *376*, 238-240.
- (8) Hammer, B. *Surface Science* **1995**, *343*, 211-220.
- (9) Goda, A. M.; Barteau, M. A.; Chen, J. G. *The Journal of Physical Chemistry B* **2006**, *110*, 11823-31.
- (10) Greeley, J.; Nørskov, J. K. *Surface Science* **2005**, *592*, 104-111.
- (11) Hoffmann, R. *Reviews of Modern Physics* **1988**, *60*, 601-628.
- (12) Santen, R. A. V. *Theoretical Heterogeneous Catalysis (World Scientific Lecture and Course Notes in Chemistry)*; World Scientific Pub Co Inc, 1991; p. 650.
- (13) Anderson, A. B. *Journal of the American Chemical Society* **1977**, *99*, 696-707.
- (14) Fukui, K.; Yonezawa, T.; Shingu, H. *The Journal of Chemical Physics* **1952**, *20*, 722.
- (15) Fleming, I. *Frontier orbitals and organic chemical reactions*; Wiley, 1976.
- (16) Kohn, W.; Sham, L. J. *Physical Review* **1965**, *140*, A1133-A1138.
- (17) Vanderbilt, D. *Physical Review B* **1990**, *41*, 7892-7895.
- (18) Kohn, W.; Sham, L. *Phys. Rev* **1965**, 385.
- (19) Hoffmann, R.; Lipscomb, W. N. *The Journal of Chemical Physics* **1962**, *36*, 2179.
- (20) Hoffmann, R. *The Journal of Chemical Physics* **1963**, *39*, 1397.

- (21) Cramer, C. J. *Essentials of Computational Chemistry: Theories and Models*; Wiley, 2004; p. 618.
- (22) Szabo, A.; Ostlund, N. S. *Modern Quantum Chemistry: Introduction to Advanced Electronic Structure Theory (Dover Books on Chemistry)*; Dover Publications Inc., 1996; p. 480.
- (23) Boys, S. *Reviews of Modern Physics* **1960**, 32, 296-299.
- (24) Edmiston, C.; Ruedenberg, K. *Reviews of Modern Physics* **1963**, 35, 457-464.
- (25) Reed, A. E.; Weinhold, F. *The Journal of Chemical Physics* **1985**, 83, 1736.
- (26) Foster, J. P.; Weinhold, F. *Journal of the American Chemical Society* **1980**, 102, 7211-7218.
- (27) Weinhold, F.; LANDIS, C. *CHEMISTRY* **2001**, 2, 91-104.
- (28) Mo, Y.; Peyerimhoff, S. D. *The Journal of Chemical Physics* **1998**, 109, 1687.
- (29) Surjan, P. R.; Ravasz, M.; Mayer, I. *Journal of the Chemical Society, Faraday Transactions 2* **1981**, 77, 1129.
- (30) Fornili, A. *Journal of Molecular Structure: Theochem* **2003**, 632, 157-172.
- (31) Coulson, C. A.; Goodwin, T. H. *Journal of the Chemical Society (Resumed)* **1962**, 2851.
- (32) Reed, A. E.; Weinstock, R. B.; Weinhold, F. *The Journal of Chemical Physics* **1985**, 83, 735.
- (33) Landis, C. R.; Firman, T. K.; Root, D. M.; Cleveland, T. *Journal of the American Chemical Society* **1998**, 120, 1842-1854.
- (34) Landis, C. R.; Cleveland, T.; Firman, T. K. *Journal of the American Chemical Society* **1995**, 117, 1859-1860.
- (35) Landis, C. R.; Weinhold, F. *Journal of Computational Chemistry* **2006**, 5.
- (36) Frenking, G.; Fröhlich, N. *Chemical Reviews* **2000**, 100, 717-74.
- (37) Pauling, L. *Proceedings of the Royal Society A: Mathematical, Physical and Engineering Sciences* **1949**, 196, 343-362.

- (38) Nilsson, A.; Pettersson, L. G. M.; Norskov, J. *Chemical Bonding at Surfaces and Interfaces*; Elsevier Science, 2007; p. 532.
- (39) Glendening, E. D.; Streitwieser, A. *The Journal of Chemical Physics* **1994**, *100*, 2900.
- (40) Anderson, P. W. *Physical Review* **1961**, *124*, 41-53.
- (41) Grimley, T. B. *Journal of Vacuum Science and Technology* **1971**, *8*, 31.
- (42) Qian, X.; Li, J.; Qi, L.; Wang, C.-Z.; Chan, T.-L.; Yao, Y.-X.; Ho, K.-M.; Yip, S. *Physical Review B* **2008**, *78*, 1-22.
- (43) Kresse, G.; Furthmüller, J. *Physical Review B* **1996**, *54*, 11169-11186.
- (44) Kresse, G. *Computational Materials Science* **1996**, *6*, 15-50.
- (45) Perdew, J. P.; Chevary, J.; Vosko, S.; Jackson, K.; Pederson, M.; Singh, D.; Fiolhais, C. *Physical Review B* **1992**, *46*, 6671-6687.
- (46) Methfessel, M.; Paxton, A. *Physical Review B* **1989**, *40*, 3616-3621.
- (47) Blöchl, P. E. *Physical Review B* **1994**, *49*, 16223-16233.